UNIVERSITY OF SOUTHAMPTON

Faculty of Engineering and Physical Sciences
School of Electronics and Computer Science
Smart Electronic Materials and Systems Research Group (SEMS)

Investigating and Developing Low-Cost Wearable Respiration Sensors

by

Mahdi Mohamed Saleh Abdulla Ahmed Shaban
BEng Electromechanical Engineering
ORCiD: 0000-0002-7219-3708

A thesis for the degree of
Doctor of Philosophy

June 2023

University of Southampton

Abstract

Faculty of Engineering and Physical Sciences
School of Electronics and Computer Science

Doctor of Philosophy

Investigating and Developing Low-Cost Wearable Respiration Sensors

by Mahdi Mohamed Saleh Abdulla Ahmed Shaban

Respiration is a vital parameter in healthcare monitoring, in which it can be used to identify and help prevent illnesses such as sleep apnoea and sepsis. Small changes in respiration can be linked to deteriorating health, where failing to detect these changes promptly can often result in poorer outcomes for the patient, and in serious cases mortality. In some cases where respiratory rate is $\geq$ 27 BPM, it can be a better indicator for cardiac arrest from up to 72 hours. This brings the importance of continuous respiration monitoring of time greater than 1 hour. The current sensors that are available for use can monitor respiration rate continuously, but not all of them can for long periods of time. An example on the importance of continuous monitoring is sepsis, where continuous monitoring could be used to identify early risk warnings for the medical professionals.

Many sensor technologies showed potential in detecting respiration, but the capaciflector sensor shined due to the low number of research done on it for applications in respiration detection, and due to the ease of use. The sensor is developed into a sensor system that is manufactured and compared to a pneumotachometer and a belt sensor which are both gold standard sensors in respiration monitoring. The data is directly compared using Bland Altman Statistical Analysis, with limits of agreement being $\pm$3 BPM for the difference between the capaciflector and the gold standard sensor. This research aims to identify and develop a low cost wearable respiration sensor that is capable of accurately (within $\pm$ 3 BPM) measuring respiration, as well as continuously monitoring respiration over long periods of time ($\geq$ 1 hour).

Two short studies with 70 participants were conducted to assess the capaciflector as a respiration sensor, where study one was done on stationary participants and the second study on participants riding a bicycle. A new algorithm was developed to process and analyse the data, which resulted in biases and lower limits of agreements of 0.05 ± 0.04 BPM and 0.70 ± 0.20 BPM in the stationary tests respectively. While the biases and agreements are 0.12 ± 0.03 BPM and 3.02 ± 0.13 BPM for the bicycle tests respectively.

A new algorithm was developed and tested in MATLAB based off a short Fourier transform which analysed the signal in the spectral plane. The results from these studies allowed a capaciflector which is PCB based to be developed. The hardware was developed to match the needed specifications and was tested with the same algorithm from the studies. The new hardware contained better and improved methods for reading the capacitance from the capaciflector, while also having more sensors such as a real time clock and an accelerometer. Results from testing the hardware showed potential in utilising the accelerometer data as part of the processing algorithm. The hardware developed is capable of continuously monitoring respiratory rate for periods spanning more than 48 hours on a single CR2032 coin cell battery.

Thus by running a small trial of 10 participants, the new sensor system was tested alongside a newly developed algorithm that can segment stationary data from data that contains movement artefacts. Three studies were conducted, the first study is a metronome study which resulted in a bias of $0.04BPM$ with ± 0.54 BPM for the limits of agreement across all 10 participants. While the second study which is a walking study achieved results of -0.04 BPM for the bias and ± 1.48 BPM for the limits of agreement. This study utilised the new algorithm which allowed the results to be within the required accuracy even while including walking data. And when compared against the initial results found, the algorithm developed proved to be very useful for monitoring respiration rate. Finally the last study is a study that aimed to explore the effects of speaking on respiratory data, in which the study showed that speaking has a unique pattern of being similar to a saw tooth wave which is reflected in the respiratory data.

Overall the capaciflector based sensor system developed proved to be within the required aims as well as satisfying the conditions set, with being compact, comfortable and capable of continuously monitoring respiration rate over long periods of time. And this research demonstrates that it is viable for use towards long term home monitoring or ambulatory care patients.

Contents

List of Figures

List of Tables

Listings

Declaration of Authorship

I declare that this thesis and the work presented in it is my own and has been generated by me as the result of my own original research.

I confirm that:

1. This work was done wholly or mainly while in candidature for a research degree at this University;
2. Where any part of this thesis has previously been submitted for a degree or any other qualification at this University or any other institution, this has been clearly stated;
3. Where I have consulted the published work of others, this is always clearly attributed;
4. Where I have quoted from the work of others, the source is always given. With the exception of such quotations, this thesis is entirely my own work;
5. I have acknowledged all main sources of help;
6. Where the thesis is based on work done by myself jointly with others, I have made clear exactly what was done by others and what I have contributed myself;
7. Parts of this work have been published as: **Published:**Nick Hayward, Mahdi Shaban, James Badger, Isobel Jones, Yang Wei, Daniel Spencer, Stefania Isichei, Martin Knight, James Otto, Gurinder Rayat, Denny Levett, Michael Grocott, Harry Akerman, and Neil White. A capaciflector provides continuous and accurate respiratory rate monitoring for patients at rest and during exercise. *Journal of Clinical Monitoring and Computing*, January 2022. doi: 10.1007/s10877-021-00798-7. URL https://doi.org/10.1007/s10877-021-00798-7
   Unpublished conference paper (Found in Appendix G): Mahdi M S A A Shaban, Daniel C Spencer, and Neil M. White. A new type of respiration sensing system for continuous monitoring. *IEEE Sensors Conference*, 2022
   Submitted for review: Mahdi M S A A Shaban, Daniel C Spencer, Harry Akerman, Isobel Jones, and Neil M. White. A new type of respiration sensing system for continuous monitoring. *IEEE Sensors Journal*, 2023

Signed:.. Date:..................

Acknowledgements

A thank you goes to both my supervisors, Prof. Neil White and Dr Daniel Spencer for their continuous support and guidance throughout my PhD journey. I would like to also thank Dr Harry Akerman who was a streamline of valuable input and insight throughout my research. Special thanks to all my friends who supported me and pushed me to the finish line.

And this work is dedicated to my family : my parents Mohamed Saleh and Amina, my siblings Zianab, Feras, Zain, and Ali and both my grandparents. Thank you for your endless support and encouragement every step of the way. You are all a guiding light towards achieving my dreams.

And lastly, a thank you to all my colleagues who I met throughout this journey, whom inspired me with interesting ideas and pushed me to complete my goals.

Definitions and Abbreviations

ADC	Analog to Digital Converter
BLE	Bluetooth Low Energy
BPM	Breaths Per Minute
CDC	Capacitance to Digital Converter
$CPET$	Cardiopulmonary Exercise Testing
CSV	Comma Separated Values
DFT	Discrete Fourier Transform
ECG	Electrocardiography
FFT	Fast Fourier Transform
IC	Integrated Circuit
IMU	Inertial Measurement Unit
$LI-PO$	Lithium Polymer
MCU	Micro Controller Unit
PCB	Printed Circuit Board
PPG	Photoplethysmogram
RAM	Random Access Memory
RTC	Real Time Clock
$RTOS$	Real Time Operating System
RR	Respiratory Rate
SNR	Signal to Noise Ratio
$TENS$	Transcutaneous electrical nerve stimulation
UWB	Ultra Wide-band radar

Chapter 1

Introduction

Breathing is a vital part of every human's body and is a set of sophisticated processes that help regulate and clean the incoming gases that we breathe. Breathing has many forms and rhythmic movement that links it to other organs movement such as the heart and lungs.

While breathing occurs on a physical level of the human body, respiration occurs at the cellular level; due to the key functionalities of both, they become part of the full breathing cycle in the human body (Negro et al., 2018). The speed of this cycle changes from age to age as a healthy person normally breathes at a standard rate of 12-20 breaths per minute while an infant can breath 25-40 breaths per minute (Yuan et al., 2013). Having slight changes in respiration rate can also be an early indicator of deteriorating health, where respiration rates of $\geq$ 27 BPM can predict cardiac arrest from up to 72 hours (Kelly, 2018).

In hospitals there are multiple methods for detecting respiration, some of the methods are in the form of machines such as a capnograph or by having a nurse manually count the number of times the chest rises and falls over a set period of time. This is typically done in 1 minute intervals at set intervals. This becomes a long and tedious task for nurses that are in charge of this process (Wheatley, 2018). The capnograph is an accurate machine which can continuously monitor the respiration of a patient, this is considered a gold standard machine in respiration detection, due to the accuracy and reliability, as it measures the amount of airflow and pressure coming from the body as well as the amount of carbon dioxide expelled (Donnelly et al., 2013). The only downside is that this method takes time and requires a machine that is not portable or comfortable to wear for long periods of time. This is the reason why they are more common in the ICU in hospitals.

This shows the need for a respiration monitoring system that is able to continuously monitor the changes in breathing over long periods of time, while also being easy

to wear and portable. This type of system should allow the detection of many different types of disorders and conditions that are directly related to respiration, such as obstructive sleep apnoea/hypopnoea (OSAHS), central sleep apnoea (CSA), and hypoventilation syndromes which are all different forms of sleeping disorders (Riha, 2015). With conditions like sepsis, pneumonia, and cardiac arrest, they can all be identified early by looking at a continuous respiration signal (Ginsburg et al., 2018).

In an analysis done by Lynn and Curry (2011) on unexpected hospital deaths, the research shows that the early detection of respiration rate changes in disease such as sepsis, could potentially identify and help prevent early death by having proper monitoring and alarm systems that are set up to identify the appropriate changes. Where one of the main factors that change in a predictable manner is the respiratory rate. Figure 1.1 shows an example of an unexpected hospital death signals, and in that figure respiration rate can be seen to have a steady increase over time in an event such as sepsis.

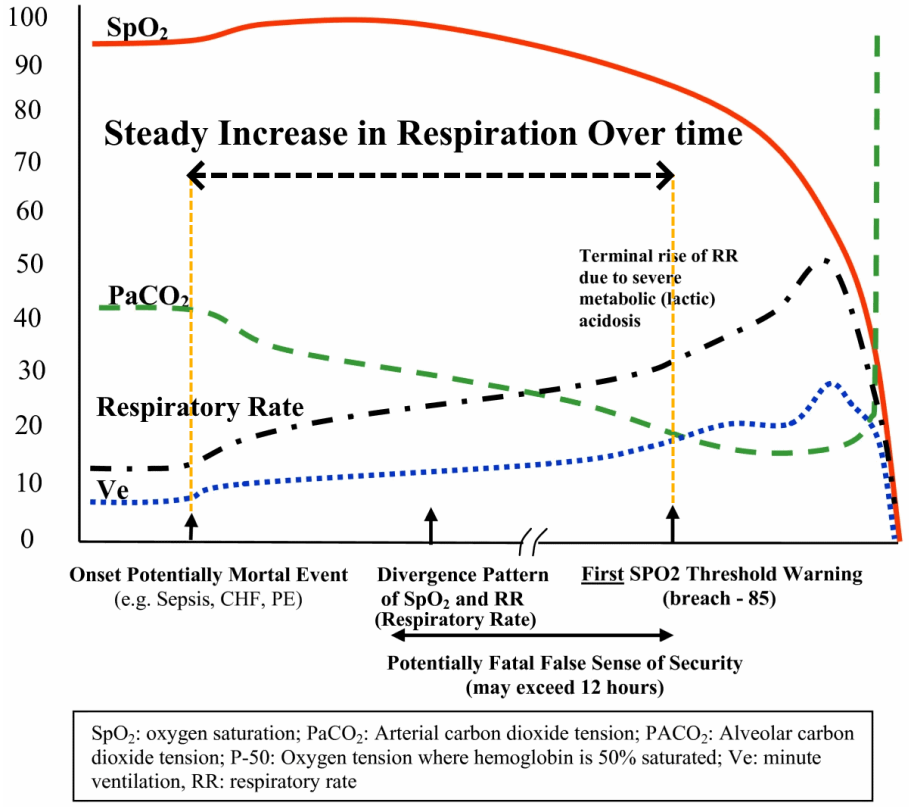

FIGURE 1.1: Pattern in unexpected deaths, where respiration can be linked to possible early detection (Sourced and edited from (Lynn and Curry, 2011))

This need for respiration data is reflected by the many different types of scoring systems that are developed to prevent many of these unexpected deaths. The widely used one in the United Kingdom National Health Service (NHS) is the National Early Warning Score (NEWS) developed the Royal College of Physicians, which was updated recently in 2017 to NEWS2. The main aim of this system is to create a standardised approach

for assessing illness (RCP, 2020). The scoring system uses six physiological parameters that produces a score representing the risk of the patient (RCP, 2020). The NEWS2 score emphasises the need of respiration rate as a primary parameter, as it is important in determining the severity of the patient. And recently there is work done on a new risk score for assessing corona virus patients, which adopts respiration as a primary parameter due to the effects the virus has on the lungs (Knight et al., 2020).

Similarly, the Quick SOFA score that is used for scoring sepsis patients uses respiration as one of the primary parameters for assessing a patients health and their appropriate mortality risk value.

This brings the topic of building such systems that can detect many of these changes in respiration by continuously monitoring the patient and potentially avoiding these deaths. An example is towards Figure 1.1 where continuously monitoring the respiration rate could have given an early warning, while potentially preventing the unexpected death. However, for the system to be effectively used in many environments such as the home and hospital, as well as to be used in low-resource environments, the system must have a low manufacturing cost without having an affect on the accuracy of the sensor/system. In this paper a low-cost sensor system is attributed to be in the range of £100 - £500, which was chosen by the exploration of the average market prices of respiration sensors.

Currently there are sensors that exist in the market to fill the gaps of continuous respiration monitoring while also being relatively cheap (between £500 - £1000), however many of these technologies are not well suited to be easily wearable and portable or more importantly continuous in monitoring respiration rate over long periods of time. Hence this research aims to produce a better sensor system that can fill in the gap in which many sensor technologies could not, while also having the goal of being low cost, continuous and accurate to be deployed in both home and hospital environments.

The sensor technology that has been decided upon to be used to fill this gap is the capaciflector. The sensor is a essentially a distance sensor that measures respiration by correlating the distance between the chest and the sensor to be attributed as breathing data. This capaciflector is evaluated by testing it in a clinical environment with a total of 70 participants. Two studies were undertaken to assess the effectiveness under stationary conditions, while the other study is to assess the effectiveness and accuracy under the movement of the body by the use of a bicycle. The results from this analysis were used to develop a different form of system that can utilise the capaciflector sensor effectively. As well as continuously data logging the breathing data of the subjects.

The developed sensor system is explored by finding the optimal capaciflector sensor design to be used for respiratory monitoring. Thus by testing seven different designs through a series of controlled tests that compare against a belt sensor. Two designs were selected and developed further alongside a new sensor system.

The sensor system was developed aimed to be small in size, as well as having the capability of continuously data logging raw capacitance data for long periods of time. The sensor system is tested against a series of tests targeting power, use case and data integrity in order to assess the new sensor system hardware. The tests resulted in a successful system capable of monitoring respiratory rate at a fixed breathing frequency with up to ± 0.1 BPM. And for the walking tests it resulted in a average respiratory rate difference of -0.24 ± 0.08. Thus assessing the system to be capable of continuously monitoring respiration rate accurately.

Lastly the capaciflector based sensor system was put to the test in a larger study of 10 participants, targeting three different studies: metronome, walking, and speaking. This helped to solidify the results gathered during the hardware development phase. The sensor system developed resulted for the first study to be within ± 0.54 BPM with a positive bias of 0.04 BPM for the metronome data. While study two resulted in higher limits of ± 1.48 BPM with a bias of -0.04 BPM for the walking study. This chapter demonstrated the accuracy of the capaciflector based sensor system as well as the algorithm developed. Thus finalising the development of the sensor system and showing that the capaciflector based systems show promising potential for becoming reliable and low-cost sensing system for respiration monitoring in ambulatory or home care patients.

1.1 Published and Peer Reviewed Chapters

1. The work done in Chapter 3 is published under the Journal of Clinical Monitoring and Computing. My contribution in this paper is performing all the analysis of the data collected from the studies by using different signal processing techniques. **Nick Hayward, Mahdi Shaban, James Badger, Isobel Jones, Yang Wei, Daniel Spencer, Stefania Isichei, Martin Knight, James Otto, Gurinder Rayat, Denny Levett, Michael Grocott, Harry Akerman, and Neil White. A capaciflector provides continuous and accurate respiratory rate monitoring for patients at rest and during exercise.** ***Journal of Clinical Monitoring and Computing*****, January 2022. doi: 10.1007/s10877-021-00798-7. URL** https://doi.org/10.1007/s10877-021-00798-7.

2. The work done in Chapter 5 was peer reviewed for the IEEE Sensors Conference 2022. The conference was not attended due to visa issues. The document can be seen in Appendix G. **Mahdi M S A A Shaban, Daniel C Spencer, and Neil M. White. A new type of respiration sensing system for continuous monitoring.** ***IEEE Sensors Conference*****, 2022.**

3. The work done in Chapter 6 is under review in the IEEE Sensors Journal. The initial work submitted to the conference is expanded upon and flushed out into a

full journal article. **Mahdi M S A A Shaban, Daniel C Spencer, Harry Akerman, Isobel Jones, and Neil M. White. A new type of respiration sensing system for continuous monitoring.** ***IEEE Sensors Journal*****, 2023**.

1.2 List of Contribution

Chapter 3 and 4: This chapter contributed in expanding the knowledge of the capaciflector as sensor for respiration monitoring. This mainly applies towards assessing the limitations and possible hybrids of the capaciflector sensor, as well as examples of some of the methods. In Chapter 3 new processing methods were explored for respiration rate monitoring, which provides a higher accuracy result that is within the error of a commercial device.

Chapter 5: This chapter contributes toward the development and implementation of the sensor system which is comfortable to wear and small in size. The system shows the capability of the capaciflector in which the sensor system's size is mainly attributed to the minimum size of the capaciflector sensor.

Chapter 6: This chapter mainly contributes towards the development of a new and improved technique of noise reduction in the calculation of respiration rate. The technique is improved upon Chapter 3's processing method, which adds the capability of reducing the noise of the captured signal by the use of the accelerometer data. This chapter also tested the algorithm on a series of participants to assess the accuracy of the algorithm and the sensor system as a whole.

Chapter 2

Respiration Background and Theory

There are many different sensor technologies that are capable of measuring respiration rate accurately. It is important for the sensor to be able to accurately capture the slightest changes while breathing. With that in mind different sensor technologies are identified with their advantages and disadvantages including cost, portability, wearability and reliability when compared against each other. These methods can range from standard manual count, to different forms of sensor technology such as: Doppler-radar, piezo electric/resistive sensors, and flow sensors.

2.1 What is a Breath?

To understand what exactly is being measured, an exact definition of what a breath is must be outlined. In simple medical terms a breath can be expressed as the expansion and contraction of the lungs in the body to clean the incoming gases by the process of inhaling and exhaling. On the other hand for sensors, the movement needed to describe a breath is primarily the movement from the lungs which in turn exhibit movement in the rib cage that is correlated to the breath data collected from the sensors. Some sensors differ as they correlate the amount of air inhaled/exhaled to the equivalence of a breath. And even though many sensors rely on different types of technologies to correlate the breath to the signal measured, this general classification helps standardise the types and methods of measuring respiration in this research.

As the breath is collected there are different approaches to measure breathing information from a signal. In this classification the breath is normalised as the full cycle of inhale and exhale, which in turn means the full positive peak and the negative peak in the signal. And by calculating how many full cycles are in a minute, respiratory rate

(RR) can be calculated and has a unit of breaths per minute (BPM). Figure 2.1 demonstrates an example respiratory signal which indicates the main breathing cycle as well as the depth, negative peaks, positive peaks, inhale, exhale and the length of the breath.

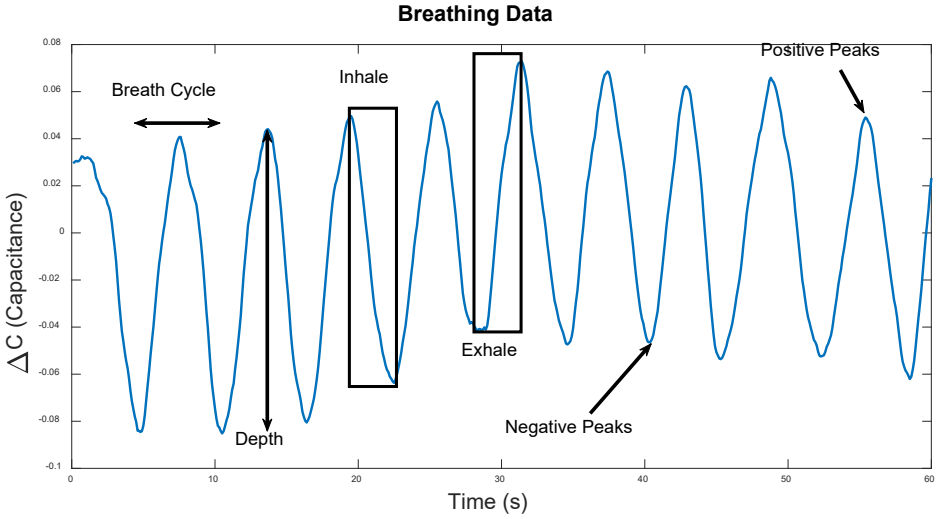

FIGURE 2.1: An example respiratory signal sampled with a capaciflector, highlights the main points that identify a breath within a respiratory signal.

To identify what a good breathing signal is, an adequate parameter must be built to accommodate the comparison between the different sensor technologies. For an accurate sensor the limits of agreement is $\pm$ 3 Breaths Per Minute (BPM) is selected as a standard in accordance with the medical limits for accuracy (Kelly, 2018). This is also what the FDA requires for a sensor to be approved (Chan et al. (2022)). This value is not with respect to time (i.e. the change in breaths per minute over a period of time), but the limits of agreements used for measuring short signals between 5-10 minutes, is going to be used for the longer signals (above 1 hour) extracted from the sensors.

2.2 Fast Fourier Transform (FFT)

The Fourier Transform is a mathematical technique that is widely used in many applications such as communications, signal processing, analysing linear time invariant signals, and spectral analysis (Brigham, 1988; Oshana, 2006; Cooley et al., 1969). The Fourier transform is generally expressed as the integral seen in equation 2.1 .The main problem with solving the Fourier transform mathematically is that the required processing time is extremely long due to the large number of operations needed to finish the computation (expressed as N^2 operations for N data points) (Cooley et al., 1969). And to process signals on a computer or a micro controller the signal must be discrete and continuous, in which a discrete Fourier transform (DFT) is used (Oshana, 2006). The discrete Fourier transform does not differ from the Fourier transform as it still needs N^2 operations to complete, where the DFT can be expressed to be the continuous

Fourier transform. The DFT can be expressed mathematically as seen in equation 2.2, where N is the number of points and y_i is the actual data (Fischer-Cripps, 2002).

$$F(\omega) = \int_{-\infty}^{\infty} f(t)e^{-j\omega t}dt \tag{2.1}$$

$$F(\omega) = \sum_{i=0}^{N-1} y_i(i\Delta t)e^{-j\omega(i\Delta t)}\Delta t \tag{2.2}$$

This brings up the fast Fourier transform (FFT) which is the faster form of the discrete Fourier transform. The way the FFT works is by separating the problem from a big problem into multiple small problems, this allows for a much faster processing of the data, which makes it more practical to use (Cooley et al., 1969). The FFT reduces the operations from being N^2 operations to being $Nlog_2N$, which is significantly faster.

The use cases in detecting respiration rate using FFT is important as it allows the signal to be analysed in the frequency domain. This allows the respiration data to be analysed, and to identify the strongest frequency throughout the sample. This technique is used throughout many research done for detecting respiration due to the simplicity of the method and the accuracy in identifying the frequency present in the signal. This technique however is very basic and can only provide information over a portion of the respiration signal, which is not useful in identifying changes in the frequency. The signal can further be segmented into equally spaced segments where the FFT can then be run on each segment to identify the dominant frequencies over time. Thus creating a spectorgram image which provides information that is much more valuable than a simple FFT.

2.3 Bland Altman Statistical Analysis

The Bland Altman analysis method is a simple method that is widely used in the medical field to compare two different methods of measurement. The method uses a graphical analysis approach to quickly convey the information to the reader (Giavarina, 2015). The way the analysis is done, is by first calculating the difference between the two data sets, this difference is then processed to get the mean difference (Bias), and the standard deviation. Where the bias is the average value above or below the zero line that shifts the limits of agreement accordingly; while the limits of agreement are the 95% confidence interval values of the two data sets. To calculate both the upper and lower limits of agreement equation (2.3) and equation (2.4) are used.

$$\textit{Upper Limit Of Agreement} = \textit{Bias} + 1.96 \times (\textit{Standard Deviation}) \tag{2.3}$$

$$Lower\ Limit\ Of\ Agreement = Bias - 1.96 \times (Standard\ Deviation) \tag{2.4}$$

An example figure can be seen in Figure 2.2 which shows 2 different example plots that compare between two data sets that are varied in each case. The plot clearly conveys the difference between the two signals, as well as quickly identifying the limits of agreement which are represented by the dotted lines. The main advantage to using this method is that patterns can be easily identified in large data sets, where Figure 2.2a would be considered a normal data set with a slight regression while the other case represents a scenario with a constant difference between all point while slowly increasing, which is seen with the increasing mean (Figure 2.2b). And in the case of respiration data that is over 10 minutes long, this makes it easier to understand and compare between the data sets. Different Bland Altman Patterns can be observed however, in the context of this research these two examples are sufficient in understanding the plots.

(A) Case A: Random Variability between Method A and B

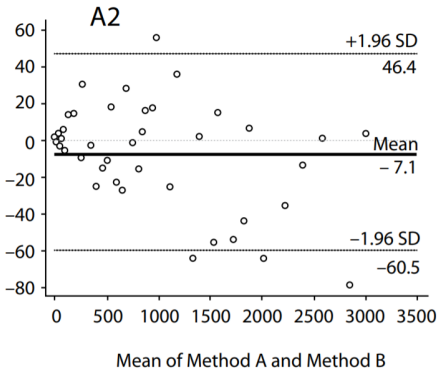

(B) Case B: Constant Variability between Method A and B (Constant Difference across all points)

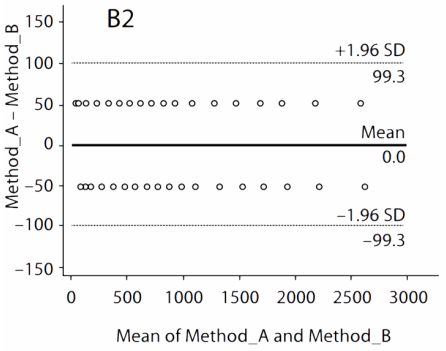

FIGURE 2.2: Shows two different examples of different forms of data displayed in a Bland Altman plot. Both cases represented use the difference as units. Plots are from Giavarina (2015)

2.4 Pneumotachometer and Cardiopulmonary Exercise Testing

Cardiopulmonary Exercise Testing (CPET) is a test that is used to assess the heart and lungs conditions during exercise, this test is generally done before a major surgery. The test uses full body sensors including electrocardiogram (ECG) for the heart and a pneumotachometer for the lung air and respiration measurements. The way the pneumotachometer works is by applying the main airflow with pressurised air of known pressure, and as the patient breathes, there is a slight drop in pressure which is then correlated to the volume of air inhaled/exhaled (Engineering, 2018). This method allows for measurements such as oxygen uptake and carbon dioxide production, both which are useful for medical professionals (Albouaini et al., 2007).

The pneumotachometer can be attributed to be one of the gold standards of respiration measurement. Where gold standard is identified as one of the best in the field. This is due to the data retrieved from the tests to be highly accurate within ± 1 BPM. Hence the use and comparison of pneumotachometer data to any of the used sensors, is highly valuable as data retrieved from the test can validate or exclude certain sensor outputs.

2.5 Doppler-Radar Sensors

Ultra Wide-band radar (UWB) or known as Doppler-Radar is a highly researched type of sensor technology that aims to eliminate the main disadvantage of existing sensors in the market; which is the method of testing (currently direct connections/interfacing with the body) (Chung et al., 2016). This type of sensor technology aims to remove the interface between the sensor and the human by using radar waves that are directed at the patients chest to measure the changes in the chest deflection. Currently only a few commercial companies which manufactures this type of sensor provide them in the form of development boards, one of them is XeThru by Novelda, which had previous runs with this technology.

More studies are being published using this technology in the past few years, and one of the most notable one's, is the study done by Yang et al. (2020) where a hybrid between a camera and an ultra wide band radar are used together to properly assess distance and changes in respiration. A test on a stationary person was conducted with three different distances, where the algorithm and system developed achieved a max error of 0.79 BPM and a standard deviation of 0.71 BPM. This is one of the better results, where movement causes the largest amount of error. Hence the need of classification of movement error is crucial in any ultra Wide-Band radar system.

This is important, as in a study by Kim et al. (2019), which used the same sensor to build a respiration monitor for newborn babies. The study used a pneumography mask to acquire the reference respiration rate. A good movement detection algorithm was put in place, where movement was classified into three levels (low, intermediate and high). The results however were not as good, where the results are analysed using the Bland Altman analysis. The results are split into three sets of results based on the movement classification. The low movement level resulted in a Bland Altman plot with a bias of -0.17 BPM and large limit of agreement (LOA) of -9.6 to 10.0. As for the intermediate and high movement classification, the accuracy is much lower than the low level movement making it unusable. Nonetheless, this method if applied successfully in software can be a more viable solution for newborns and infants which are more sensitive to patch based respiration sensors.

Even though this type of sensor technology is still under research, the applications for this sensor in real world scenarios is yet to be practical. This is mainly due to the extreme amount of precision the radar wave must achieve to measure the deflection with minimal amount of noise, hence adding the need for the sensor to be targeted accurately at the patients chest. This was demonstrated by XeThru in their initial product which was discontinued due to the impracticality of it. Its successor is now a patch based antenna using the same Ultra Wide-band Radar however with a different approach of using the device as close as possible to the chest of the person using it (Novelda, 2021).

2.6 Belt Respiration Sensor

Belt sensors are commonly seen as one of the easiest types of sensor technology to be used, as they mainly utilise force sensors to measure the expansion of the chest which is correlated as respiration. This sensor technology already excels and is well used in the medical field and in research due to its low cost in both setup and manufacturing, and for its precision. The disadvantage for this type of sensor technology is mainly the comfort of the user; this is due to the design of the belt sensor, where the belt must be tightly wrapped around the chest and or abdomen area in order to function properly and get good results. This makes the sensor comfortableness subjective to the person being used on, especially for long periods of time. (Chu et al., 2019)

There are companies both medical and non-medical that provide this sensor as a product. And many of them provide the raw data output from the sensor to easily be used in custom algorithms for detecting respiration rate. In this case the sensor used is the Go Direct^{TM} Respiration Belt (Vernier, 2020) which provides both the raw and processed data, which can be accessed through Bluetooth or through a direct connection with a computer.

This sensor choice is primarily because it lies within the low cost range specified earlier, while also being accurate enough to be compared against hospital grade equipment. Another reason for using this sensor is also because of its certification, making it easier to apply for ethical approval for when testing needs to be done on participants.

2.7 Accelerometers as Respiration Sensors

Accelerometers are widely used sensors that can be used in many different fields, and the way they work is by measuring the forces applied to them which also means gravitational forces. As for the usage in respiration sensing, the sensor is used to measure the small amount of changes in either the chest or the abdomen region. This type of

sensor technology is much more easier to integrate as its already a part of many devices especially phones and tablets. However, the nature of the sensor and the method of extraction makes it extremely unreliable in any other case from laying down or sitting in a still position (Fekr et al., 2014). Nonetheless, the sensor technology is good in the right conditions, making it a good candidate to be used as a low cost sensor, that is easily portable however lacks the flexibility to be used in many other conditions.

One of the other major use cases for an accelerometer is to measure steps and movement, which is a feature commonly found on modern smart phones. This will be useful in assessing respiration while walking or running, to allow the identification of movement and correlating them to the respiration data (i.e sitting and lying). Accelerometers also can be accompanied by other sets of sensors such as a gyroscope and a magnetometer, which are useful in identifying device positioning on the body. But if only movement frequency and identification of the type of movement is needed an accelerometer is enough. Modern accelerometer IC's are also very efficient and don't require much current to run continuously making them very well suited for this type of work.

2.8 Piezoelectric and Piezoresistive Sensors in Respiration Sensing

There are two main types of sensors that are named base on the fundamental effect that occurs on the material; the piezoelectric effect and the piezoresistive effect.

Piezoelectric sensors work by converting the changes in stress to electrical voltage, this is a physical phenomenon that happens in both directions. Which means applying voltage to the material causes stresses on the surface of the material (Pohanka, 2018). The way this is used to detect respiration is by converting slight changes in the stress to voltage that is then converted to signal information. One prominent example is the Respirasense in collaboration with the NHS. The sensor used by Respirasense uses the piezoelectric effect to measure the changes between each breath (Pmd-solutions, 2020). This is done by applying the sensor specifically to the lower abdomen region in order to correlate the movement of the body to the piezo sensor. The sensor boasts an accuracy of $\pm$ 2 Breaths Per Minute (BPM) and a range of detection of 6-60 Breaths Per Minute.

A study on the Respirasense was conducted to compare the device against the industry gold standard, the capnography test; where it was tested with 17 patients for two hours against the capnography with manual counts every 15 minutes. The test measured stationary data in the first hour and movement data in the second. The results from the capnography where compared using a Bland Altman Plot which resulted in a bias of 0.38 BPM with limits of agreement of $\pm$2.17 BPM during the first hour at rest. While the manual count for the first hour resulted in a bias of $-$0.7 BPM and limits of agreement

of ± 4.2 BPM. Lastly for the second hour the results that included movement showed a great change in the results, with a bias of -1.72 BPM and limits of agreement of ± 5.08 BPM.(Subbe and Kinsella, 2018). The results from these tests show that the device is accurate for stationary movement while being inaccurate during any movement event.

The second type is the piezoresistive sensor which relies on the resistive changes of the material that are related to the stresses applied on the surface. This type of sensor is most commonly known as a strain gauge sensor. This sensor can be used similar to the piezoelectric sensor to measure the changes in respiration by measuring the changes in stress on the surface of the skin, however the main difference will be the electronics used to gather the information as well as the materials used to manufacture this sensor. (Arja et al., 2019)

These sensors are extremely accurate, well developed, and are available in many different forms. However as respiration requires special methods of collection, the sensors must be manufactured in different materials and shapes, causing them to be potentially expensive when used as a disposable solution. This is a key point in Respirasense which uses a single use sensor that is disposable after use, making it a potential source of cost. Currently this device is not available for commercial purchase and hence cost is a factor that is currently unknown.

2.9 ECG Sensor in Healthcare and Respiratory Monitoring

Electrocardiography sensors (ECG) are the most versatile and widely used sensors in hospital environments to asses a patient health. They work by monitoring the heart activity through surface contact with the patient's skin, and by reading the electrical signals from the sensor (Rashkovska et al., 2020).

However this signal does not just include heart information, but also more information about the patient's respiration rate. Research done by Charlton et al. (2016) shows the possibilities in extracting respiration information from ECG signals using a software approach which means minimal hardware integration on already existing devices in hospitals. The research done was performed on a single simulated ECG electrode, with 44 algorithms tested to run with ECG sensors. The way the data was extracted is through a 3 step process to filter out unneeded signal information. A high pass filter is first applied to remove low frequencies (as low as 4 Breaths per minutes), followed by a feature extraction filter to extract the respiration data, and finally a band pass filter to retrieve information only within human breathing range. The final results from the best algorithm yielded results of ± 4.7 BPM with a bias of 0.

Considering that the algorithms described by Charlton et al. (2016) only achieved that accuracy using a single ECG electrode; there can still be improvement done in terms

of refining the algorithms, as a standard ECG system can have up to 12 electrodes connected to a patient at one time. Overall the ECG data can be said to have a direct link to respiration rate, hence opening up possibilities for other sensor technologies to link other vitals as well.

2.10 PPG Sensors as Respiration Sensors

Photoplethysmogram sensors (PPG) are a widely used sensor type in both medical and consumer level products, these range from professional medical monitoring devices to smartwatches and fit bands that monitor vitals such as heart rate, respiration and other activities in the human body (Mouradian et al., 2014). The sensor works by using an optical method to find small changes in the blood volume (Mouradian et al., 2014), thus by using this information, many other activities can be correlated to this data.

PPG sensors are a great low cost, non invasive solution to respiration detection, however the way the sensor works, there is little to be done to improve upon, as there is already a large amount of papers that research this technology, including the fusion of other vital signals such as ECG signals (He et al., 2017). The current research does not improve much upon the hardware, but is mainly focused on the processing on the software side.

A paper by Ravichandran et al. (2019) where the sensor algorithm was optimised using a deep learning model to better extract the respiration data from the PPG data. The main reason for this is due to the PPG raw data containing multiple vital information that could make it hard to extract the respiration signal. Another study by Chang et al. (2018) focuses on extracting respiration rate by using Holo-Hilbert Spectrum. The study was able to get a good low cost device which still needs a heavy amount of processing to get the respiration rate, for both the PPG signal and the extracted respiration signal. Nonetheless the results of the tests against a transthoracic impedance plethysmography resulted in a difference of 0.04 ± 0.96 BPM for patients at rest. While the second set of test were under a metronome value resulted in a difference of 0.01 ± 0.70 BPM.

2.11 Image Processing

Image processing can be an extremely versatile method of measuring respiration, as the main sensor used is only a camera, which is commonly available everywhere. The difficulty in using a camera as a sensor is the amount of post processing that is required to produce good and fast results. The way most of the image processing algorithms work

is by analysing the difference between the different frames from the camera, which differs with the frequency of capture (30 - 60 Hz for webcams). Therefore, most of the algorithms that are written to monitor respiration require heavy processing and computation power to run effectively.

A paper by Massaroni et al. (2018) shows a viable algorithm solution for detecting respiration rate using a standard web camera, most commonly found in laptops and computers. The method focuses on extracting the data from "intensity variations of reflected light at the level of the collar bones and above the sternum"(Massaroni et al., 2018) by using a standard 720 pixel webcam. This algorithm hence make it easier to allow for direct measurement of respiration over video calls. The algorithm was tested on multiple different types of webcams with the best results of $\pm$ 2 BPM.

A commercial company Xim developed similar technology called lifelight that utilises image processing to take fast reading of many vitals over a laptop camera. A video demonstrated on their website shows a quick demonstration of the speed in which metrics such as respiration can be gathered in 40 seconds (Xim, 2020). No metrics are available on the accuracy of such algorithm, however the existence of such algorithm commercially makes using image processing a viable solution in use for home an ambulatory patient care.

And recently google released their google fit update which is now capable of measuring vitals through the camera on the phone (Google, 2021). This includes respiration detection, by the use of the front camera. There is currently no analytical data towards the accuracy of the application but, this shows clear advancements in image processing as a potential respiration sensor in less intensive care environments both at home or at the hospital.

The only downside of using this technique is that when collecting the data the patient must be stationary towards the camera, which means its not viable towards continuous respiration monitoring. Nonetheless, using a camera with a good processing algorithm proves to produce good results for short term data collection/monitoring.

2.12 Flow Sensor

Flow sensors are the sensors that are commonly used in hospitals to directly measure the output flow of CO2 and inflow of oxygen (Sensirion, 2021). The way the sensor works makes it extremely accurate in detecting small changes in breaths as well as other vital information about the lungs. However, this sensor must be enclosed around the nose and mouth to function properly, in order to create a proper seal for the sensor

(Sensirion, 2021). Not all forms of the flow sensor need this to function. But nonetheless, this causes the sensor to be less portable and more uncomfortable for monitoring over long periods of time.

There has been many research papers that explored portable versions of it, but due to the method of construction the sensor has; the cost of manufacturing may contribute to the final cost. Research by Jiang et al. (2019) shows this in more detail, where a flow sensor is constructed to be attached underneath the nostrils in order to measure the changes in heat and airflow around the nose. This type of sensor is less invasive than hospital masks, and because it is a resistive sensor, its easy to read the output from any micro controller.

Another research undertaken by Dinh et al. (2020) to construct a new flow sensor, shows better results when testing the sensor. The sensor is designed to be flexible and worn underneath the nose and above the mouth. From the tests done for this sensor, the results show a very good response towards being a good portable solution. Where standard breathing tests as well as blowing tests were conducted with the respiration accurately getting picked up. The only downside with this type of sensor and the one designed by Jiang et al. (2019), is that external interference's from movement can be a big factor towards a more portable solution.

The main use case for this sensor is the capnography test which monitors the changes in carbon dioxide continuously (Kerslake and Kelly, 2017). This is mainly found in intensive care or for monitoring patients during anaesthesia. The capnography test is considered to be the gold standard in monitoring respiratory changes, and is much better than a pneumotachometer. Access to a capnography machine is generally extremely limited and too costly so the more realistic alternative is the pneumotachometer. Nonetheless, having data to compare against a capnograph is the best way to assess a sensor.

2.13 Capaciflector Distance Sensor as a Respiration Sensor

The capaciflector sensor is investigated by White et al. (2017) at the University of Southampton to be capable of monitoring respiration rate, this is the first study that is published to explore the capaciflector as a respiration sensor. The sensor uses technology researched by Vranish (1991) from NASA. The capaciflector is a 3-electrode proximity-based capacitance sensor, that works by measuring the variation in capacitance between the sensor electrode and ground. The sensor plat projects a field out and is done by exciting the plate and ensuring sure that there is no potential difference between the reflector and sensor plate. This creates a return path for the field. And as an object enters the field the field is disrupted causing the new object material to affect the

capacitance of the sensor. This field effect is demonstrated in Figure 2.3 more clearly alongside the model of the sensor.

(A) Shows the capaciflector side view against skin. Red field lines indicate the field effect from the reflector while the blue lines are from the sensor plate.

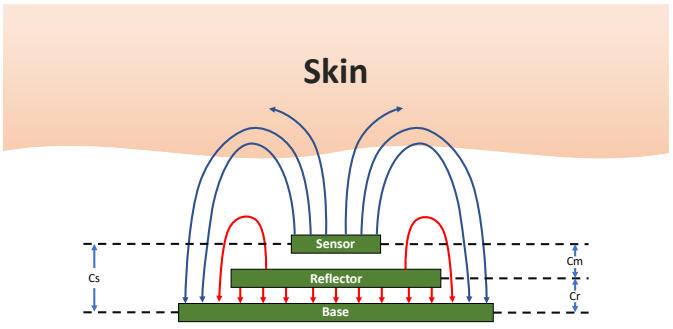

(B) Shows the model of the capaciflector circuit with how the layers connect (Note: Cm should be 0 pF in theory).

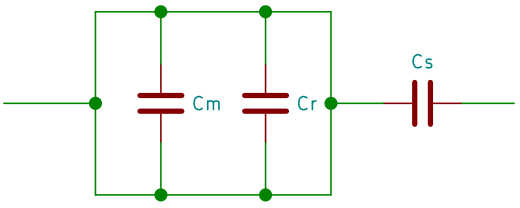

FIGURE 2.3: Shows the capaciflector sensor layers and the circuit for the sensor model.

To be used as a respiration sensor the capaciflector is scaled down, and the breathing signal is correlated to the change of the skin thickness due to chest expansion and contraction during a respiration cycle, which causes the capacitance to change. The paper shows that the capaciflector is viable to be used as a respiration sensor, however there are still many parts of the sensors that can be improved upon. The capaciflector construction consists of three main parts, which is the base, the reflector, and the sensor plate; the materials for constructing the sensor can be any type of metal separated by an insulator between each layer as seen in Figure 2.3. This type of construction allows the sensor to be thin and portable while also lowering the cost significantly compared to other types of sensors. For example the capaciflector could be directly integrated into a printed circuit board (PCB) allowing the device to be thinner and much more cost efficient. Some of the other benefits includes the unnecessary need to be placed on the skin to work, while also not requiring much electronics to gather the data, as the only metric that needs to be read is the capacitance.

2.14 Hardware: Sensor Comparison

Table 2.1 shows the sensor comparison that was done to highlight the existing gap in the hardware side of the sensor. As can be seen most of the sensors either have one or two disadvantages, while the capaciflector shows dominance over the other types of sensors with much more potential to be developed and researched.

Sensor Type/Technology	[1]Non-Invasive	[2]Low Cost	[3]Portable	[4]Accurate	[5]Wearable
PPG Sensor	✓	×	✓	✓	×
ECG Sensor	×	×	×	✓	×
Piezo Electric Sensor	×	×	✓	✓	×
Belt Sensor	✓	✓	✓	✓	×
Flow Sensor	×	×	×	✓	×
Doppler-Radar	✓	×	×	×	N/A
Accelerometer	✓	✓	✓	×	✓
Image Processing Sensors	✓	✓	×	✓	N/A
Capaciflector Sensor	✓	✓	✓	✓	✓

TABLE 2.1: Comparison table for different commercial and non-commercial respiration sensor technologies.

2.15 Software

Most of the sensors that have been investigated use standard algorithms to measure the respiration rate, mainly peak detection. Peak detection is done by analysing the highest points of a signal and classifying the peaks through a threshold that is set either manually or automatically. And as the information retrieved from peak detection algorithms are based only on the highest point in a breath cycle, it can cause many issues in the analysis as sometimes the peaks identified don't necessarily correlate to a breath from the signal.

There are many research papers that prioritise the signal processing part, however the focus of the processing is not for a general solution but only a part of the bigger problem. An example would be on sleep apnoea which is a disorder that is caused by the "partial blockage of the upper airway during sleep" (Selvaraj and Narasimhan, 2013); this disorder requires specific algorithms and detection sequences to accurately detect when an apnoea event is happening.

Thus peak detection algorithms are only just part of the beginning, where building an algorithm that can adapt and overcome many of the difficulties in measuring respiration is a goal yet to be accomplished. This is because respiration data contains so much

[1]Does the sensor require skin contact to function?
[2]Does the cost of the sensor and the electronics range between £100 - £500?
[3]Is the sensor easy to use in while moving at home, or at the hospital?
[4]Is the sensor accurate to within $\pm$ 3 BPM over a period of time ($\geq$ 60 minutes)?
[5]Is the sensor comfortable to wear for long periods of time?

information that can be retrieved and used by the medical professionals. But due to the drastic change that can happen to the signal in minutes, it poses a challenge as on how to classify and differentiate between the different forms of the signal. This could also include noise that is generated from external sources such as walking, running or even talking. A comparison to existing software developments is in the ECG sensors, where the algorithms have reached the maturity stage and rarely gets advancements in their field.

An alternative in which respiration can be detected is by using an FFT, more specifically a segmented FFT where the respiration data is segmented and then analysed on the spectral plane to get the frequencies present per segment. Thus by building up the data from multiple segments of this data a spectrogram can be constructed to inspect the changes in frequencies. So through the proper post processing and filtration of the data, respiration could be detected over time. This can be expanded upon by introducing different forms of segmentation where rather than a standard rectangular window, different windows could be tested to explore the effectiveness. Some of the most common windows used in spectrogram analysis are the Kaiser and Hann Window.

2.16 Opportunity in Respiration Sensors Technology

The current opportunity that exists within the respiration sensors technology can be seen in the capaciflector. This is because there is little work done in the region of developing the sensor itself into a respiration sensor, with only one short paper that describes the use case of the sensor as a respiration sensor (White et al., 2017). From the paper itself the sensor could potentially be developed as a much better respiration sensor which is very low cost to manufacture, while also being accurate to compete with the many existing sensor technologies.

The main challenges in detecting and converting respiration data from the sensor into user readable data, is that the software side mainly uses very basic processing methods (Lynn and Curry, 2011). The very basic methods of peak detection are used readily throughout the commercial and researched sensors, in which they have a major setback in terms of accuracy. A solution could potentially be fusing different sensors, as well as different algorithms to detect respiration rate accurately and reliably.

Another opportunity that also exists within the respiration sensors technology is ”Home Monitoring”, where the sensor systems that are designed and researched are mainly tested to be used in an ideal environment, and do not account for home use cases. The home monitoring can be a very ideal entry point for the capaciflector due to the low cost barrier as well as the perceived accuracy from basic results, hence making it much more viable for this challenge. The challenge that comes from home monitoring can be

the unpredictable use cases the sensor system has to go through. Which includes movement artefacts. The secondary challenge in home monitoring is how the data could be presented to the medical professionals, which is important when the data must be then interpreted into some useful information.

Chapter 3

Analysis of the Capaciflector in a Clinical Environment

Research was conducted to test the capaciflector in a clinical environment and on patients while exercising and while at rest. The aim of this analysis is to evaluate the potential of the capaciflector and measure its effectiveness. The analysis is split into two studies that evaluate each data set separately; the first study is done on patients at rest for a period of 10 minutes using a chest-belt sensor (Go Direct^{TM} Respiration Belt (Vernier, 2020)), while the second study is done on real patients that are performing a Cardio Pulmonary Exercise Test (CPET). The first study was conducted by Isobel Jones who is a medical student studying at the University of Southampton, while study 2 was conducted by Nick Hayward, a former anaesthetist and an academic clinician at the University Hospital Southampton. Both studies contained 4 capaciflectors at different locations on the chest as seen in Figure 3.1. The analysis was done using a post processing script that was specifically developed for this research, which used the short Fourier transform (FFT) method to evaluate the respiration rate.

3.1 Methodology and Post Processing Techniques

The capaciflectors used in both these studies were screen printed devices used in a previous study by White et al. (2017) to demonstrate the effectiveness of the capaciflector. They were wrapped in polythene, for cleanliness and interchanged between subjects. The polythene was replaced for each test and this method was used in both studies.

The studies used a shared hardware and software platform. The capaciflectors used a relaxation oscillator circuit to convert the change in capacitance to the change in frequency (The circuit diagram can be seen in Appendix A). To capture the frequency

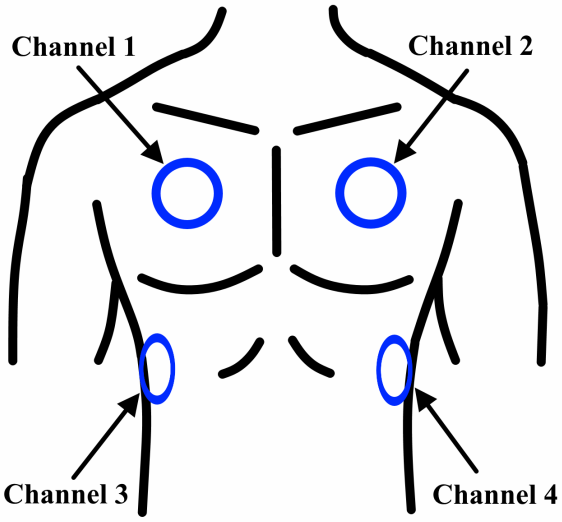

FIGURE 3.1: Capaciflector Placement in both Study one and Study two

change, a data acquisition device (DAQ) from National Instruments (USB-6003 (National Instruments, 2020)) is used. The DAQ's analogue to digital converter sampling at 25 kilo samples per second (ksps) is used to convert the relaxation oscillator analogue output frequency into digital time series data. The speed of sampling is determined by the number of active channels, with a minimum of 6.25 ksps with 4 active channels and a maximum of 25 with one. The device and relaxation oscillator were powered through a laptop USB connection (running at 5V and 10mA) and kept tethered throughout the entire sampling duration. The raw data is converted into a time series data set by the use of a custom written LabVIEW (2018) application which samples the data from all 4 channels at a rate of 10Hz and writes it into a text file to be processed later in MATLAB (2019) version r2019b. The output range for the relaxation oscillator was 3.1kHz with a fluctuation of $\pm$25% of the base value.

For the first study the Go Direct respiration Belt (Vernier, 2020) data was used as the comparison between the capaciflector data. The belt is mounted on the chest and is sampling the raw force output in Newtons from the chest expansion at 10Hz. This data is converted to a comma separated values (CSV) file which was processed using MATLAB (2019). The testing was conducted with 20 healthy participants that performed three different exercises: sitting, controlled metronome breathing, and laying tests. This total number of tests was 60, with each test comprising 4 channels. The method of testing is done by tasking the participant to breath on a predefined metronome frequency between 6 and 12 BPM, the belt and capaciflector data was synchronised by having

the participant take two deep breaths at the start before matching the metronome frequency. The metronome test is a test which tasks the participants to breath (inhale/exhale) a full breath on every metronome click, which results in a periodic, sinusoidal looking breathing signal. This study aims to collect capaciflector signals that are under a stationary condition hence providing much cleaner data.

For study two, the CPET tests were performed on 50 patients with the data from the pneumotachometer as the data that is compared to the capaciflector data. The data did not come in a raw time series format but came in a format where the registered peaks and their timings are recorded. A peak is registered as a spike in airflow recorded to the nearest second. The data is then converted to the sum of breaths in a given minute by summing the total number of peaks in that minute. The resultant data is then comparable to the capaciflector data but with a reduced resolution of $\pm 1 BPM$ due to the format it's in. This test is a test that targets the body movement changes effect on the capaciflector signal.

The data processing introduced a new and unique method of detecting respiration, by analysing the signal in the frequency time domain. A short-time Fourier transform (FFT) is applied with an overlap of 90% and a window of size 60 seconds to convert the data into the frequency time domain with a resolution of 6 seconds per point. Before applying the FFT, the raw data is filtered appropriately to ensure movement artefacts and noise are removed. The data is first filtered using a high pass filter with a 0.02Hz cut off frequency to remove the DC offset present in the raw signal and to remove low frequency noises and to remove any breathing signal below 1.2 Breaths Per Minute (BPM). Secondly a low pass filter with a 1 Hz cutoff frequency is used to remove any high frequency signals that may be present due to movement artefacts or passive noise. This is then put into the FFT and the results are averaged per minute to give the final results in breaths per minute (BPM). The new method allows a higher resolution tracing of changes in respiration rate, which can be useful in identifying more information about the signal including the presence of motion artefact.

Other filtering methods were tested in order to find the optimal filter and parameters used in the pre-filtering stage. The process started by testing selective filters including Butterworth and Chebyshev type one and two. The choice for these filters were strong filters that had a steep, flat, or sharp roll off at the pass band stage, in which the Butterworth and Chebyshev filters performed very well when tuned appropriately. Each filter was manually tuned and adjusted to fit the data which was not ideal, thus the choice of using the low pass filter with a high cutoff frequency was selected as it had the least impact on the signal. The issue that came up with using singular values for each filter for the entire data-set caused data loss to occur throughout the signal. This is mainly due to the effect on the different parts of the signal which vary in frequency, where the filter cutoff frequency causes the signal to be dampened. In order to use these

filters effectively, they will need to be adaptive filters that change with the frequency of the noise.

As for the FFT, the window overlap percentage was the most influential parameter in this as it concluded how much of the data is seen in each block, where the higher the value the higher the resolution, but the lower the processing speed. Therefore the 90 percent selected, captured all of the important data while also being fast enough to go through the entire data. The window size chosen is the minimum number of seconds to accurately read respiration rate, where values of 15, 30, and 120 seconds were also tested but were not as effective as the 60 second window size which was fast and accurate. The resolution between each point was determined by the overlap percentage and window size, and in this case results in a resolution of a data point every 6 seconds.

The output from the post processing script is converted into a Bland Altman plot for the ease of analysis. Every Bland Altman plot represents the different channel which correspond to the locations in Figure 3.1 which are compared against the data collected from the pneumotachometer.

3.2 Data and Results

After the data sets were collected, the data was manually analysed to ensure that any invalid data was eliminated using the criteria mentioned above. A test will be marked as invalid whenever the data output from the relaxation oscillator exceeds the limits of 3.1 kHz by a margin greater than 25%. A table was formed with all the tests and channels in order to observe the data patterns on each channel and calculate the total usable test data.

For the results from the Bland Altman the best result for the bias is to have values equal or close to zero, while the limit of agreement being $\pm$ 1 BPM. The limit of agreement value selected is the minimum accuracy needed for when comparing against the gold standards of the industry. In which the FDA apporval for a respiratory monitoring device is $\pm$3 BPM (Chan et al., 2022).

3.2.1 Study One Results

For the first study the data is separated into three different sets to make it easier while comparing the data. The data is manually collated into a table to show the usable data. This helped in identifying the failure points and at which sensors/tests this happened in. The tests were grouped per type (Laying, Metronome, and Sitting), and the results for the usable data are seen in Figure 3.2, Figure 3.3, and Figure 3.4.

Laying Tests

Patient	Test	Channel 0	Channel 1	Channel 2	Channel 3
1	LIE	0	1	1	0
2	LIE	1	1	0	0
3	LIE	0	0	1	0
4	LIE	1	1	1	1
5	LIE	0	0	1	1
6	LIE	0	0	1	1
7	LIE	1	1	0	0
8	LIE	0	0	0	0
9	LIE	0	0	0	0
10	LIE	0	0	0	0
11	LIE	0	0	0	0
12	LIE	0	0	1	1
13	LIE	1	1	1	1
14	LIE	1	0	1	0
15	LIE	0	0	0	0
16	LIE	1	0	0	0
17	LIE	0	0	0	0
18	LIE	0	0	0	0
19	LIE	0	0	0	0
20	LIE	0	1	1	1
Total Usable Channels		6	6	9	6

FIGURE 3.2: Laying test results which highlights all usable data in Green

Metronome Tests

Patient	Test	Channel 0	Channel 1	Channel 2	Channel 3
1	MET	0	1	1	0
2	MET	1	0	1	0
3	MET	1	1	1	1
4	MET	1	0	1	1
5	MET	1	1	1	0
6	MET	1	1	0	0
7	MET	1	1	1	0
8	MET	1	1	0	1
9	MET	0	1	0	0
10	MET	1	1	1	0
11	MET	1	1	1	1
12	MET	1	0	1	1
13	MET	1	1	1	1
14	MET	1	1	1	0
15	MET	0	1	1	1
16	MET	1	1	1	0
17	MET	0	1	1	1
18	MET	0	1	0	0
19	MET	1	1	1	0
20	MET	1	1	0	0
Total Usable Channels		15	17	15	8

FIGURE 3.3: Metronome test results which highlights all usable data in Green

		Sitting Tests			
Patient	Test	Channel 0	Channel 1	Channel 2	Channel 3
1	SIT	1	1	1	0
2	SIT	0	0	0	0
3	SIT	0	0	0	0
4	SIT	1	0	1	0
5	SIT	1	1	1	1
6	SIT	1	0	0	0
7	SIT	1	1	1	0
8	SIT	1	1	1	1
9	SIT	0	0	0	0
10	SIT	0	0	0	0
11	SIT	0	0	0	0
12	SIT	0	0	0	0
13	SIT	0	1	0	1
14	SIT	0	0	1	1
15	SIT	0	0	0	0
16	SIT	0	1	0	0
17	SIT	1	0	0	0
18	SIT	0	0	0	0
19	SIT	0	0	0	0
20	SIT	0	0	0	0
Total Usable Channels		7	6	6	4

FIGURE 3.4: Sitting test results which highlights all usable data in Green

3.2.1.1 Metronome Results

The metronome data was post processed in three different groupings, where the first set of results is to test all channels that are usable, the second is to test all participants with 3 usable channels, and lastly is to test all participants with all 4 usable channels. The reasoning behind these three choices is to understand the effects of position, as well as identifying whether or not position matters for the capaciflector to be used effectively.

The first set of results from all usable channels showed good results as the data was very close to the belt data. Figure 3.5 and Table 3.1 shows the 4 different channel outputs with a very low bias (0.05 ± 0.04 BPM) as well as low limits of agreement between the belt and the capaciflector data (0.70 ± 0.20 BPM). As for the test for 3 usable channel per participant, this resulted in Figure 3.6 and Table 3.2 for a total of 9 participants (27 tests). The resulting data showed very similar values of 0.10 ± 0.01 BPM for the bias and 0.84 ± 0.36 BPM for the limits of agreement. Lastly the test which contained all usable channels per participant resulted in Figure 3.7 and Table 3.3 for a total of 3 participants (12 tests). This test aimed to identify whether or not the position of the capaciflector affected the accuracy, which resulted in very similar limits and biases between all channels.

TABLE 3.1: Results from Study One Metronome Study with all usable channels compiled into a table.

Channel	Bias (BPM)	ULOA (BPM)	LLOA (BPM)	Difference (± BPM)
1	-0.01	0.49	-0.50	0.50
2	-0.05	0.85	-0.95	0.90
3	-0.05	0.85	-0.95	0.90
4	-0.09	0.62	-0.81	0.71

TABLE 3.2: Results from Study One Metronome Study with 3 usable channels per participant compiled into a table.

Channel	Bias (BPM)	ULOA (BPM)	LLOA (BPM)	Difference (± BPM)
1	0.09	0.57	-0.39	0.48
2	0.09	0.58	-0.39	0.49
3	0.10	0.93	-0.74	0.83

TABLE 3.3: Results from Study One Metronome Study with 4 usable channels per participant compiled into a table.

Channel	Bias (BPM)	ULOA (BPM)	LLOA (BPM)	Difference (± BPM)
1	0.11	0.33	-0.10	0.22
2	0.11	0.34	-0.11	0.23
3	0.11	0.35	-0.12	0.24
4	0.12	0.37	-0.14	0.25

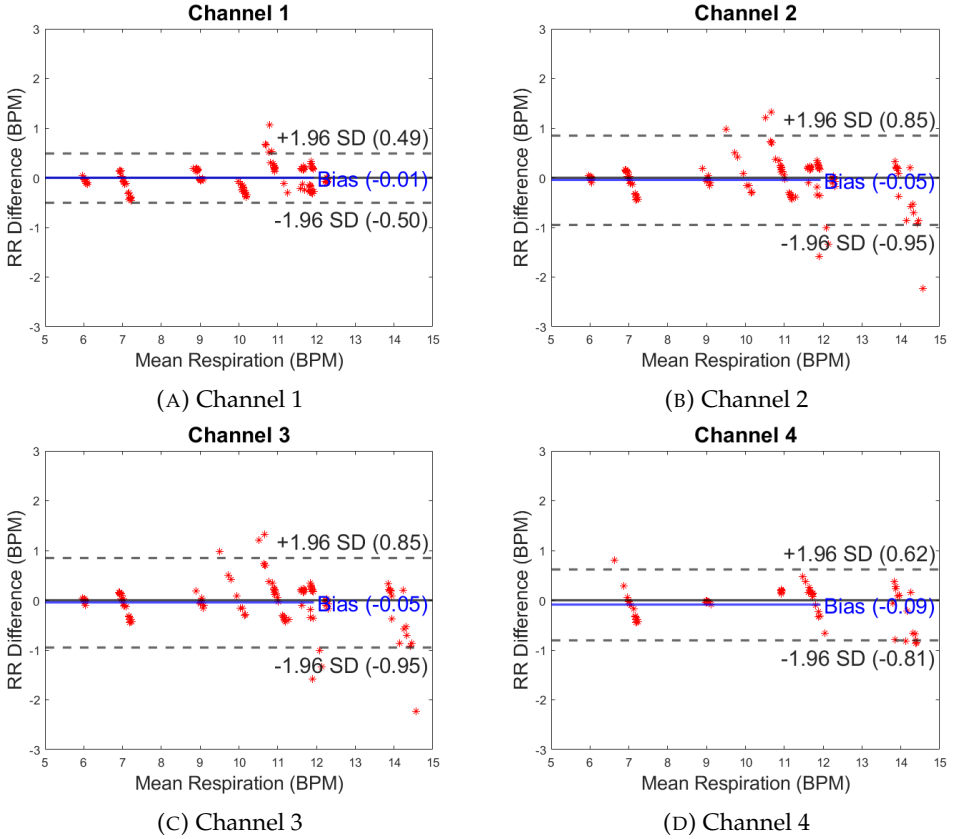

(A) Channel 1

(B) Channel 2

(C) Channel 3

(D) Channel 4

FIGURE 3.5: Shows the results from the Metronome Belt tests for all usable data

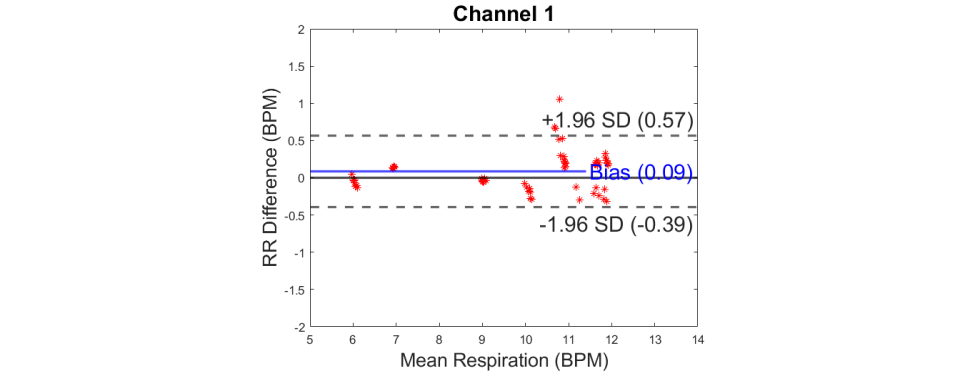

(A) Channel 1

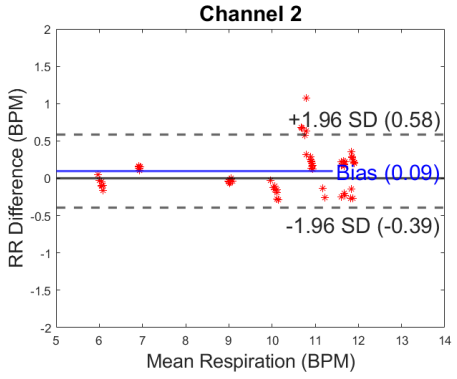

(B) Channel 2

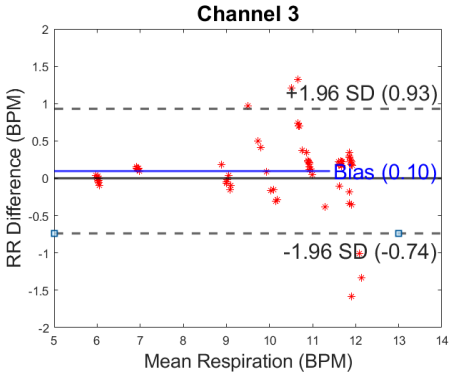

(C) Channel 3

FIGURE 3.6: Shows the results from the Metronome Belt tests for 3 usable channels per participant

3.2.1.2 Sitting Results

For the sitting tests, little usable data remained after discarding invalid data, which resulted in a smaller number of tests used in generating the plots. From Figure 3.4 only a handful of tests were usable out of the 20 tests per channel, which didn't allow for a similar processing method as the metronome data-set. So for the sitting tests all the available tests were used regardless of whether or not the participant had more than one usable channel. The results can be seen in Figure 3.8, also seen in Table 3.4. The bias from the plots fluctuated between channels, with values as low as 0.02 BPM and as high as 0.8 BPM with a limit of agreement that was as high as ± 3.1 BPM, which is close to the limit of error set. The reason why many tests from the sitting portion of the study were bad is due to the sensor failure or due to high noise which caused the signal to carry false data. This is apparent in Channel 2 which has a higher bias and limits of agreement when compared to the other channels. The outliers above the limits of agreement show that some of the tests have a higher difference in the higher breathing ranges, which is expected as the sensors on Channel 2 exhibited the highest failure rate between the other channels.

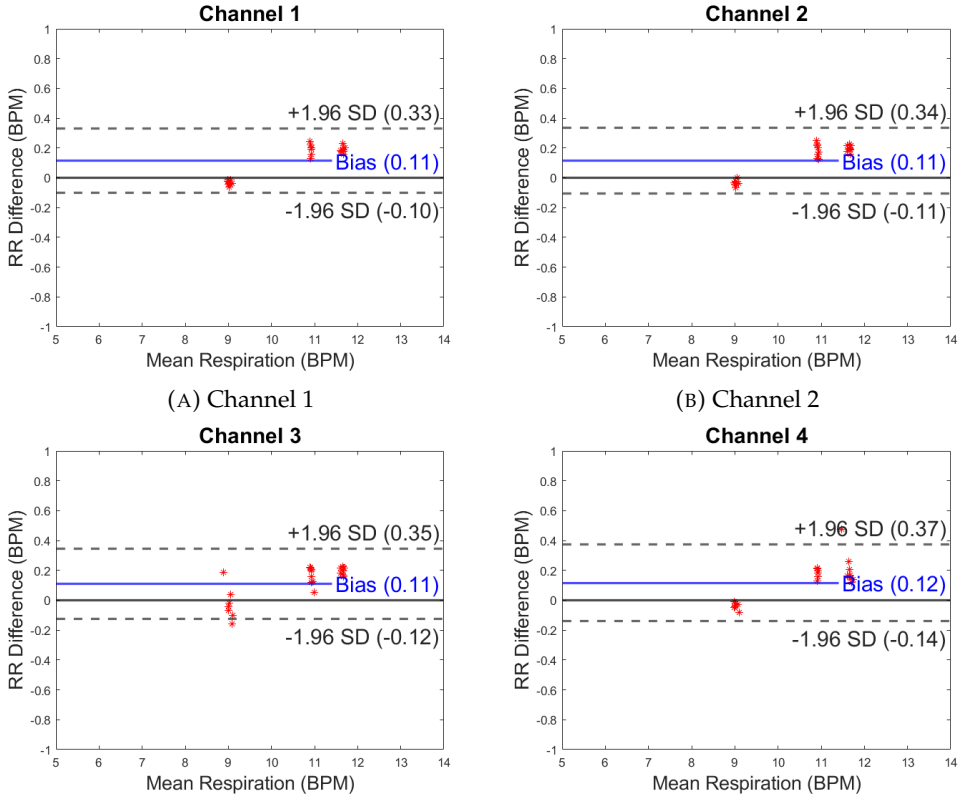

(A) Channel 1 (B) Channel 2

(C) Channel 3 (D) Channel 4

FIGURE 3.7: Shows the results from the Metronome Belt tests for all tests which have 4 usable channels per participant

TABLE 3.4: Results from Study One Sitting Study with all usable channels compiled into a table.

Channel	Bias (BPM)	ULOA (BPM)	LLOA (BPM)	Difference (± BPM)
1	-0.16	1.39	-1.72	1.55
2	0.80	3.90	-2.30	3.10
3	-0.02	2.18	-2.22	2.20
4	0.42	2.85	2.00	2.43

3.2.1.3 Laying Results

Similar to the sitting portion, the laying portion of the study was also processed in the same manner due to the same sensor failure, which can be seen in Figure 3.2. Figure 3.9 shows the Bland Altman's of the laying portion, also seen in Table 3.5. The results are very close when compared to the sitting portion, with the laying part performing better. The bias maintained a value of 0.01 BPM between channel 4 and 2, while channel 1 and 3 had a value of 0.22 BPM and 0.09 BPM respectively. As for the limits of agreement, channels 1 and 2 performed extremely well with a value of ± 0.66, while channel 3 and 4 had higher limits which are greater than 1.

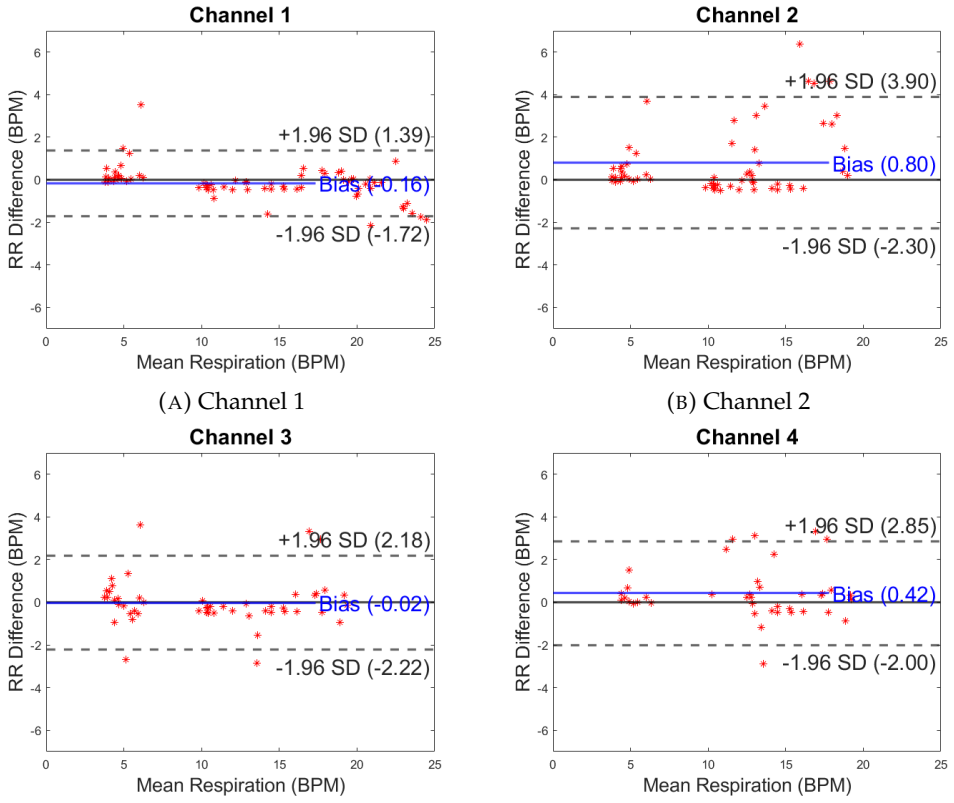

(A) Channel 1

(B) Channel 2

(C) Channel 3

(D) Channel 4

FIGURE 3.8: Shows the results from the Sitting tests for all usable channels per participant

TABLE 3.5: Results from Study One Laying Study with all usable channels compiled into a table.

Channel	Bias (BPM)	ULOA (BPM)	LLOA (BPM)	Difference (± BPM)
1	0.22	0.88	0.43	0.66
2	-0.01	0.66	-0.68	0.67
3	0.09	1.99	-1.81	1.90
4	-0.01	1.58	-1.59	1.59

3.2.2 Study Two Results

For study two the same process is started by constructing a table for all usable data, this is seen in Figure 3.10. This table was important in identifying the cause of failure, as when comparing the trend of the failure between channels it seems too sporadic. This can be attributed to the fact that the sensors for each channel were not the same throughout the study. As for the failure itself, it is due to the nature of the study which introduces high moisture buildup causing the sensor layers to separate. This is mostly visible with channel 2 which showed a trend with the sensor failing continuously at the last few tests. Exactly as study one the failure is identified by looking at the sharp change in the relaxation oscillator output frequency. Figure 3.11 shows a raw signal with a bad capaciflector signal, in which it starts failing at the end of the test. The data

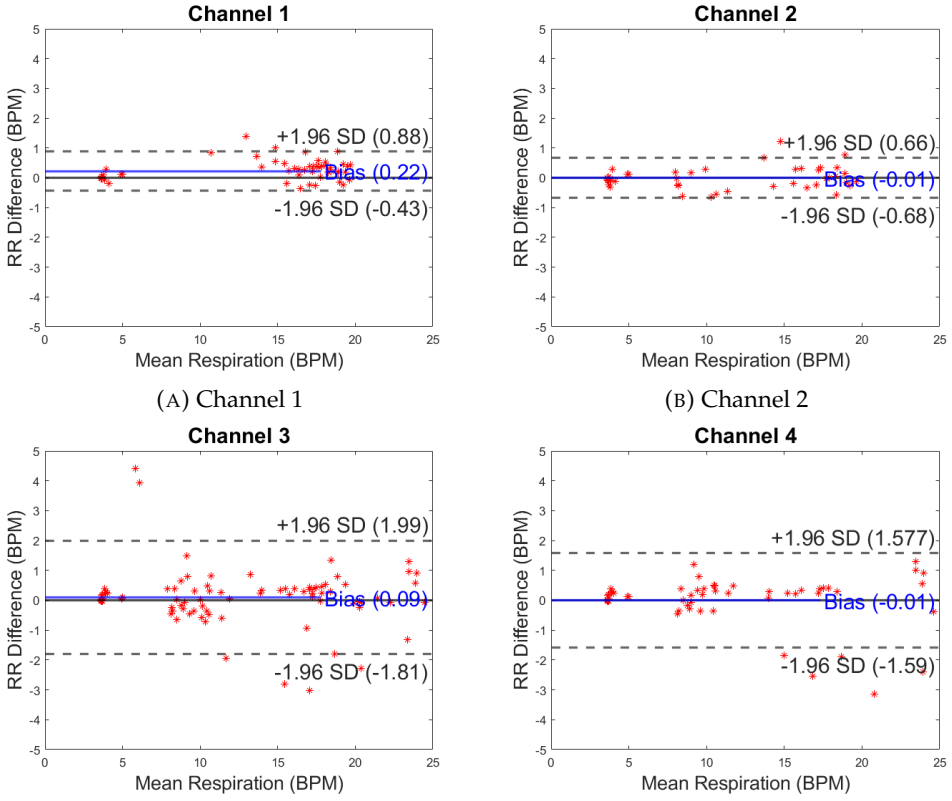

(A) Channel 1

(B) Channel 2

(C) Channel 3

(D) Channel 4

FIGURE 3.9: Shows the results from the Laying tests for all usable channels per participant

does contain some usable information during the first half however due to having the sensor fail in the end, this data was deemed as unusable.

The results after running the algorithm on all the usable data sets, (Same as sitting and laying tests in study one) showed promising results for having the participants undergo physical exercises with body movement, hence the result seen in Figure 3.12 and Table 3.6 are within the limits of agreement of the expected error. The results for this study is a bias of 0.12 ± 0.03 BPM and a limit of agreement of 3.02 ± 0.13 BPM. This shows that even at extreme scenarios the capaciflector was able to pick up respiration rate data. However due to the data from the CPET tests being a whole number for the number of breaths per minute, it caused the data to be less accurate when compared to the data extracted from the short Fourier transform which contained much higher resolution data (6 seconds per point). While this data shows potential it does not fairly assess the capaciflector properly due to the mismatch in the way the data is processed, which is why the first study was undertaken to provide a fairer comparison.

Test File Name	Channel0	Channel1	Channel2	Channel3
Test1	0	0	0	0
Test2	0	0	0	0
Test3	0	0	0	0
Test4	0	0	0	0
Test5	1	1	0	1
Test6	0	1	1	1
Test7	1	1	1	1
Test8	1	0	1	1
Test10	1	1	1	1
Test11	1	0	1	1
Test12	0	1	1	0
Test13	1	1	0	1
Test14	1	1	0	0
Test15	0	0	0	0
Test16	1	0	1	0
Test17	0	0	0	0
Test18	0	0	0	0
Test19	0	0	1	0
Test20	1	0	1	1
Test21	0	0	1	1
Test22	0	1	0	0
Test23	1	1	1	1
Test24	1	0	1	1
Test25	1	0	1	1
Test26	1	0	0	1
Test27	1	1	1	1

(A) First Half of the table

Test File Name	Channel0	Channel1	Channel2	Channel3
Test28	1	0	1	1
Test29	0	0	0	0
Test30	1	0	0	0
Test31	1	0	1	0
Test32	0	0	0	0
Test33	0	0	1	0
Test34	1	0	1	1
Test36	1	0	0	1
Test37	0	0	0	0
Test38	1	1	0	0
Test39	0	1	0	0
Test40	0	0	0	0
Test41	0	0	0	0
Test42	0	1	0	1
Test43	1	1	0	0
Test45	0	1	0	0
Test46	1	1	0	1
Test47	0	0	0	1
Test48	0	1	0	0
Test49	0	0	0	0
Test50	0	1	0	0
Total Usable Tests	22	18	18	20

(B) Second half of the table

FIGURE 3.10: Shows the tests from the second study with the usable data in Green

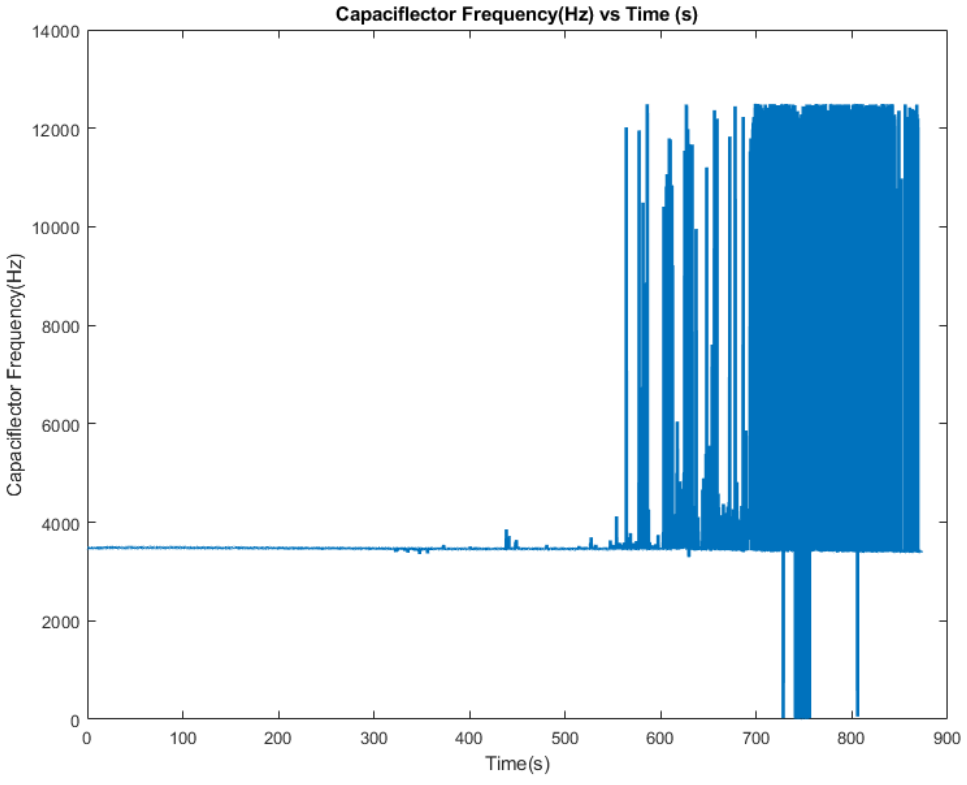

FIGURE 3.11: A sample signal from one of the tests from the second study showing failure at the end of the sampling period, where the frequency spikes to 12kHz

TABLE 3.6: Results from Study two compiled into a table.

Channel	Bias (BPM)	ULOA (BPM)	LLOA (BPM)	Difference (± BPM)
1	0.18	3.07	-2.71	2.89
2	-0.31	2.89	-3.51	3.20
3	0.32	3.36	-2.71	3.04
4	0.27	3.23	-2.69	2.96

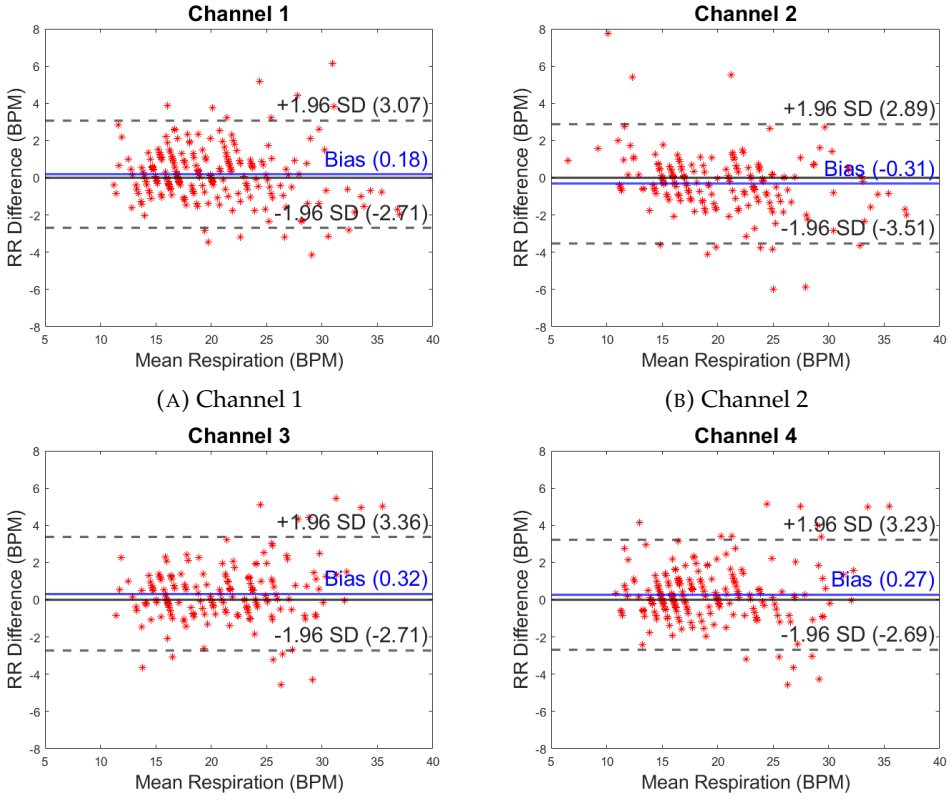

(A) Channel 1

(B) Channel 2

(C) Channel 3

(D) Channel 4

FIGURE 3.12: Shows the results from the post processing done on the data from the second study

3.3 Analysis

A short analysis is done on the data in order to answer the hypothesis and identify the main point regarding the usability and effectiveness of the capaciflector as a respiration sensor. As well as assess the effectiveness of the capaciflector as a sensor in both a stationary and high movement setting.

3.3.1 Data and Channel Usability

As the data was manually checked after using an automated script, this poses a slight limitation to the data quality as some data may be deemed unusable due to the low signal to noise ratio. This however, is only done for study two as the results from the

study contained high amounts of noise due to the bicycle movement, thus requiring a more thorough look on the signal quality. This results in a slightly lower number of usable channels per participant as they cause the data points to be low hence providing a slightly biased result towards the only good results. This can be justified by running a proper analysis on the first study by fully automating the script to avoid any bias in the results.

3.3.2 Study One

The data for the metronome portion of the study contained a large amount of usable tests which helps in building a more solid set of results. The results show that a tuned system with no movement can easily follow along the breathing in a stationary position. This data was used to evaluate the effectiveness and maximum accuracy of the capaciflector for a stationary position, while also helping calibrate the post processing algorithm to detect these repeating breathing frequencies. This is not the best method to calibrate, in which a more valid test would be sitting at rest for a long period of time or variably changing the breaths per minute over time. All the data contained biases which are less than 0.1 breaths per minute, with limits of agreement that are as high as 0.8 breaths per minute. Where the tests for the 3 channels and all channels are done in order to ask questions related to the number of capaciflectors needed as well as the position to accurately get all the information. And from this we can see that there is no visible difference between all of the channels.

The results from the sitting tests are more inaccurate when compared to the metronome tests, this was due to the large amount of noise which was surprising as there was no movement in the human body. This noise originated from the sensors failing as well as the shallow breathing that was done and not picked up by the relaxation oscillators. This is an issue as most of the home use cases are going to be either sitting or laying down, and will breath shallower as time passes. And even though many data sets were unusable, the results are still within the limits of agreement chosen, causing this test to be a successful one.

Lastly for the laying tests these were closer to the expected values from stationary tests, where the results are within the range of expected values. However there are some slight noticeable changes between channels 1 and 2 and channels 3 and 4 where there is a bigger change in the limits between the two ($\approx$ 1 BPM). This means that in a laying position the capaciflector attached to the sides was able to capture less of the data and introduced more error into the system, and hence the location for the capaciflector is preferably placed in the upper chest area. This was an interesting point as the metronome tests which were also stationary tests did not have any noticeable differences between the two sets of channels.

Overall, the first study showed very promising results in assessing the capaciflector as a usable sensor in detecting respiration during a stationary scenario.

3.3.3 Study Two

When analysing Figure 3.10 a trend for the data loss can be seen due to the failure of the sensors after continuous use. And because the sensors were interchanged between each other for every participant this makes tracking the faulty sensor a bit more difficult, hence why the bad sensors kept switching between different channels.

Looking at the bias of the system in Figure 3.12 shows that the average breathing rate is very close between each channel, where a value of less than or equal to 0.12 breaths per minute is seen on average, this value is calculated from averaging the biases between all 4 channels (Table 3.6). The difference in values was identified as a timing error in the Lab View App which sampled the data. The problem originated from the DAC (Digital to Analogue Converter) which was sampling at 100ms but with a small error of $\pm 1ms$. However, this error scaled over a period of time escalating into a bigger data shift. This was identified later during the processing stage, after the data was collected, which means the data wasn't sampled at the exact 10Hz but at a different rate, which was found to be a constant of 10.4Hz by averaging the total sample rate change from multiple samples. This change was applied to the rest of the data collected through the Lab View Application, which provided better results from the original sample rate. A comparison of the before and after can be seen in Figure 3.13 where the shift that is constant is seen, the figures are outputs from the post processing that were run with the 10Hz sample rate and the 10.4 Hz respectively. The increase in the sample rate for analysis accommodated the average bias throughout all the signals, fixing the results to be closer to the actual sample rate collected during the tests.

This shows that even under extreme scenarios the capaciflector was able to capture the data accurately. Even if at some cases there are outliers between the two signals compared. This is seen more clearly in Figure 3.12b where there are three points that have a positive difference of 6 BPM.

Overall, study two is a success and helped answer the question to whether or not position matters. The answer is that no position matters for when performing an exercise, as all channels performed equally well, when accounting for the sensor failure that occurred throughout the testing.

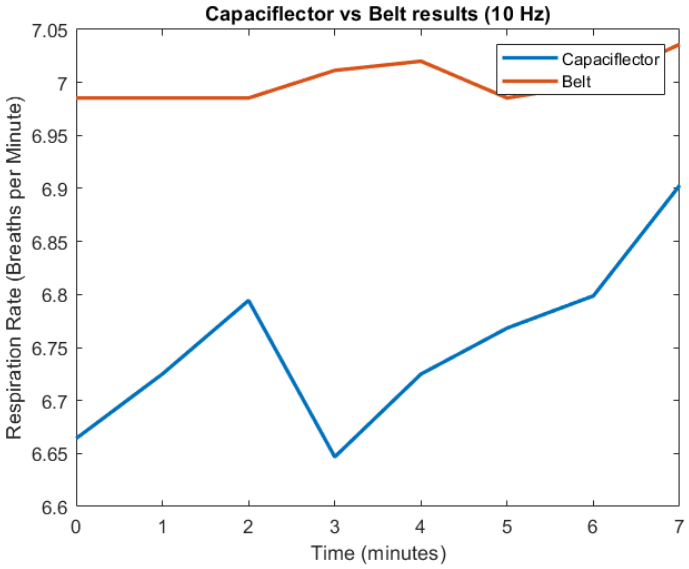

(A) Metronome Test Results for Channel 1 with 10Hz Sample Rate

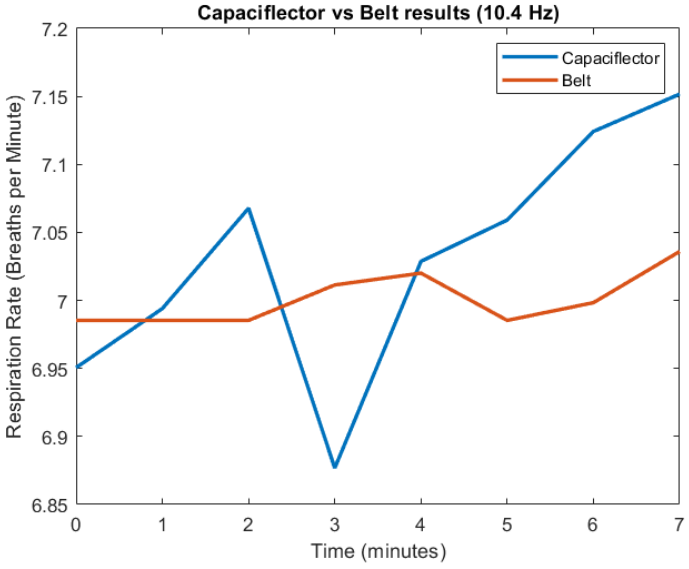

(B) Metronome Test Results for Channel 1 with 10.4Hz Sample Rate

FIGURE 3.13: Results from adjusting the sample rate of the processing algorithm, from 10Hz to 10.4Hz

3.4 Chapter Summary

In the end both studies helped provide a very good insight on the way the sensors are designed as well as how important the hardware and software used matters for the capaciflector to successfully capture the respiration signal. Where study one managed to verify that the capaciflector is well suited for stationary situations, whereas study two is more focused on body movement and is more extreme. Nonetheless study two managed to stay within the limits of agreement as well as properly detecting the respiration in a reliable manner. The results from these tests are important towards developing

a newer system which is more reliable and accurate. And the next set of steps are to investigate the capaciflector and identify if there is a more easier and reliable way of manufacturing as well as having the system be untethered and battery powered for longer sample lengths.

Chapter 4

Capaciflector Sensor Configuration Analysis

Finding the best configuration for the capaciflector is vital towards building a system that is more compact and easily adapted between different systems and environments. Thus by assessing the different ways the capaciflector can be used, it can help maximise the capaciflector's effectiveness for detecting respiratory rate (RR). This chapter focuses on the limitation found in Chapter 3, which is the continuous failure of the sensor during exercise due to layer separation. Another key aspect that this chapter tackles is the different modes in which the capaciflector can be constructed and used in detecting RR.

4.1 Introduction

Seven designs were designed, manufactured, and tested under a set of different methods (modes) and materials in order to compare the effectiveness of each design for detecting RR. Three of the sensors are rigid sensors while the other four sensors were flexible sensors. The sensor designs selected allowed a wide range of tests to be conducted to explore the different methods the sensor can be used and the type of data that is expected from it.

The sensors were compared against each other in order to see the effects of changing the frequency and method of connection in detecting RR. The assessment of all the sensor designs is done by performing a short a breathing exercise (25-30 seconds long). Two main modes are tested, the capaciflector mode and the capacitance mode. The capacitance mode was also tested with two different methods of connection in order to find the best method that yields the best accuracy. The results from the sensor were

compared against a belt sensor which provided the force exerted from the chest movement.

The study compared both the maximum capacitance change as well as the maximum force change from the belt sensor. The analysis ended up with the capacitance mode outperforming the capaciflector mode. With the best sensor being the flexible sensor design one.

4.2 Methodology

Seven different designs were adapted and scaled from the work done by White et al. (2017). The capaciflector's were designed in KiCad (KiCad Development Team, 2021) a PCB design software, whereas the testing hardware and software used is an evaluation board and its accompanying software for the capacitance to digital converter (CDC) IC (FDC2214) from Texas Instruments. The FDC2214 evaluation module board allows the user to prototype the system with easy access to the FDC2114 IC through a computer interface with data logging capabilities. The choice of using the module over custom hardware is due to the already existing solution with good support from Texas Instrument, while also having all the features needed for this type of testing already built in onto the accompanying software.

Two different modes of operation were tested: capaciflector mode and capacitance mode. The key differences between them is the use of the reflector plate as part of the stack-up to build the sensor, in which the capaciflector mode requires a buffer to operate the sensor properly while the capacitance mode does not. With each mode, different configurations were also tested with different inputs between the IC and the sensor. Different frequencies were also tested for all sensors: 100kHz, 1MHz, and 10MHz.

The data collected from the tests is compared against a belt sensor (GO Direct^{TM} Respiration Belt) by Vernier (2020) with the same method of testing, this resulted in the truth vs measured values. Further processing was done on all the data collected in order to compare the different sensor designs through the use of MATLAB (2019).

4.2.1 Capacitance to Digital Converter IC

The FDC2214 IC is a capacitance to digital IC manufactured by Texas Instruments which uses an LC tank to measure the capacitance of the target (Texas Instruments Incorporated., 2015). The sensor allows measurement of capacitance values with resolution's of up to 28-bit, which is more than enough to capture all the signals needed for this experiment and for any future development. And in conjunction with the evaluation module board, all the necessary starting software to data log and modify the

hardware is available for purchase. This made matching the testing conditions between all the sensor designs from a hardware perspective to be the same. One of the key features of this IC is the ability to read from multiple channels (up to 4 channels) which helped speed the process of testing by having each channel tuned to a separate tank frequency. The IC uses an external Inductor Capacitor (LC) tank which can be seen in the schematics in Figure C.3 in the Appendix which allow the IC to be configured at different frequencies. In order to adjust the LC tank frequency, the inductor and capacitor pair were tuned to output a frequency as close as possible to the target frequency needed. A list of the inductor capacitor pairs can be seen in Table 4.1 alongside the measured frequencies. One thing to note is the capacitor inductor used for the 100kHz frequency which required extreme values in order to lower the frequency, this is due to the nature of the IC and the limitations on the evaluation module board which had a small footprint for the inductor. The results from the desired frequencies are all calculated based on the resonant frequency of an LC circuit in parallel (4.1).

TABLE 4.1: Outlines all the channels used and the appropriate calculated and measured frequencies.

Channel	Calculated Frequency	Measured Frequency (Unconnected)	Inductor (L)	Capacitor (C)
1	100kHz	98kHz	680uH	3.3nF
2	1MHz	550kHz	470uH	47pF
3	10MHz	3.2MHz	18uH	12pF

$$f = \frac{1}{2\pi\sqrt{LC}} \tag{4.1}$$

The IC uses two inputs per channel to measure the capacitance, this allows for multiple different methods of connection to the sensor. The only thing to account for when switching between different sensors and different frequencies is the drive current of the sensor IC. The value can be changed through the software provided, however each value differs between different settings as the IC will not measure the capacitance properly if the current drive value is not calibrated per sensor. The method of calibration is done by ensuring that the output value from the LC tank oscillates between 1.2V and 1.8V while the sensor is attached to the skin as values that go beyond or lower than these volatges generates flags that indicate overflow and underflow in the IC registers. A representation of valid calibration voltage can be seen in Figure 4.1.

4.2.2 Capaciflector Mode

The capaciflector mode is a mode of operation in which the sensor operates as originally designed by Vranish (1991) and can be seen in Figure 4.2. In the original patent the proposed method of reading the capacitance value is by the use of a relaxation

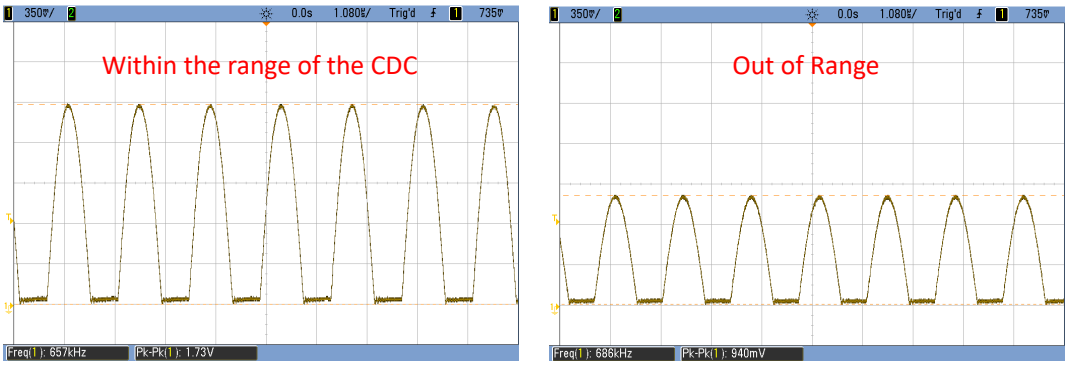

FIGURE 4.1: Valid and Invalid calibration voltages for the CDC.

oscillator and a buffer to drive the reflector plate of the sensor. The operation principle of this mode stays the same as the original design, where the main change is the method of measurement, in which a more accurate sensor IC was chosen to drive the sensor and the reflector plate through the buffer. The same CDC IC used in series with a buffer (BUF602 IC) from Texas Instruments makes the capaciflector behave the same way as the original proposed method. The buffer selected has a wide bandwidth of 1 GHz which is more than enough for the operating frequencies of the the CDC which is between (100kHz - 10 MHz). The key advantages to using the capaciflector mode is the reduction of interference and directionality of the field generated when driving the sensor plate. This configuration makes the sensor less prone to external capacitive interference's, as the field's directionality reduces the chance of the sensor picking up any external movements/interference such as touching .

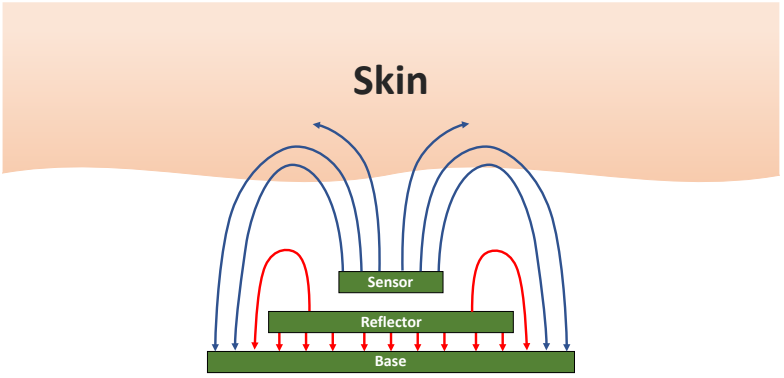

FIGURE 4.2: Capacitor in capaciflector mode showing the field lines between all layers.

4.2.3 Capacitance Mode

The capacitance mode when compared to the capaciflector mode is similar in structure with the main difference being the removal of the reflector plate. This makes the capacitance mode a two plate sensor consisting of a ground and sensor layer. The key difference in the operation of the sensor is the reduction of directionality of the sensor, but by reducing the plate count and removing the buffer, the drive electronics become simpler as fewer components are needed. With the removal of the reflector plate, the sensor is more prone to external interference depending on the different ways the sensor is connected (Capacitance mode seen in Figure 4.3).

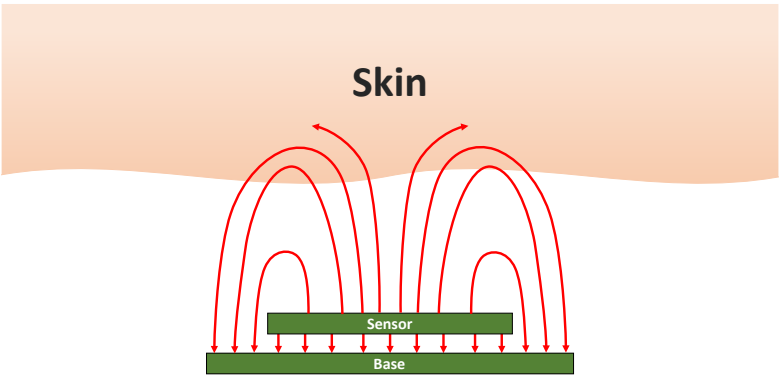

FIGURE 4.3: Capacitor in capacitance mode showing the field lines between all layers.

For this mode two different configurations were tested by utilising the different methods of connection to the CDC IC. The different connections can be seen in Figure 4.4 with inputs A and B being the inputs to the channel. One of the methods of connection uses a standard ground and signal pair while the other drives both the ground and signal plate with the inputs from the channel. Different configurations were also tested with different layer pairs however these designs were omitted out of this test as the testing introduced too many parameters to fairly compare the sensors. The configurations for these tests can still be seen in Appendix B.

4.2.4 Sensor Specifications and Manufacturing

The sensors were manufactured by two PCB manufacturer's in two different materials, one is a standard FR-4 material while the other is a flexible polymide material for PCB's. Three designs were manufactured for the rigid material and 4 designs were manufactured for the flexible material. Figure 4.5 shows the seven different designs. The choice for these sizes and ratios is based off the initial work done by White et al. (2017), which provides a starting ratio which already works for detecting respiration, and was modified to assess slight variations of the design.

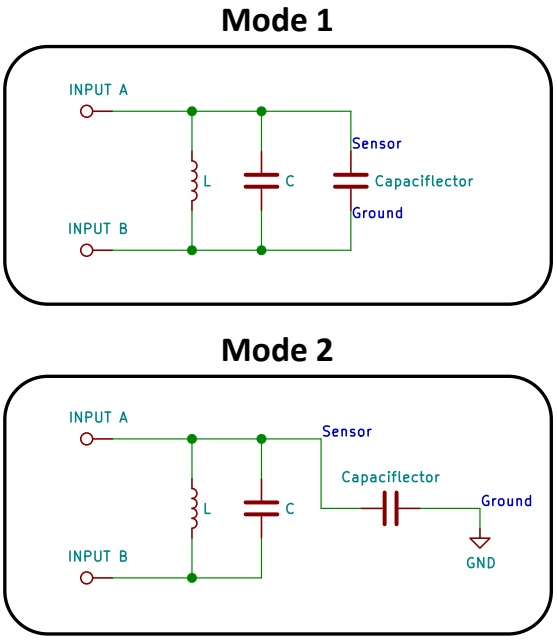

FIGURE 4.4: Modes used for the capacitance mode, where Mode 1 is using both the sensor and ground layer while Mode 2 uses only the sensor layer.

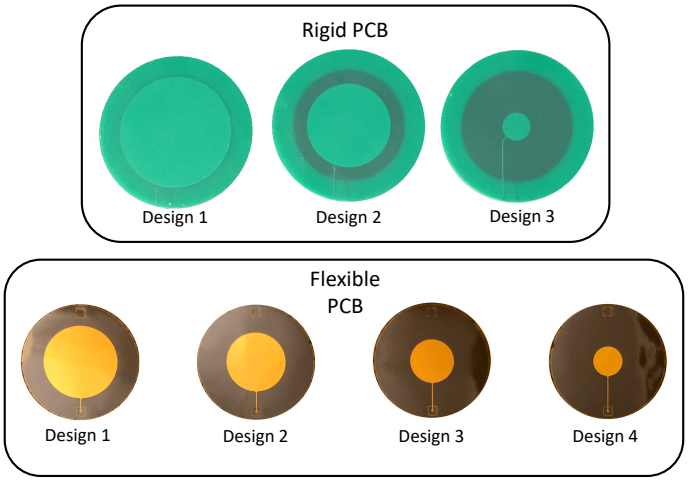

FIGURE 4.5: All sensor designs used, with 3 rigid sensors and 4 flexible sensors tested (Rigid PCB's are 50mm in diameter while the Flexible PCB's are 40mm).

For the rigid sensors three designs were manufactured with a diameter of 55mm and a thickness of 1.6mm using standard FR-4 PCB materials (TG130 (JLCPCB (2021))) with a dielectric constant of 4.6. While the flexible sensors were manufactured with a smaller diameter of 40mm and a thickness of 0.1mm using polymide flex material from PCB-Way with a dielectric constant between 3.3 and 3.5 (PCBWay (2022)). The rigid sensors

are 4 layer PCB's with a sensor, reflector and base plate being in a separate layers while also allowing one extra layer for any electronics. The flexible PCB's were manufactured with 2 layers and contained the sensor and base layer only.

The ratios between the sensor and base layer are seen in Table 4.2. For the flexible sensors the diameter stepped up by 5mm per design with a starting sensor diameter of 10mm, while the rigid sensors used the ratios from the patent (Vranish (1991)) with a base diameter of 50mm.

To connect both sensors for testing, the rigid sensors were connected with the base and sensor layer for the capacitance mode, while the capaciflector mode uses all layers. The other configurations mentioned previously are to connect the different layer pairs for example, the sensor layer and the reflector layer, in which the reflector layer acts as the base layer in this configuration. This was not possible for the flexible PCB's hence were left out of the results in this chapter.

The flexible PCB's were connected as normal with a sensor and base layer as manufactured. However to test the sensor in capaciflector mode two sensors were stuck to each other through double sided tape in which the base layer used in the bigger sensor is used as a reflector while the new sensor attached becomes the base layer. This allowed the sensor to be tested in capaciflector mode even though the sensor was only manufactured with 2 layers. A side view and top view of the sensor can be seen in Figure 4.6 below. Thus making the sensors have a configuration with a base and reflector plate of equal diameters, with only the sensor plate changing between the sensors.

TABLE 4.2: Ratios and layer sizes for all the sensor designs.

Design	Base Diameter (mm)	Refelector Diameter (mm)	Sensor Diameter (mm)	Ratio (Base:Sensor)
Rigid Design 1	50	40	40	1:5
Rigid Design 2	50	40	30	3:5
Rigid Design 3	50	40	10	4:5
Flexible Design 1	40	-	25	5:8
Flexible Design 2	40	-	20	1:2
Flexible Design 3	40	-	15	3:8
Flexible Design 4	40	-	10	1:4

4.2.5 Testing Method

To test the sensors, the method needs to be a fair test between all the sensors in order to effectively compare the results. So the choice of testing the sensors on the skin by the use of a TENS (Transcutaneous electrical nerve stimulation) electrode gel pad gives a more realistic output of what is expected from the sensor as well as providing a repeatable method of attaching the sensor to the skin. Due to the way the CDC works, each sensor frequency and design requires its own setting that is tuned manually to allow the sensor to read the capacitance properly. A small portion of this list can be seen in Table 4.3 while the full list for all the frequencies and designs can be seen in Appendix

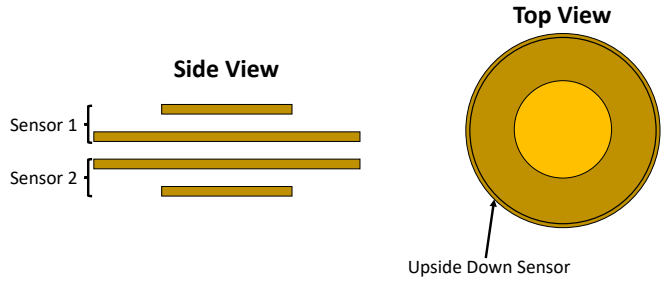

FIGURE 4.6: Side view and top view of the flexible sensors modified to allow the sensor to run in capaciflector mode.

B. The TENS gel pad used was modified from a generic reusable pad, where the sensors were attached face down onto the pad using double sided sticky tape. The sensors were all mounted on the top right side of the chest during this test for consistency.

TABLE 4.3: A sample of one of the current settings per mode for some of the designs.

Design	Mode	Frequency	Sensor Calibration (uA)
1	1	1MHz	38-60
2	1	10MHz	264-356
3	2	100kHz	264

As part of the testing the evaluation module needed to be isolated due to interference issues whenever the module was connected to a device which is connected to mains power (Issues mentioned in Texas Instruments Forums Page Texas Instruments Incorporated. (2021)). To avoid this issue an unplugged laptop was used, while also having the belt sensor plugged in through USB to ensure that no data loss occurs. The data collected is saved as a csv file for both the belt sensor and the capaciflector sensor, where the belt outputted the values as force in Newtons (N), and the evaluation module is capacitance in pico Farads (pF).

Each test had a single sensor connected at a time with a different frequency, at the same time the belt sensor was collecting data to compare against the capacitance data. The data was collected at 50 Hz for a duration of 20-30 seconds for each test for both the belt and the capaciflector.

The test sequence is completed by breathing hard for the first few breaths, then breathing normally for a few breaths and finally ending it with more deep breaths. Figure 4.7 shows an example of this sequence output from the belt sensor where the y-axis represents how hard the breath was, as well as the belt data for reference. This sequence was selected as it allows the sensor to be tested for maximum change during both light and heavy breaths. While the detection of the type of breath is not important in the

respiration rate measurement its useful to identify which sensor design allows the differentiation between breathing depths.

4.2.6 Processing and Analysis Method

After collecting the data, MATLAB (2019) was used to process the data into coherent figures which show the capaciflector mode against the capacitance mode. The key points between the figures is that the capaciflector mode only has one data-set per frequency as the design uses all three plates for the sensor. The analysis is compiled into a maximum change of capacitance table which allows the sensor modes to be compared. The change of capacitance is used as the capacitance value is not important as only the relative change is useful in identifying chest movement. As for the maximum change of force, the point in which the maximum capacitance change is found, the same time instance is used to calculate the equivalent change in force. Thus the capacitance and force changes are synchronised by the same time.

For the analysis of the data, the highest sensitivity sensor with the smallest current calibration constant will be selected as the best sensor. This is done in order to optimise the amount of current the sensor needs for when the hardware is to be developed. An example of these calibration currents used can be seen in Table 4.3.

4.3 Results and Analysis

The results for each mode and configuration is combined into a single table with the maximum change in capacitance and force. The results from the capaciflector configuration only has a short table for the different frequencies as only one method of connection can be used. While the capacitance configuration has multiple tables representing the different modes and frequencies used in the test.

4.3.1 Capaciflector Mode Results

Table 4.4 and Table 4.5 shows the results from the rigid PCB's and flexible PCB's respectively. The best results are represented as the maximum change with respect to the force, this changes with the design as the capacitance is not linear with the force. Which is why the deciding factor is the lowest current drive.

Looking at the results we can see that the capaciflector data in the rigid PCB's has a decreasing maximum change as the frequency increases. This however does not indicate poor performance in higher frequencies as the difference between the frequencies is the signal cleanliness and the stability. An example can be demonstrated in Figure 4.8

TABLE 4.4: Results from the testing the rigid sensors Designs with the capaciflector mode.

Design	Frequency (Hz)	ΔC (pF)	ΔF (N)
Rigid Design 1	100k	1.060	10.83
Rigid Design 1	1M	0.012	10.56
Rigid Design 1	10M	0.093	14.21
Rigid Design 2	100k	N/A	22.83
Rigid Design 2	1M	0.066	11.89
Rigid Design 2	10M	0.166	10.18
Rigid Design 3	100k	0.700	16.18
Rigid Design 3	1M	0.233	13.48
Rigid Design 3	10M	0.0381	20.27

TABLE 4.5: Results from testing the flexible sensors with the capaciflector mode.

Design	Frequency (Hz)	ΔC (pF)	ΔF (N)
Flexible Design 1	100k	0.202	35.46
Flexible Design 1	1M	0.195	37.14
Flexible Design 1	10M	2.409	30.89
Flexible Design 2	100k	0.312	34.10
Flexible Design 2	1M	0.868	31.12
Flexible Design 2	10M	0.092	36.77
Flexible Design 3	100k	0.546	33.02
Flexible Design 3	1M	1.651	36.10
Flexible Design 3	10M	0.630	29.34
Flexible Design 4	100k	0.212	40.13
Flexible Design 4	1M	0.076	39.59
Flexible Design 4	10M	2.045	31.66

which shows the difference between the different frequencies for the capaciflector rigid design 1. And even though the maximum change in the sensor is minimal it s much smoother and has little noise in the captured data.

As for the flexible sensors, they performed slightly better with higher changes overall throughout all the sensor designs. The sensor output varied between designs and frequencies with fluctuations between the results from the 1MHz and 10MHz, where one will outperform each other across different designs. A clear case of this is between design 4 and design 3 in which the results between the two frequencies are exact opposite. A key point as well is the maximum force change which is higher overall for the flexible sensors. This is due to the mounting method of the belt sensor which was tighter for these tests.

Overall this shows that the sensors in capaciflector mode perform in a stable manner and have very good sensor responses at the higher frequencies of 1MHz and 10MHz. And equally so, the flexible and rigid PCB's both had much cleaner signals at the higher frequencies while also exhibiting higher capacitance changes when compared to the lower frequency of 100kHz.

4.3.2 Capacitance Mode Results

Table 4.6 shows the results from the rigid PCB's for both modes. While Table 4.7 shows the results for the flexible PCB's.

TABLE 4.6: Results for the rigid sensor designs in capacitance mode.

Design	Mode	Frequency (Hz)	ΔC (pF)	ΔF (N)
Rigid Design 1	1	100k	0.590	11.36
Rigid Design 1	1	1M	0.370	7.98
Rigid Design 1	1	10M	0.220	7.40
Rigid Design 1	2	100k	1.180	14.72
Rigid Design 1	2	1M	0.231	15.38
Rigid Design 1	2	10M	0.088	12.02
Rigid Design 2	1	100k	N/A	15.02
Rigid Design 2	1	1M	0.180	10.38
Rigid Design 2	1	10M	0.148	9.49
Rigid Design 2	2	100k	0.220	14.85
Rigid Design 2	2	1M	0.084	13.05
Rigid Design 2	2	10M	0.319	16.88
Rigid Design 3	1	100k	0.240	7.28
Rigid Design 3	1	1M	0.266	16.63
Rigid Design 3	1	10M	0.479	17.50
Rigid Design 3	2	100k	0.370	14.20
Rigid Design 3	2	1M	0.069	14.51
Rigid Design 3	2	10M	0.169	14.56

As for the capacitance mode the results from the rigid sensors exhibit similar behaviour between each other in mode 2 especially designs 2 and 3 while design 1 follows the same patterns of decreasing capacitive changes as the frequency increases. For mode 1 the results from design 1 initially started with decreasing capacitance values, however as designs 2 and 3 are tested an inverted behaviour is seen on design 3 with an increase in the capacitive changes as the frequency increases.

Between the three frequencies the 1MHz performed the lowest in terms of capacitive change across mode 2 and in mode 1. And the 100kHz performed poorly which can be seen in the results of design 2 where there was little to no signal making the results closer to zero. This behaviour was seen in the flexible sensors however the results from this type of sensor are much better than the rigid sensors, as the maximum change is also higher (4pF higher). This is due to the flexibility of the sensor which forces the sensor to change shape, which in turn affects the capacitance value greatly. This is good as it makes the sensor much better at picking up changes in the chest but also has the disadvantage of picking up any other movement due to the flexibility of the sensor.

Overall both sensors performed equally well between the capaciflector and capacitance mode, where the clear difference between both sensor modes is the amount of noise the

TABLE 4.7: Results from testing the flexible sensor designs in capacitance mode.

Design	Mode	Frequency (Hz)	ΔC (pF)	ΔF (N)
Felxible Design 1	1	100k	5.630	33.24
Felxible Design 1	1	1M	4.179	33.17
Felxible Design 1	1	10M	4.036	40.23
Felxible Design 1	2	100k	0.610	25.41
Felxible Design 1	2	1M	3.789	27.64
Felxible Design 1	2	10M	0.444	30.45
Felxible Design 2	1	100k	2.230	27.57
Felxible Design 2	1	1M	1.628	33.38
Felxible Design 2	1	10M	2.776	34.69
Felxible Design 2	2	100k	0.530	35.77
Felxible Design 2	2	1M	N/A	29.63
Felxible Design 2	2	10M	0.188	32.82
Felxible Design 3	1	100k	0.540	34.26
Felxible Design 3	1	1M	0.821	30.31
Felxible Design 3	1	10M	0.792	38.08
Felxible Design 3	2	100k	0.260	41.62
Felxible Design 3	2	1M	0.244	42.95
Felxible Design 3	2	10M	2.465	30.9
Felxible Design 4	1	100k	0.530	32.01
Felxible Design 4	1	1M	1.434	29.86
Felxible Design 4	1	10M	0.459	35.80
Felxible Design 4	2	100k	N/A	50.55
Felxible Design 4	2	1M	0.070	36.27
Felxible Design 4	2	10M	1.112	33.00

capaciflector mode omits out of the signal, as well as the maximum change of capacitance detected. Nonetheless, the flexible sensor design one performed the best between all the other sensors, due to the method of construction (PCB manufacturing). The construction method is more accessible with the benefits of being resilient to wear and tear. This does not apply just for the flexible sensors, but also for the rigid PCB's. This comparative analysis shows that the capacitance mode which is much easier to implement, and also performs the best, while also requiring a lower number of layers to manufacture. Thus making it more suitable to be used in a low cost wearable systems. The main advantages to using the capacitance mode is the cost and scalability of the device, as the capacitance mode requires far less components in the sensor system in order to let it run, while the capaciflector mode requires additional passive and driven components to make it work. As for the cost factor, the ability to manufacture 2 layer PCB's make the price of the capacitance mode much cheaper to manufacture on a large scale, while the capaciflector mode requires at least 3 layers hence making the manufacturing process more expensive, especially with flexible materials. While the capaciflector does make the sensor more resilient to noise, it doesn't justify increasing the complexity of the system in order to achieve minimal performance gains.

4.4 Chapter Summary

Summing up the work done, four main points are to be gained from this analysis. One is the benefit of the CDC in detecting RR, making it a prime target to be used in the sensor system. The second point is that the capacitance mode performs better than the capaciflector mode which requires more components. And the last point is that the sensor designs which use a sensor plate closer in size to the base plate generally gives better performance, with the best sensor design being the first flexible sensor design in capacitance mode. And finally the CDC IC performs better at the higher frequency range (1MHz - 10MHz) for all the sensor designs.

This makes the next steps of developing the wearable sensor system to be clear as the type of sensor and CDC IC are already examined and tested in this chapter. The next chapter goes through the process of developing and testing a wearable respiration sensing system which is capable of continuously monitoring RR for long periods of time. The sensor system will be designed to utilise the sensors explored in this chapter, with the sensors being designed to run in capacitance mode.

(A) Shows the results from Flexible Design 4 for the capacitance mode.

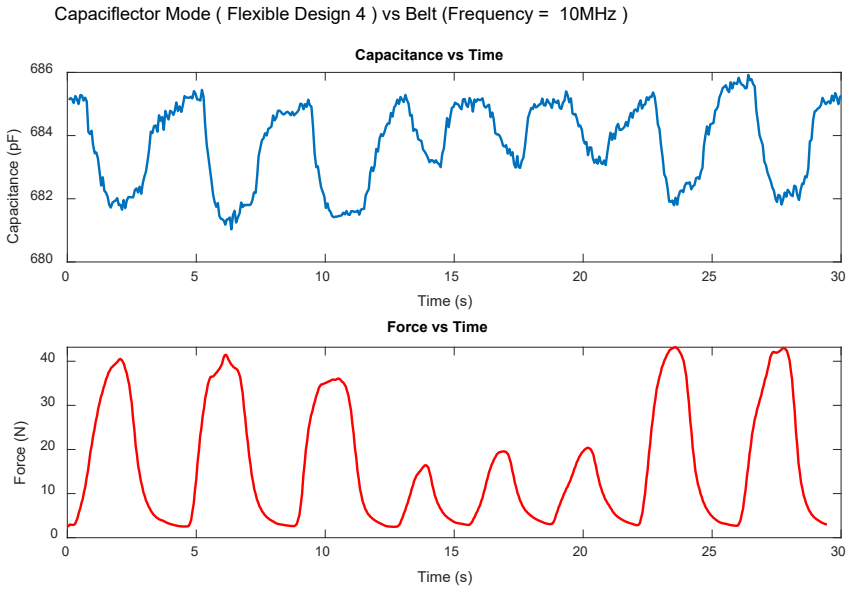

(B) Shows the results from Flexible Design 4 for the capacitance mode.

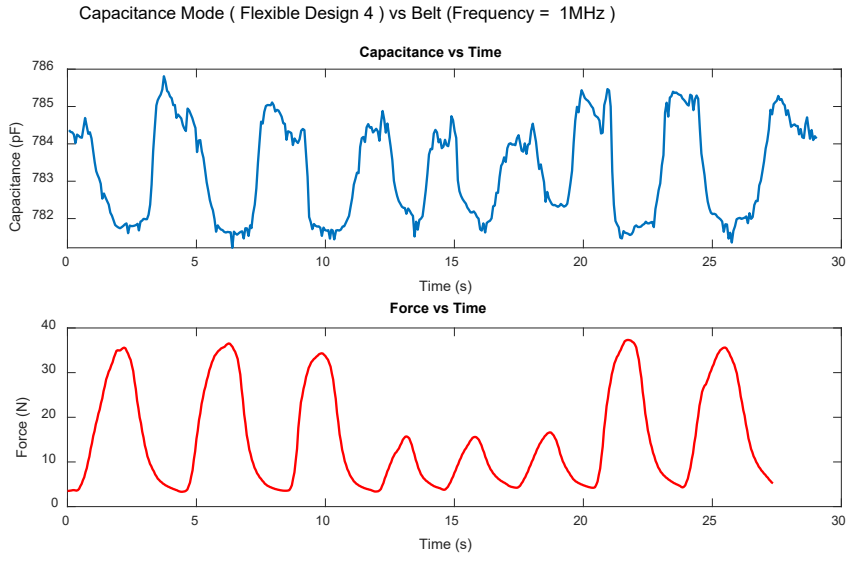

FIGURE 4.7: Compares the belt against the capaciflector and capacitance mode for a selected design, showing the light and heavy breaths as part of the test. The signal is inverted from the capaciflector due to the calculation from the CDC, however the negative peaks of the capaciflector match the positive peaks from the belt.

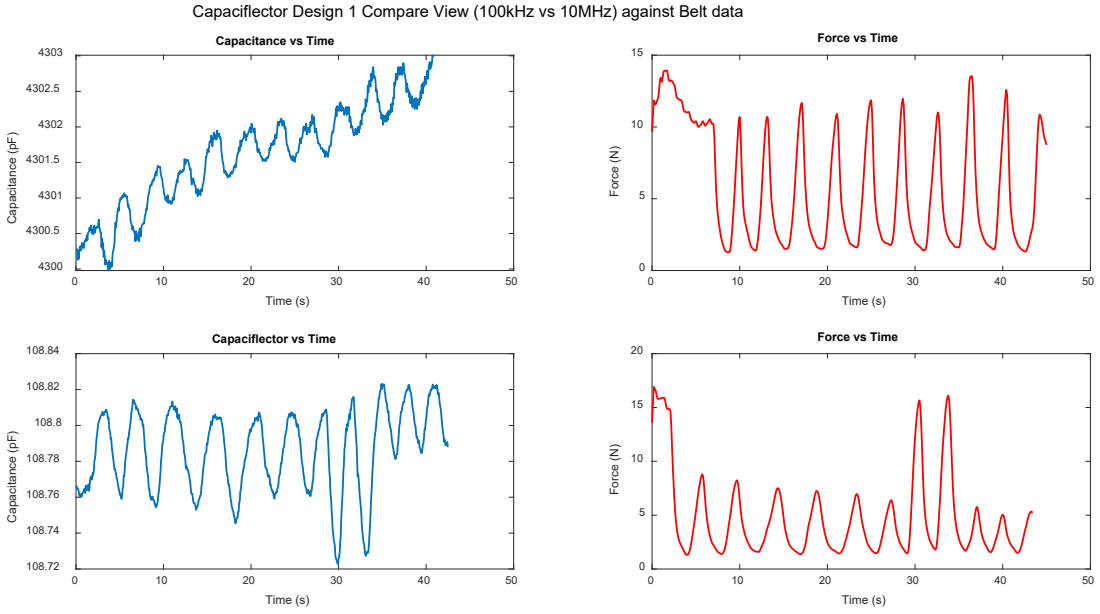

FIGURE 4.8: An example comparing two signals from design 1 but with a different frequency in capaciflector mode (100kHz and 10MHz).

Chapter 5

Wearable PCB and Software Development

Chapter 4 and Chapter 3 findings gave insight on the direction in which the sensor system needs to be developed. Where the hardware was developed with the aim of creating an untethered solution that can data log capacitance data from the sensor at the highest resolution possible. While also being small enough to be comfortably worn for long periods of time. To effectively test this system, it will be power tested, case tested and data integrity tested. The sensor system will be power optimised to get the longest run time for the system. And lastly run the sensor system through a series series of short tests to be compared against a belt sensor (Go Direct^{TM} Belt Sensor) while under a known metronome frequency to compare the data. A more extensive set of testing is done in the next chapter in which both the software and hardware are assessed against participants. The sensor design used will be both the rigid sensor design 2 and the flexible design 1 in capacitance mode as mentioned in the results of Chapter 4.

5.1 Hardware and Software Development

Four iteration's of the PCB hardware underwent development with slight changes between the components, and the main change being the size and compactness, as well as connection changes to accommodate for different features. The main development of the PCB's and the schematics was done in KiCad (KiCad Development Team (2021)), while the micro controller software was developed in Code Composer Studio and Sensor Controller Studio from Texas Instruments (Texas Instruments Incorporated. (2020)). Finally the testing of the data was done by building a graphical user interface (GUI) in MATLAB (2019) which included the data processing scripts to convert the capacitance data to respiration rate through extracting data from a spectrogram. For this chapter

the development of the two final iteration's will be discussed, the rest of the design's schematics and dimensions can be found in Appendix C.

5.1.1 Hardware Development and Testing

The initial design which contained the same components was designed with efficiency and longevity over size, which resulted in a large diameter of 70mm, this size felt much larger in person due to the large surface area. This was further scaled down to 32mm in the final version.

5.1.1.1 Components and Sensors

The main component of this hardware design is the use of a capacitance IC (integrated circuit) to measure the capacitance from the sensor. The IC used is the FDC2214 from Texas Instruments, which is the same 28-bit Capacitance to digital converter IC used in Chapter 4.

As for the main micro controller unit (MCU), the CC2640R2F chip from Texas Instruments was used due to the versatility of the chip itself and the family of that chip. The family of this MCU allows drop in replacements which are pin to pin compatible, hence provides the flexibility of choice in case more flash space or different features are needed. The main feature for this chip is that they come with a built in Bluetooth Low Energy (BLE) RF (Radio Frequency) core, which allows for future upgrades by the use of this wireless connectivity to allow for newer features to be developed.

Two other sensors were added, mainly the accelerometer IC (LIS331HHTR), which is going to be used in addition with the capacitance data for the exploration of better post processing techniques. This is a key point from Chapter 3 where the second study faced many issues due to the motion artefacts from the body movement. The other sensor is a real time clock (RTC), which is used for the time keeping of the system while its in a shutdown state. The M41T62LC6F chip is used due to the low power requirements and small scale.

For power, two options were used for the final two designs. One design used a single coin cell (CR2032) with a capacity of 220mAh to power all the electronics. While the other final design used a rechargeable 190mAh Lithium Polymer (Li-Po) battery. In the previous designs there was an extra coin cell battery (CR1225) that was used for the timekeeping of the RTC in case the main battery is disconnected, but this was later removed due to the space requirements and the practicality of having two batteries in a small system.

The inputs for the system are two components, the small push button and the micro-SD card. The micro-SD card is used to data log the sensor data, with two LED indicators (red and green) to indicate whether or not the device is active or in sleep mode. And the push button is used to start and stop the sampling as well as restart the device. Table 5.1 shows the overall specification of the hardware used for both designs, while Figure 5.2 shows the two iteration's assembled side by side. The key difference is that the hardware side is flipped to the top side for the Li-Po version when compared against the CR2032 version, as the battery is protected in a 3D-printed case and sandwiched by the PCB. The schematic for both PCB designs can be seen in Appendix C.

Both sensor systems were mounted on a 3D printed case that served to house the electronics and protect them. This is one of the risks this sensor system has as the Li-Po battery design must protect the battery from both damage and shorts. As looking back at the experiments done in Chapter 3, sweat was a big problem for the sensors. And it could still pose a higher risk for the battery. Thus the case design was built to protect the battery rather than just house it. Figure 5.1 shows a render of the 3D design of the case.

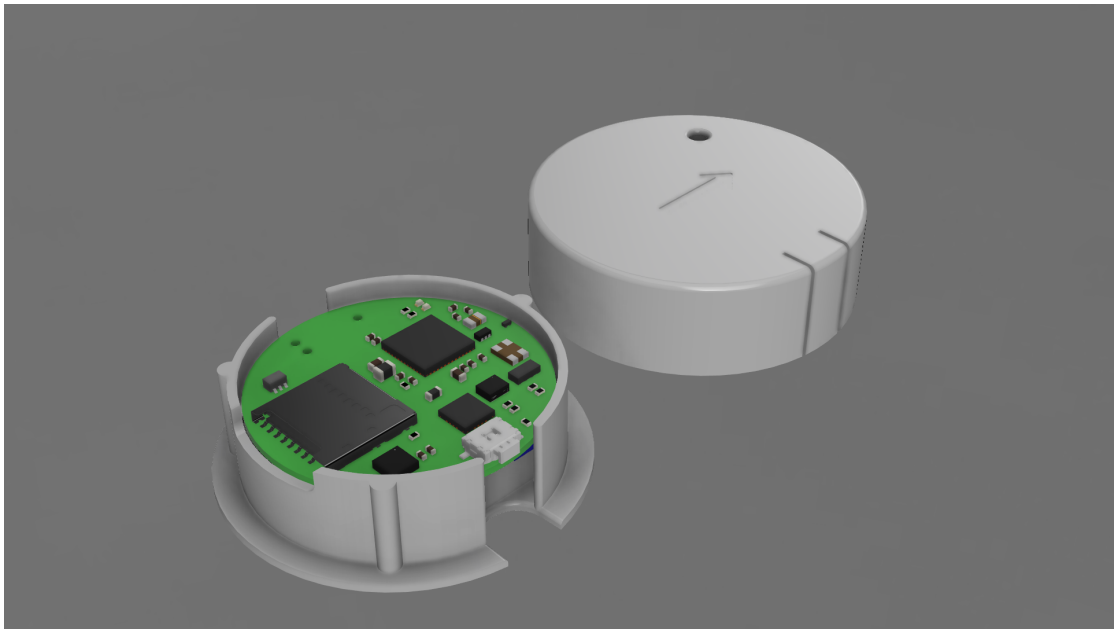

FIGURE 5.1: Render of the 3D printed case used for the Li-Po battery system.

5.1.1.2 Data Integrity and Timing Testing

The data integrity tests are done to ensure that data loss is minimal, which includes the data which is influenced by noise from the system (normally happens at low voltage levels). It also aims to test the timing of the device and ensures its accuracy. The tests conducted are seen below:

TABLE 5.1: Sensor system specification, detailing the main components used in the design.

Specification for the Sensor System PCB	
Processor	Main micro controller is CC2640R2F Bluetooth LE micro controller (128kB Flash Memory running at 24MHz).
Sensors	FDC2214 Capacitance IC, M41T62LC6F Real Time Clock, and LIS331HHTR as an accelerometer.
Power Input	CR2032 coin cell battery (Capacity of 200-220 mAh) or 190 mAh Rechargeable Li-Po Battery.
User Inputs	One Button for control, and a micro-SD card for data storage (up to 16 GB in size).
Dimensions	32mm in diameter with a thickness of 0.8mm.
Weight	10 grams (With the battery and sensor installed) 6 grams without.

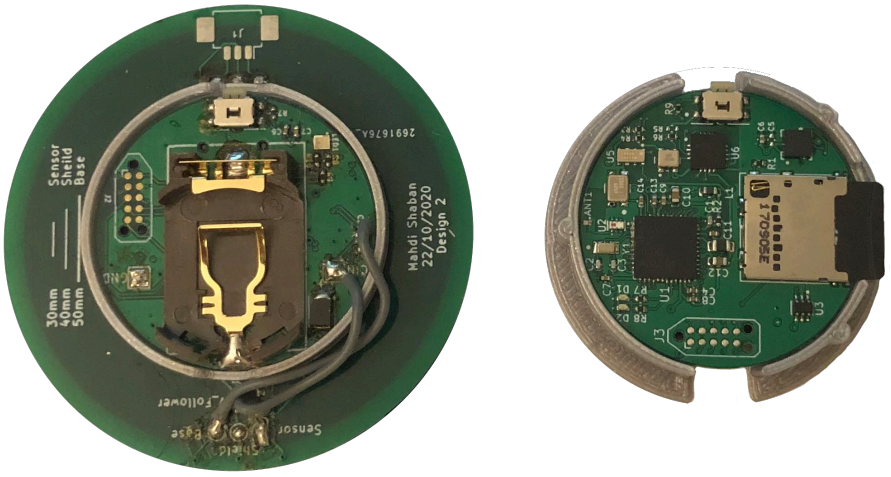

FIGURE 5.2: Final sensor systems developed with sensors attached to them. On the left is the rigid sensor design 2, and on the right is the flexible sensor design 1.

- The first test is the ADC test which will run a signal generator at a specified frequency for a ten minutes to make sure that the frequency captured is the same as the one generated.
- The second test will have the Testing the system against a metronome to test the data accuracy in a controlled scenario. The test will be 5 minutes long and the results will be compared against a belt sensor for validation.
- The third set of tests is the walk test which is done with a belt sensor to compare signals captured alongside the sensor system data. The test will be 5 minutes long.

- The final tests are long duration tests that run till the device runs out of battery (Sampling both respiration and accelerometer data). This test will be conducted for a minimum of 6 hours. No belt will be used for comparison as the belt is uncomfortable to wear for more than a few hours.

For the first test, the ADC test, it is the simplest test to perform out of all the other tests. It is done by connecting a single ADC pin in the sensor system MCU to the output of a signal generator. The signal generator was set to output a 0.3Hz sine wave signal simulating a person breathing at 18 breaths per minute. The data from the signal generator was sampled on the hardware at a rate of 20Hz. Figure 5.3 shows the output data over the span of 10 minutes to check for any data loss. The processed signal showed a frequency which was equal to 0.3Hz, hence proving the timing of the system is well within the required accuracy for sampling at 20Hz. The data was processed by having the signal generate a spectrogram with a window size of 60 seconds and a 90 percent overlap. And by tracing the maximum strength at each point a trace of the frequency changes can be extracted. A more detailed explanation is found in the software section of this chapter which details both the hardware firmware and the processing software and method used.

For the rest of the three tests, the results can be seen in the results section of this chapter.

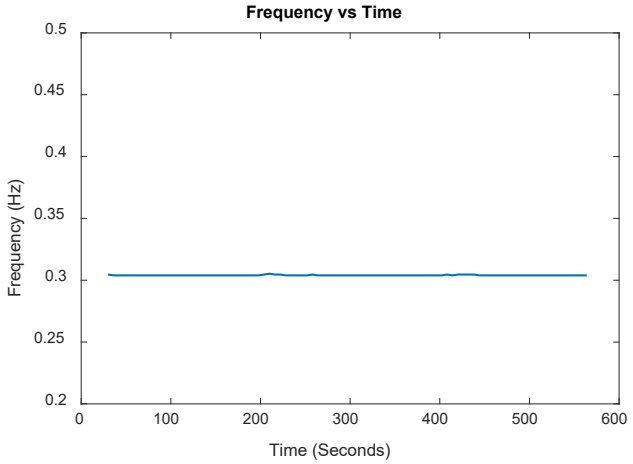

FIGURE 5.3: ADC test results, tested over the span of ten minutes.

5.1.1.3 Use-case Testing

The use case testing is a list of possible scenarios that the user will be preforming. This allows for predictable behaviour and proper assessment of what went wrong if the device fails at any instance. This allows for the software to have fail safe measures in case any of these scenarios are met during the testing phase.

TABLE 5.2: Use Case Testing Table

Use Case	Expected Result	Implemented?
SD card is ejected while sampling.	Sampling should stop and flash a red-light indicating failure in writing data. And hence waits for the SD card to be reinserted to restart sampling.	✓
SD card is not inserted when clicking the sample button.	A quick flash of the red light to indicate that something is not connected, or an error has occurred.	✓
SD card is inserted, and the sample button is pressed once.	A green light will flash every second to indicate that the device is sampling, and no error has occurred.	✓
Power is lost while the device is sampling (battery disconnected), and is then reconnected.	Device will fully restart as well as the RTC module which will need to be re synced. The device will start as normal just with the RTC module being out of sync (i.e 0 hrs 0 mins).	✓
Battery voltage drops below operating voltage of sensors.	Data will fail to sample, and a red light will flash instead of a green one.	✓
SD card fills up while sampling.	Red light will flash while sampling to indicate that the SD card is full. This will also safely stop sampling and go to sleep mode.	✓
Sample Button is pressed for 5 seconds while sampling.	The device will safely close the file and stops sampling. The device enters sleep mode.	✓

Currently the list in Table 5.2 are the only implemented fail safe scenarios, however, they are more than enough for the sensor system to sample data continuously and accurately for long periods of time. The implementation strategy is to focus on the behaviours from the software side, which means there are no hardware fail safes implemented and only software ones.

5.1.1.4 Power Testing

For the power testing three different tests are used in testing to ensure that the sensor system adheres within the specifications needed. These tests target the maximum and average power draw of the sensor system, failure points and battery life tests for both the coin cell battery and the Li-Po. A list of all the tests is outlined below:

- The first test tests the current consumption of the sensor system without having any input connected (micro-SD card) and the device is not in data logging mode.

- The second test is the minimum voltage test which finds the failure point of the device (i.e The point at which the device does not start or the data is no longer getting logged) by slowly reducing the input voltage .
- Lastly a long term test is conducted by letting the device run on a new battery/-fully recharged battery to test the total run time of the device until the device or data logging stops or fails. The test's conclusion is indicated by the flashing LED light which stops flashing when the battery is drained.

The tests were conducted in a lab with the battery voltage monitored and stored through a digital multi meter over the entire duration of the test. The data is stored in a comma separated values (CSV) file and is compiled into the results table found below (Table 5.3) though the use of MATLAB (2019).

TABLE 5.3: Power testing results for both the CR2032 coin cell PCB and the Li-Po battery PCB.

	CR2032 Battery	**Li-Po Battery**
Average Current Draw	2.45 mA	2.45 mA
Minimum System Voltage	2.5 V	3.0 V
Total run time of the system	45 Hours	70 Hours

The results from Table 5.3, shows that the average current draw for the system is approximately 2.45 mA rounded up for both the PCB's which is expected as the hardware is exactly the same. This means that with a CR2032 cell which has a capacity of 220 mAh (Panasonic, 2005) the system will have an average run time of approximately 90 hours. And a Li-Po battery with a capacity of 190 mAh will have an average run time of approximately 78 hours. However the actual value does not match the expected results due to sharp current spikes in the system whenever the data is written to the micro-SD card, which according to the data sheet for most micro-SD cards are upwards of 100 mA when writing large files (SanDisk Corporation, 2015). Nonetheless, this is more than good enough as the data captured is better and longer. And from the results of the tests the value of 45 hours was found to be the limit at which the device can sample continuously for the CR2032 battery while the Li-Po battery resulted in 70 hours. The main reason for this is that Li-Po batteries have a much higher current limit that the battery can supply. And with a high current component such as a micro-SD card the CR2032 struggled to supply that much current, even in bursts. Thus by recalculating the current of the coin cell from the results, it gives out a capacity of 110 mAh which is more reasonable considering the current draws.

As for the minimum system voltage it is tested by finding the failure point, in which the micro-SD card failed to write the data properly, this was tested to be at voltages below 2.5V for the CR2032 system. During the total run time test the actual voltage dropped below 2.5V however this was during the writing cycle, while the data acquisition from

the sensors had the battery maintained a voltage of 2.9V. This can be seen in Figure 5.4 where the hardware was run for 20 hours using a CR2032 battery. The battery voltage did not start from 3V as the battery was used from the previous testing and because it was closer to the minimum voltage needed. This test ran till the device failed to write to the micro-SD card by itself. As for the Li-Po battery system, the battery did not have sharp spikes in the voltage as the maximum current drained by the system was being supplied by the battery. Thus resulting in a sharp cutoff at 3.0V due to the battery management IC in the battery stopping the cells from discharging in order to not damage the batteries.

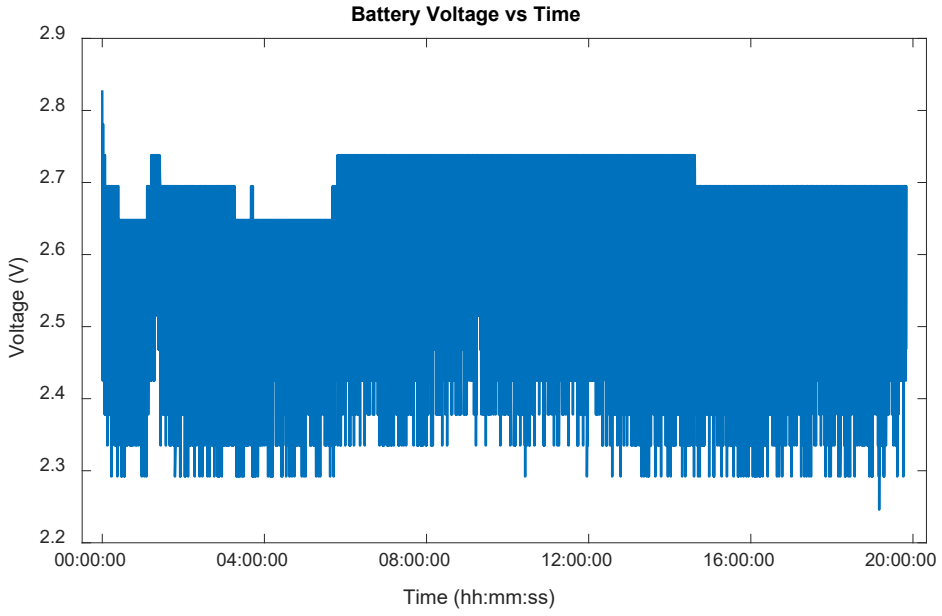

FIGURE 5.4: Battery Voltage test results for a duration of 20 hours with the CR2032 battery.

5.1.2 Software Development

The software aspect of this paper is split into two parts, the processing algorithms and the accompanying micro controller firmware that will do the main data logging. The post processing is done in MATLAB (2019) and will expand upon the work developed in Chapter 3. While the micro controller firmware is programmed through Texas Instrument's proprietary software, Code Composer Studio and Sensor Controller Studio (Texas Instruments Incorporated., 2020)

5.1.2.1 Micro Controller Firmware

The current micro controller hardware, supports both local storage using the micro-SD card connector, and the use of Bluetooth Low Energy (BLE) for connectivity and data

logging. However, for the current prototype the data logging is implemented in a more refined manner to allow reliable acquisition of respiration data for further processing, and the Bluetooth only works for demonstration as there is no application to interface with it yet.

The micro controller code was written in C while also making use of TI-RTOS which is a (Real time operating system) RTOS provided by Texas Instruments. This allowed for the code to be more structured as well as utilising many of the features the MCU offers. The main feature with this MCU is the sensor controller, which is a smaller MCU that is interconnected with the main CPU internally. This controller can run separately from the main CPU allowing for higher power optimisations while also ensuring that the sensors will always be sampled even if the main CPU is busy.

To utilise this feature a task operation diagram is constructed to show the appropriate timeline for when the user starts logging data. This diagram helps when coding the actual code and for testing and debugging in case of any failures. This diagram can be seen in Figure 5.5. This is done only for the data logging part, where the other parts of the code are simple to implement and do not need a task diagram.

The main part of this diagram is the initial start and the repeating tasks. For the initialisation the Datalogger task turns the micro-SD card on, initialises a file name, creates the file, and finally return a boolean indicating success or failure. Internal checks in the function check if there is space in the micro-SD card, and if the file name is a duplicate and if so creates a new file incremented by two digits starting from zero. Parts of this code can be seen in Appendix D. During the repeating task portion of the code, semaphores are used to send the interrupts from the sensor controller indicating that the data is ready to be written to the micro-SD card file. This section is critical as the maximum sampling rate is determined from the CPU side and not the sensor controller side, where the timing is calculated on the higher resolution timer of the main CPU. After many iterations a timing method was selected to ensure that the sample rate does not drift throughout long data logging sessions. The method calculates the amount of time the sensor controller takes to take one sample, and then based on the sample rate finds the amount of time remaining for the task to start another sample. Thus putting the task into sleep mode for the remainder of time for that one sample. This method ensures that even if the sample rate from the sensor controller studio fluctuates the resulting sample rate from the sensor system is stable while data logging.

The data coming from the sensor controller goes through the Datalogger task which in turns stores it in a global buffer which is shared by the SD write task and the Datalogger task. This buffer has two states to ensure that at no instance of time the data that is written to the micro-SD card is overwritten by the sensor controller. The SD write task uses a FATFS file system to write the data into a .TXT file. The file written prints a header showing the sample rate as well as the other sensor data.

Finally during the run time state, the LED task is continuously reading a global volatile variable which checks if the device is sampling, or if there is any error flag from any of the other tasks. This allows independent control of the LED's to allow for custom error led messages.

Once the main tasks are coded, a flow chart is constructed to represent the full flow of the system and can be seen in Figure 5.6. The firmware was developed over many iterations and changed throughout many hardware changes.

Future upgrades are relatively straight forward with extra additional tasks to be implemented in order to turn on the BLE and communicate with external devices. The code was left in a state where the framework was written but not implemented completely.

The sensor controller code initialises the sensors to be in the highest resolution possible. This is mainly for the CDC IC which is sampling 28-bit data at a sample rate of 10Hz and up to 40Hz that can be configured in the firmware. This mode makes the sensor IC sample without a power limit hence the sensor was power cycled per sample to reduce the current consumption.

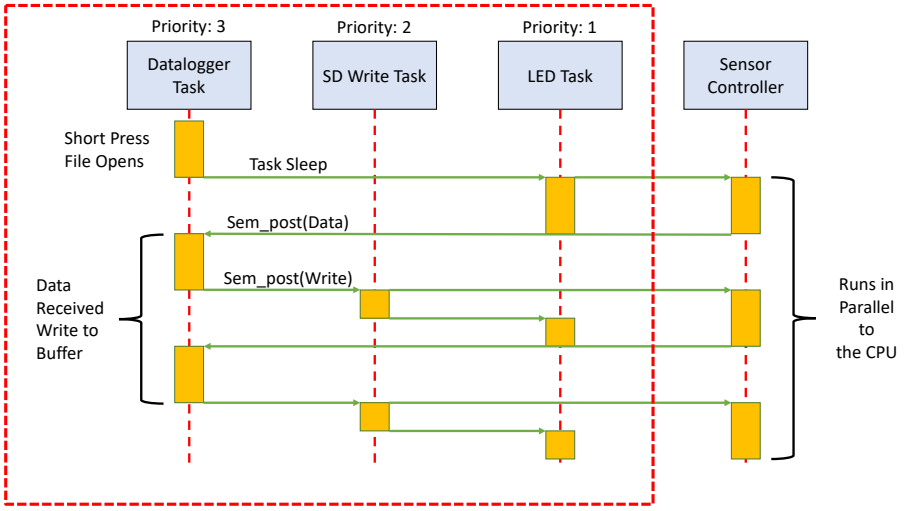

FIGURE 5.5: RTOS task diagram during the operation of the data logging. The tasks are repeating for the entirety of the data logging.

5.1.2.2 Processing Software

For the processing of the data, a GUI was built in MATLAB (2019) to allow the data gathered from the sensor system to be easily processed into readable data. The scripts also allows for direct comparison of belt sensor data. The main MATLAB (2019) script that converts the raw data to respiration rate is used for both the sensor system data and the belt data. This makes sure that the two different signals are compared fairly. This is different from the results in Chapter 3 in which the compared respiratory data

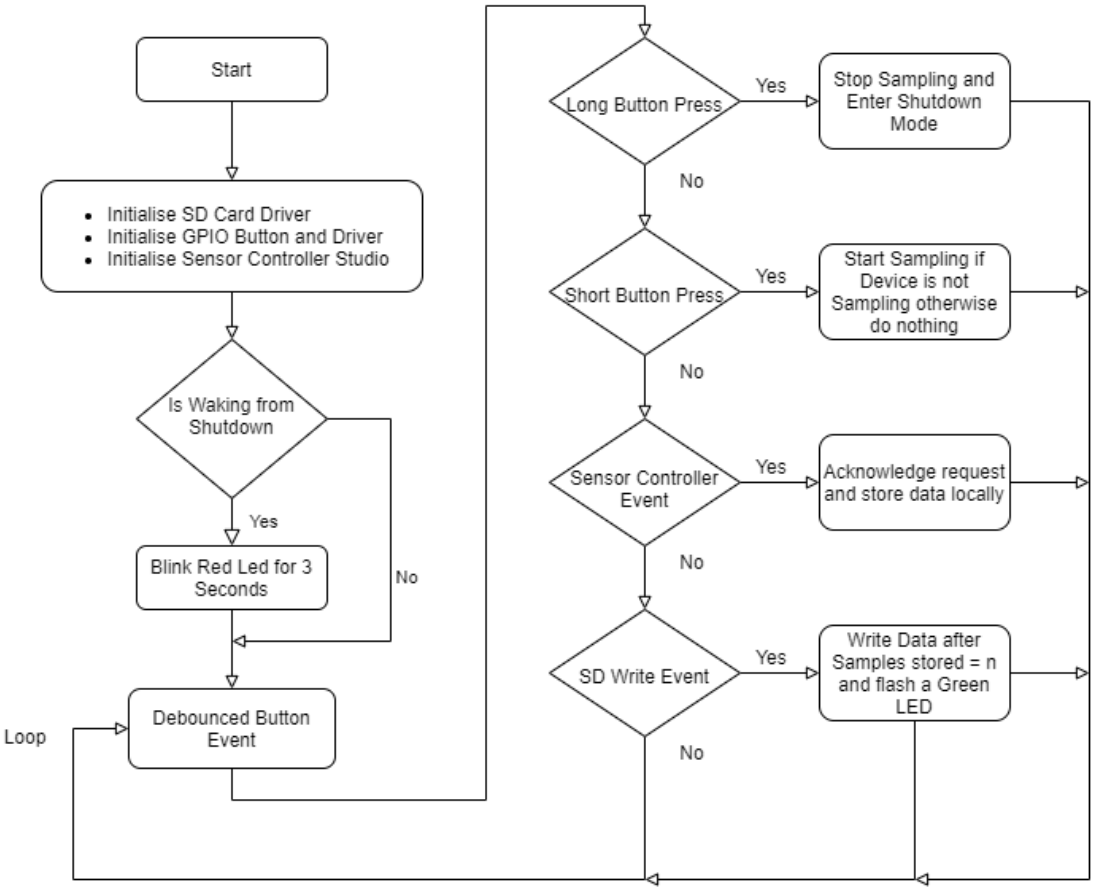

FIGURE 5.6: Flow chart for the sensor system simplified with the main functions shown.

is already calculated. As for the comparison the same Bland Altman plot will be used to convey the results from all the tests in this chapter. Direct compare figures are also going to be plotted to demonstrate the results in the time scale and in the Bland Altman plot.

The main method developed builds upon the spectrogram method that was initially explored in Chapter 3 which is more superior than the peak detection method, this is more apparent in noisy signals. Hence the method of calculating the respiration rate, is split into three different steps that can be found in Figure 5.7. The first step is to have the signal trimmed to the appropriate captured signal. This step is to ensure that any noise captured from the start of the test til the end is not included in the processed data. The trimming at this stage is manually calculated for each test. The second step is to apply the filters to the trimmed signals. The first filter applied is a high pass filter that is configured at a frequency of 0.02 Hz (1.2 BPM) to allow all frequencies above it to pass, this filter is used to remove any bias that is in the signal. The second filter is to apply a low pass filter set at a frequency of 1 Hz (60 BPM) to allow only frequencies up to 1 Hz to remain in the signal. Lastly the resulting filtered and trimmed signal is then run through a spectrogram with a sampling frequency that is equal to

the sample rate of the tests, and a window size of 60 seconds (Kaiser Window) with an overlap of 90% and leakage of 0. The values for the window and overlap used are based on the resolution needed, in this case the resulting window and overlap result in a 6 seconds interval between each point in the spectrogram in the time axis. The 60 seconds window size is determined by the minimum amount of signal needed to be present in order to calculate the frequency at that window. In this case 60 seconds is the minimum value needed to calculate the frequency of breathing for a person, hence resulting in minutely frequency windows with the maximum power representing the dominant frequency in that window. The 90% overlap is the parameter that tunes the resolution and speed at which the spectrogram is calculated, in this case 90% is a suitable value that gives a high enough resolution for calculating respiration rate. For a much higher resolution analysis a value of 99% is used to get a resolution of 0.6 seconds per time step. An example of this process can be seen in Figure 5.8 below which demonstrates the signal cleaning process into a spectrogram.

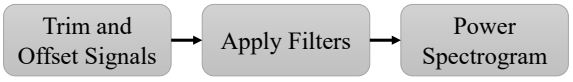

FIGURE 5.7: Three step process of cleaning the data into a spectrogram.

Finally to get the respiration rate a trace of the dominant frequency per time step is calculated and traced in order to get the change of frequency over time. This is converted to BPM by multiplying the frequency by 60 seconds. The process is not perfect as sometimes the identified dominant frequency at a given time step is abnormally different from the previous and next time step. To solve this issue a limit of change is introduced to check the next maximum change that is within the given set width, this process is then repeated for the next set of values until a trace is found. This method allows calibration of the maximum change that can be present within a signal. This method already exists as a function in MATLAB (2019) called ”tfridge” which is used throughout the testing process. Understating the way the function works allows for future development of the processing software to be filly embedded on to the MCU side. This process is repeated between both the belt data and the sensor system data and the results are compared through a Bland Altman Plot with the truth being the data from the belt sensor. Figure 5.9 presents an example of tracing the frequency from the spectrogram.

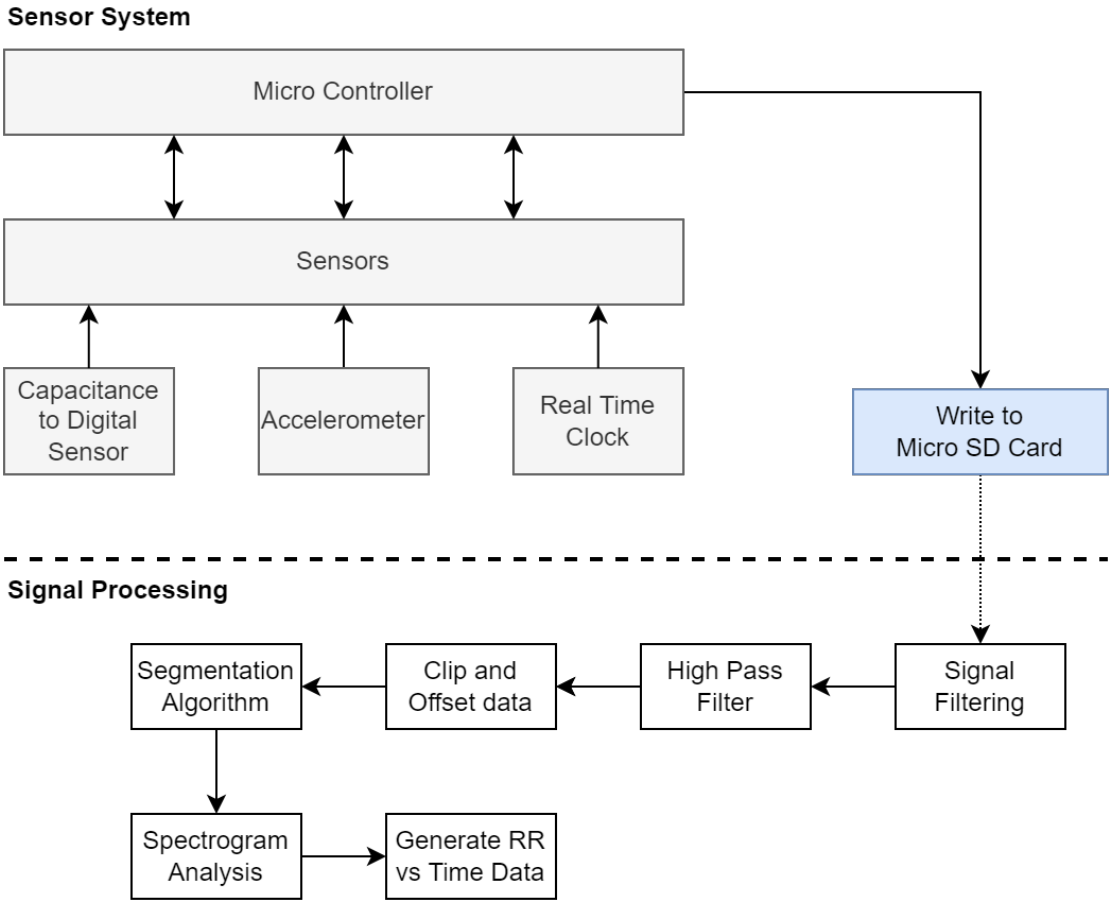

FIGURE 5.8: Shows the full block diagram of the full system from data acquisition to generating the respiration rate data.

5.2 Results

For the hardware tests, a series of simple test were conducted to assess the signal quality and accuracy, mainly for the data integrity tests. All these tests had the sensor system with the capaciflector placed on the top left side of the chest, with a single sensor in place. The sensor system was mounted through the use of a TENS gel pad, the same pads used in the testing done in Chapter 4. The data was sampled at a rate of 10 Hz alongside the belt which sampled at the same rate. The same Go Direct^{TM} Respiration belt was used throughout these tests.

5.2.1 Metronome Test Result

The simplest of these tests is the metronome test which is a controlled breathing exercise that uses a known metronome frequency. For this hardware validation test, metronome tests between 2 and 4 minutes were preformed and one of them was evaluated against the belt sensor data.

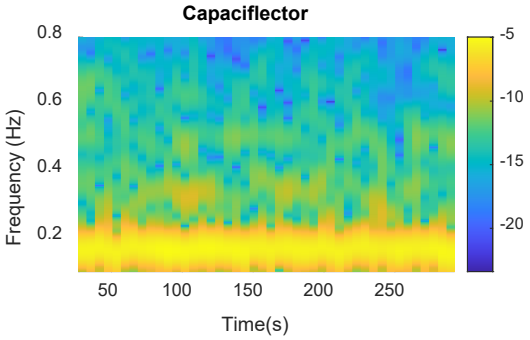

(A) Resulting spectrogram before the frequency tracing is done, in this example a clear dominant frequency is seen.

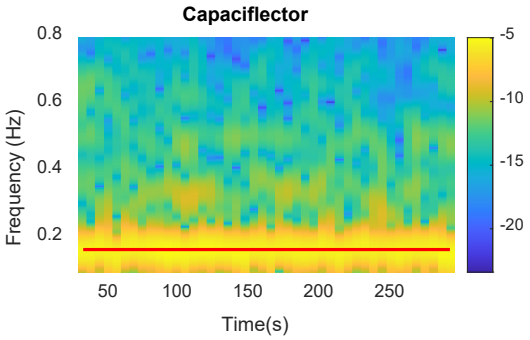

(B) Spectrogram example of the traced frequency.

FIGURE 5.9: Frequency tracing example before and after.

The four tests were performed with metronome values of 13, 13, 14, and 15 BPM respectively. The 13 BPM tests were sampled in tow different positions: laying down and sitting upright on a chair. The 14 BPM test was done by sitting upright on a chair while the 15 BPM test was done by laying down. Figure 5.10 shows the raw data sampled from the sensor from the 13 BPM sitting test, which is then processed through MATLAB (2019) to get the respiration rate change per minute. Comparison between the result and the known frequency shows that the 13 BPM test resulted in a value of 12.91 ± 0.03 BPM. The figure also shows the resulting spectrogram with the traced signal output. As for the rest of the results (13 BPM Laying and 15 BPM laying) they can be seen in Figure 5.11 where only the results are shown, and by comparing them against the known frequencies we get 13 ± 0.1 BPM and 15.05 ± 0.1 BPM respectively. And even though all of the samples were short tests of less than 5 minutes they still hold good information on the sampling accuracy. Thus resulting in a good accuracy against a static known frequency.

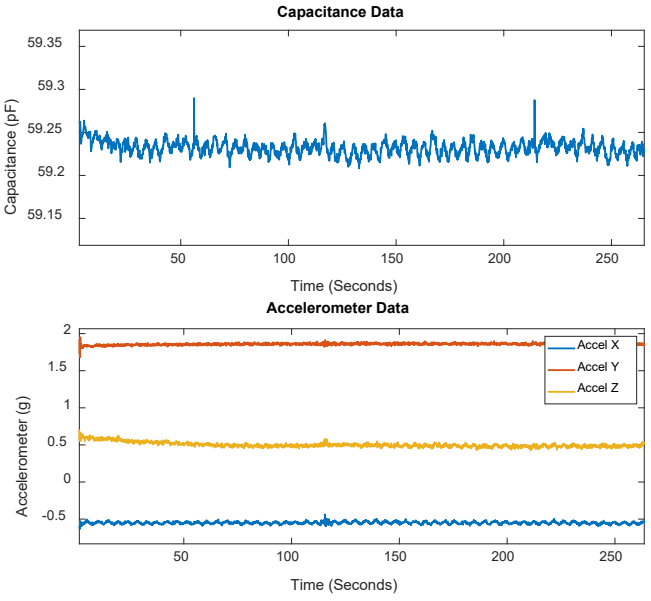

(A) Raw capacitance and accelerometer data from the metronome 13 BPM test.

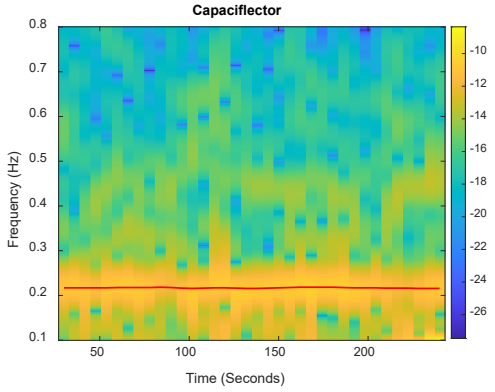

(B) Processed data spectrogram for the capaciflector data.

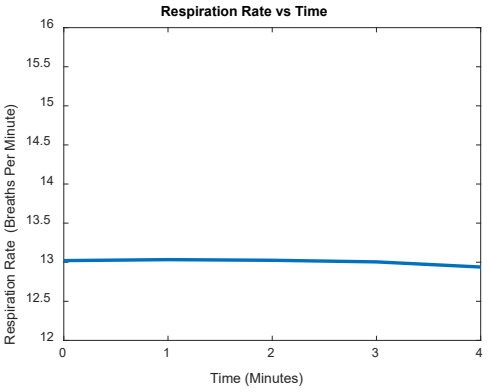

(C) Respiration rate plot for the 13 BPM test.

FIGURE 5.10: Raw and processed results for the 13 BPM sitting metronome test.

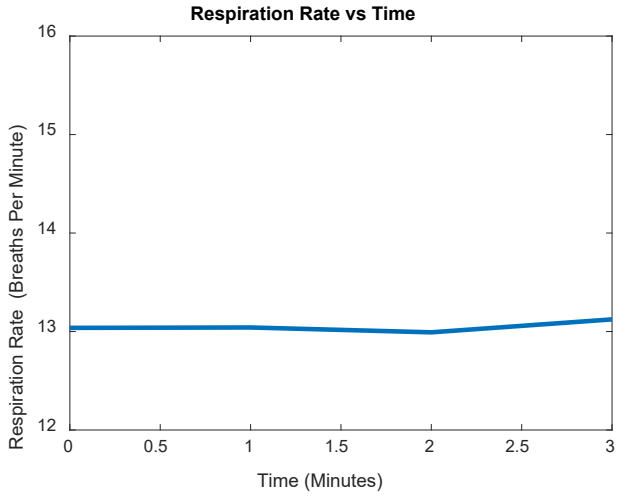

(A) Results from the processed 13 BPM laying down metronome test.

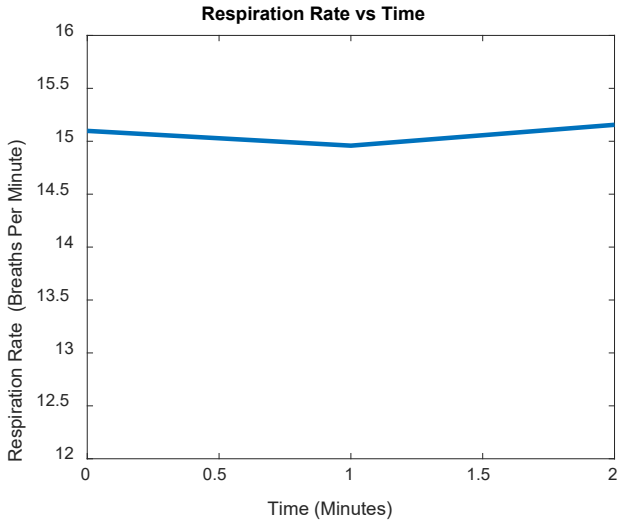

(B) Results from the processed 15 BPM laying down metronome test.

FIGURE 5.11: Processed results for the 13 and 15 BPM laying down metronome tests.

5.2.1.1 Belt Metronome Comparison

The metronome test is performed at 14 BPM with the belt sensor and sensor system was synchronised manually by starting both of the sensors at the same time. The data is then processed by the use of the same techniques mentioned previously. The resulting values are used to create a Bland Altman plot which compares the two resulting signal values. This can be seen in Figure 5.12b. A direct view can also be seen in Figure 5.12a which allows for a more visual comparison to be seen . The results from running the 14 BPM test resulted in -0.38 ± 0.11 BPM from the Bland Altman. The results do have a negative bias which means the sensor values are higher than the belt data, but the limits of agreement are within 0.11 BPM which is well within the required accuracy for the sensor system to be compared against a gold standard. Nonetheless, the results

from this test validate that the timing is within the required accuracy and that the new hardware is ready for longer and more dynamic tests.

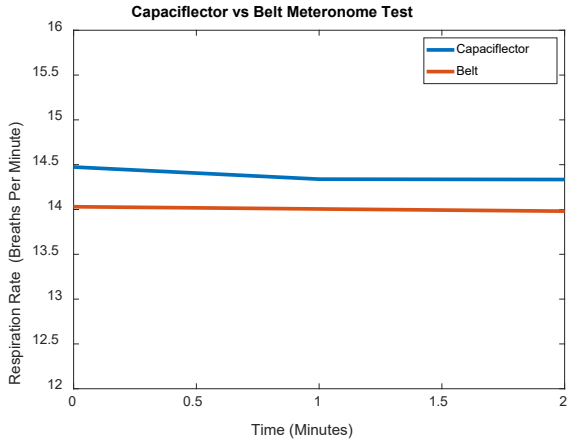

(A) Respiration rate compare plot for the 14 BPM metronome test.

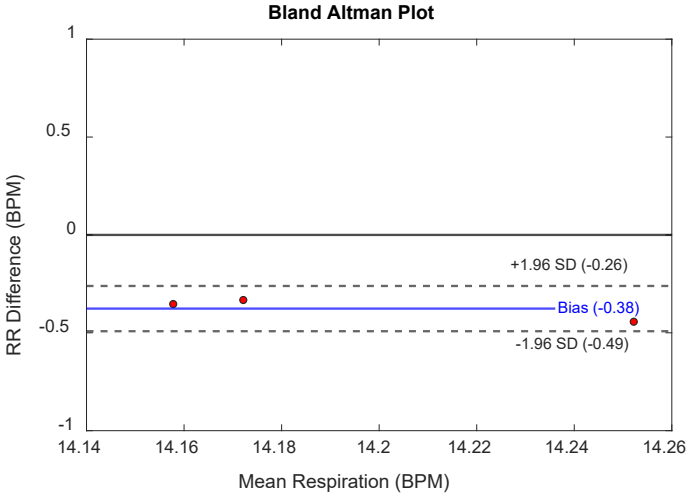

(B) Resulting Bland Altman Plot for the 14 BPM metronome test

FIGURE 5.12: Processed results for the 14 BPM metronome test.

5.2.2 Walking Test Result

As for the walking test a single five minute test was conducted which included a couple of stops where two deep breaths were taken, this allows for a peak to peak synchronisation in software at those time instances. The belt and sensor were mounted in the same position as the metronome test. The GUI was used to compare both results as well as generating a Bland Altman Plot.

Figure 5.13 shows the raw captured results as well as a segment of the raw signal from the sensor system compared against the belt sensor, and also the processed results. The Bland Altman results in an accuracy of -0.24 ± 0.08 BPM, which can be seen in

Figure 5.13c and visually in Figure 5.13b. The walking introduced moving artefacts in the raw signal which are filtered down by the low pas filter which is run throughout the entire raw signal. The current algorithm does not separate the walking segments from the non walking segments which means when the signal is filtered a large amount of data is lost due to the walking noise. For the next steps, an implementation of the signal segmentation process must be developed to allow segmented processing of the signal. Overall for the walking test the sensor system demonstrated high accuracy even for a short term test. Thus even in an un-optimised state it shows promising results for a sensor system that can be used outside a hospital environment.

5.2.3 Long Term Test Result

For the long term test a sleeping test was conducted for 6 hours. The test was done without the belt sensor, this is due to the uncomfortability factor which made it hard to wear the belt for periods more than 1 hour. The sensor system was mounted with the TENS gel pad on the top left side of the chest. This test is performed to test signal stability and the capability of continuously monitoring for periods longer than 1 hour.

After acquiring and processing the data the compiled results using the algorithms developed is seen in Figure 5.14. When looking at the raw data the accelerometer captured movements during sleep, both in different orientations such as sleeping on the side and sleeping on the back. The result from running the data through the spectrogram analysis resulted in a some flat areas in the signal, this corresponds to the minimum and maximum limits the spectrogram is set at. The limits were set to be from 6 to 48 BMP (0.1 to 0.8Hz). As for the breathing rate that was captured, the results do have some noise in the change however, the key point to note is that the x axis scale is 6 hours which means these changes happen over large portions of time. The resulting signal was also processed with 6 second points meaning many of these points correspond to the change of respiration rate every 6 seconds. To cross validate some sections of the signal which have clear defined breathing data, the peaks were counted and cross verified. This was only done for a small portion of the signal. The dips in the signal are the corresponding points in which there was movement present in the data, and with the current method, data with movement artefacts is not processed differently from clean breathing data.

Overall the sleeping test demonstrated the capability of the sensor to monitor respiration rate continuously. As well as showing that the sensor system is capable of capturing stable signals in a stable setting.

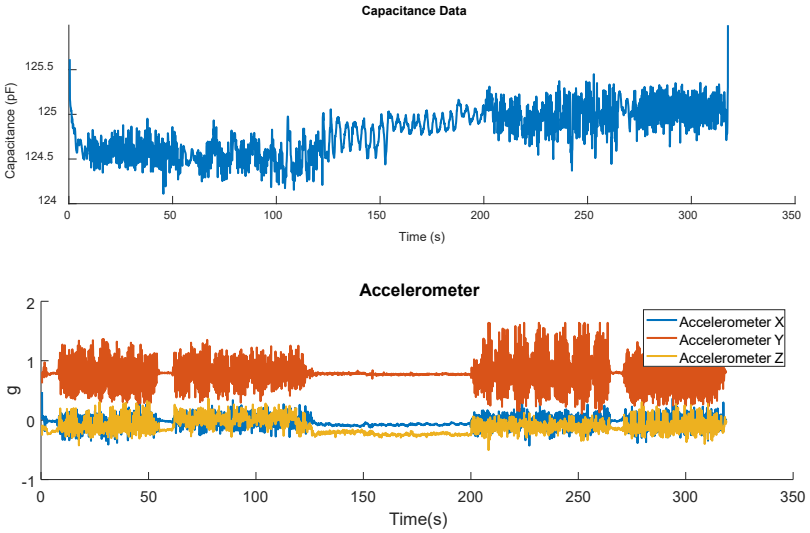

(A) Raw capacitance and accelerometer data from the walking test.

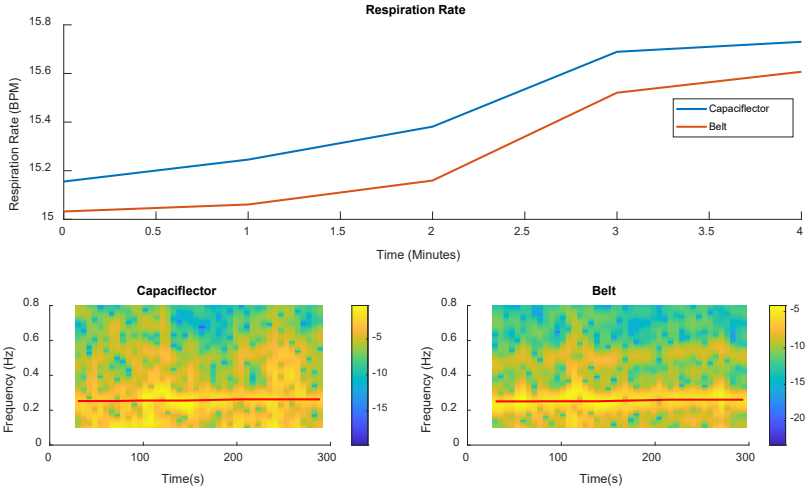

(B) Processed data alongside the spectrograms for the respective sensors.

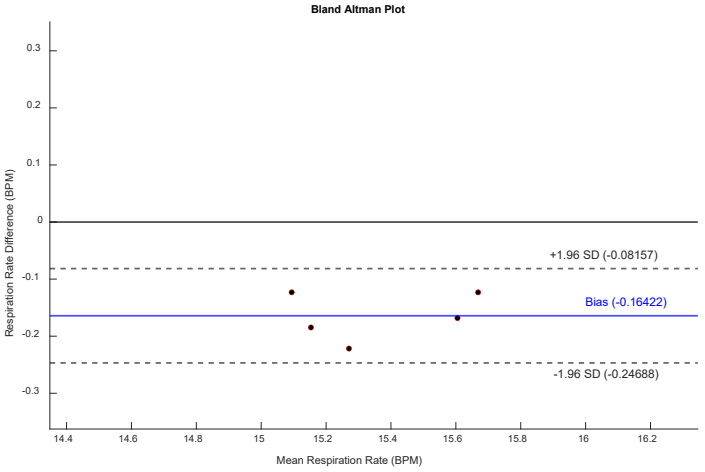

(C) Bland Altman Plot for the two resulting sensor data.

FIGURE 5.13: Walking test results and raw data.

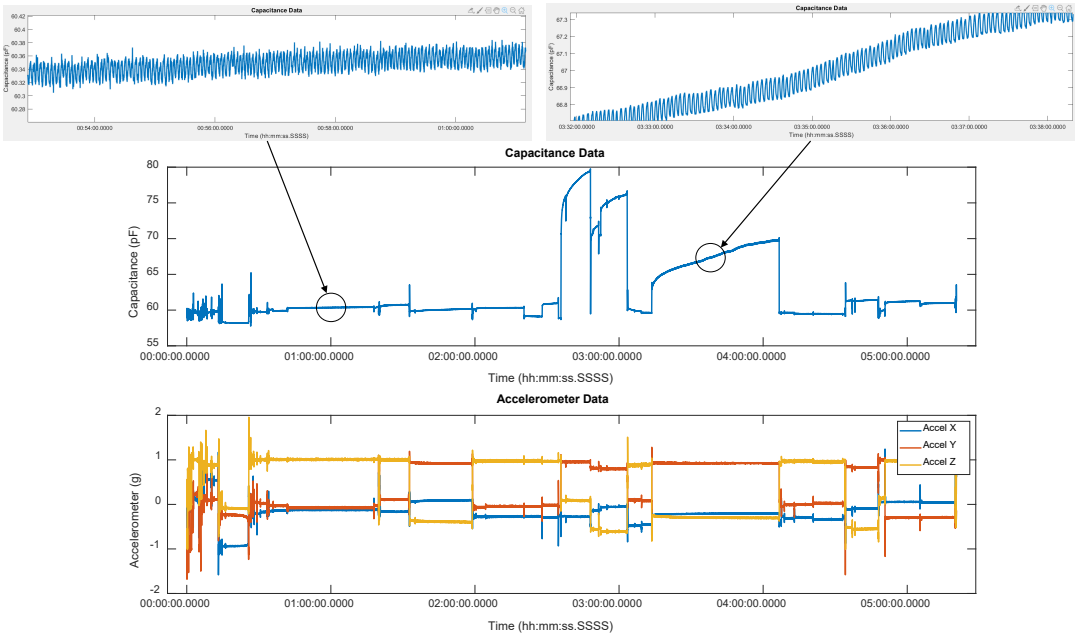

(A) Raw capacitance and accelerometer data for the sleeping test, some sections are zoomed in to show the actual signal.

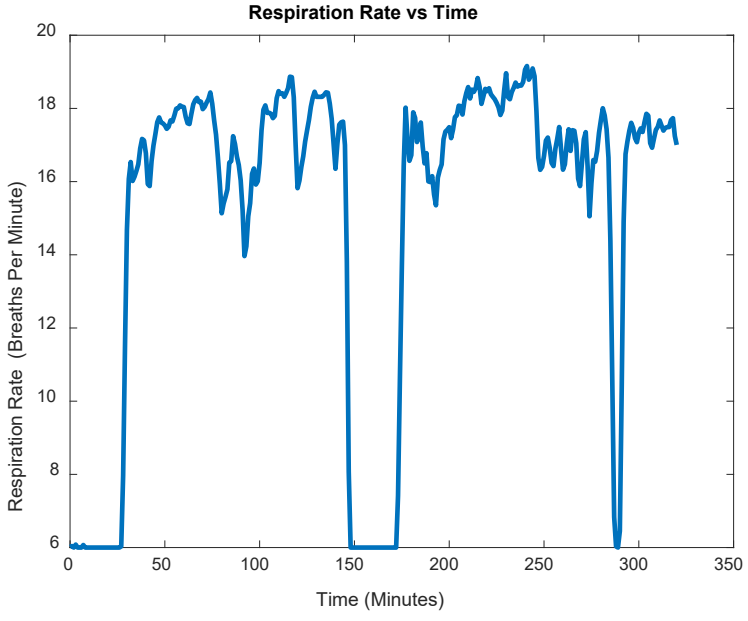

(B) Resulting respiration rate plot for the sleeping test.

FIGURE 5.14: Raw and Processed results for long sleeping test.

5.3 Analysis

The post processed values from the different tests showed very promising results. Especially in the long 6 hour sleeping test where the new hardware managed to successfully capture the sleeping frequency even with occasional body movement. Even after manually counting some of the data points to verify, this shows that the new sensor system hardware is capable of capturing respiration rate continuously.

The metronome data also displayed good results where the values calculated matched the metronome values closely within a tenth of a breath. This leads to the comparison of the belt and the sensor system where the resulting Bland Altman generated showed results from the hardware that are as good as the belt sensor. Overall for the metronome results, they show that a sensor in a controlled test it can be as comparable as a belt sensor which can be considered close to a gold standard respiration sensor. But with the advantage of being comfortable to wear, while being small and compact when compared to the belt style sensors.

For the walking test, even though it is a short test it managed to capture the appropriate breathing data from the sensor system during a walking event. The results are better than expected with the walking test achieving results within ± 1 BPM. These results are processed through a filtration stage which does not target walking segments. Nonetheless the test managed to show that the data captured from the capaciflector and the sensor system is good enough for most applications, while also being accurate enough to be used in a home environment. And for this stage of testing, the results are expected.

Lastly for the long sleeping test, this test targeted the capability of the sensor system to continuously monitor respiration rate. And it succeeded in demonstrating that, as well as showing that the signal quality for the sensor system is good even with basic filtration. Overall the tests all passed the data integrity and timing testing showing that the system is ready for more large scale testing.

5.4 Chapter Summary

The chapter successfully demonstrated the process of developing and testing the new system. The sensor system developed ended up being 32mm in diameter while being 11 mm high in a fully enclosed 3D printed case.

For the developed sensor system, the tests on the system are considered a success as the system managed to perform well in all of the tests. And when compared against the initial hardware and the analysis study performed in Chapter 3, the results from the tests done show better improvements in both accuracy as well as capabilities of

continuous monitoring of respiration rate. The tests are not perfect in any way and still have more things to improve upon, especially the processing software and methods. The key starting point is to conduct a proper study on anonymous participants to test the device across as many people as possible. This will help gather more data especially data with movement artefacts, this is to help develop and test the processing side of data with movement artefacts.

Chapter 6

Analysis and Verification of the capaciflector hardware data

The newly constructed sensor system is put to the test against a gold standard belt sensor to properly assess it in both real world scenarios and in controlled settings. The tests are done to show the effectiveness of the capaciflector, while also showing the flexibility of the capaciflector which is easily integrated in a smaller package, with the benefit of being more convenient to wear when compared to the belt sensor. The same hardware sensor system developed in Chapter 5 with the sensors selected from Chapter 4 are used for this analysis and assessment. And finally the new data is processed through the new filtration process which is mentioned at the end of Chapter 5.

6.1 Methodology

Three different studies were performed, comparing the newly developed capaciflector hardware and the belt sensor by Vernier (Go Direct^{TM} Respiration Belt). The tests were conducted on 10 healthy participants which consented on performing all the tests under the ethics approval from the University of Southampton ERGO (ERGO 68839.A1). The exclusion criteria is that the participant undergoing the tests are healthy and have no history of respiration illness. All the tests conducted were anonymous and no information on the participants is stored except the respiration data from the tests. A simple representation of the system and the mounting can be seen in Figure 6.1.

6.1.1 Hardware Details and Sensor Mounting

The capaciflector hardware is the same hardware developed in Chapter 5. The device used is the one powered by a single CR2032 coin-cell battery which allows the device

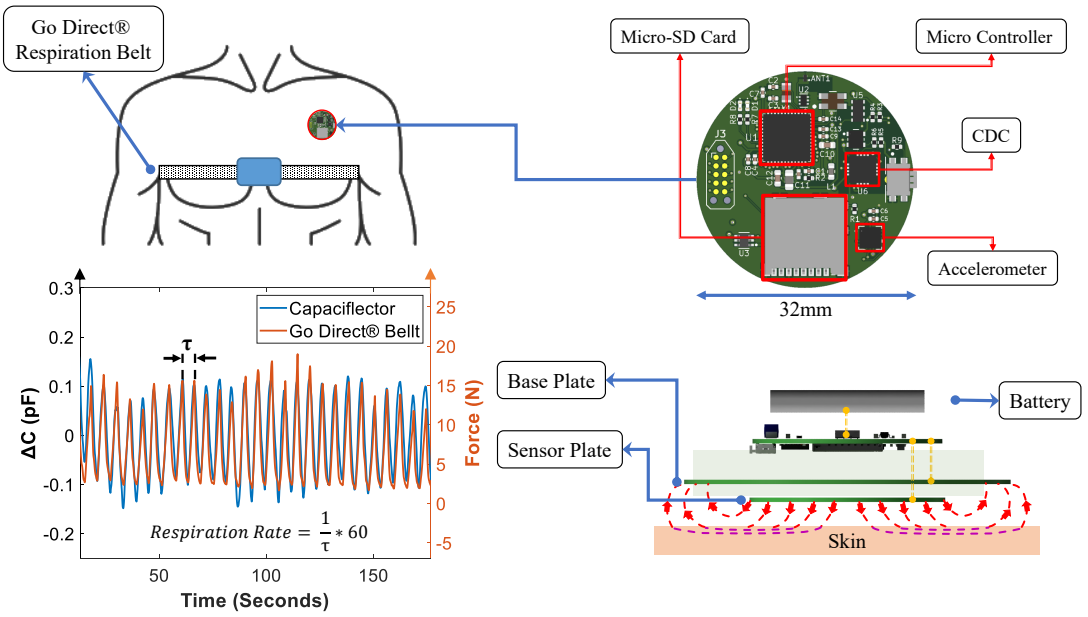

FIGURE 6.1: Overview of the respiration sensing system alongside the setup and a sample output of the comparative comparison of the belt and the capacitance based system.

to run for up to 45 hours in data logger mode. The sensor of choice is the rigid sensor design 2 developed and explored in Chapter 4., where the device is placed on top of the sensor through the use of double sided tape. The device used can be seen in Figure 6.2. The capacitance data alongside the accelerometer and RTC data is sampled at a 10Hz sampling rate and is logged onto the micro-SD card continuously once the button on the device is pressed. The sample rate of the belt sensor is also set at 10Hz. Both the belt and sensor system were untethered to a computer throughout the tests. The only thing that was connected was the belt sensor which used a Bluetooth connection to send the data.

To start the sampling between the belt sensor and the capaciflector hardware, both sensors were manually timed. However, the capaciflector sensor has a slight delay on the initial start which can sometimes make the sensor synchronisation harder as this delay is based off how long it takes the system to create the file in the micro-SD card. To deal with this problem, the participants would be tasked to hold their breath for a couple of seconds before pressing the button, which is long enough for both the sensors to start sampling data. This allows the synchronisation of the data to be easily done by finding the point in which the participant stopped holding their breath. An example on that is seen in Figure 6.3 below where the belt data clearly shows a constant force just before the participant starts breathing again.

The mounting of the sensor system was done by the use of disposable gel pads that are used for TENS (transcutaneous electrical nerve stimulation) applications (the same

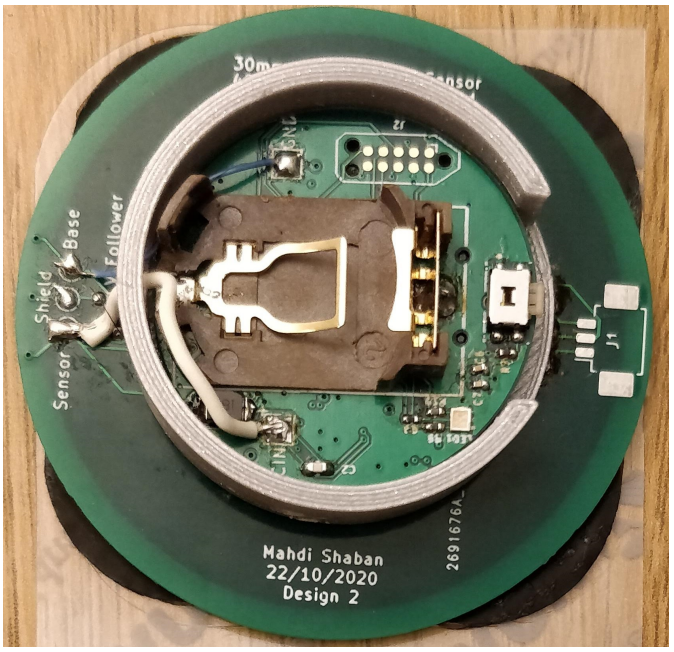

FIGURE 6.2: The newly developed Capaciflector Hardware

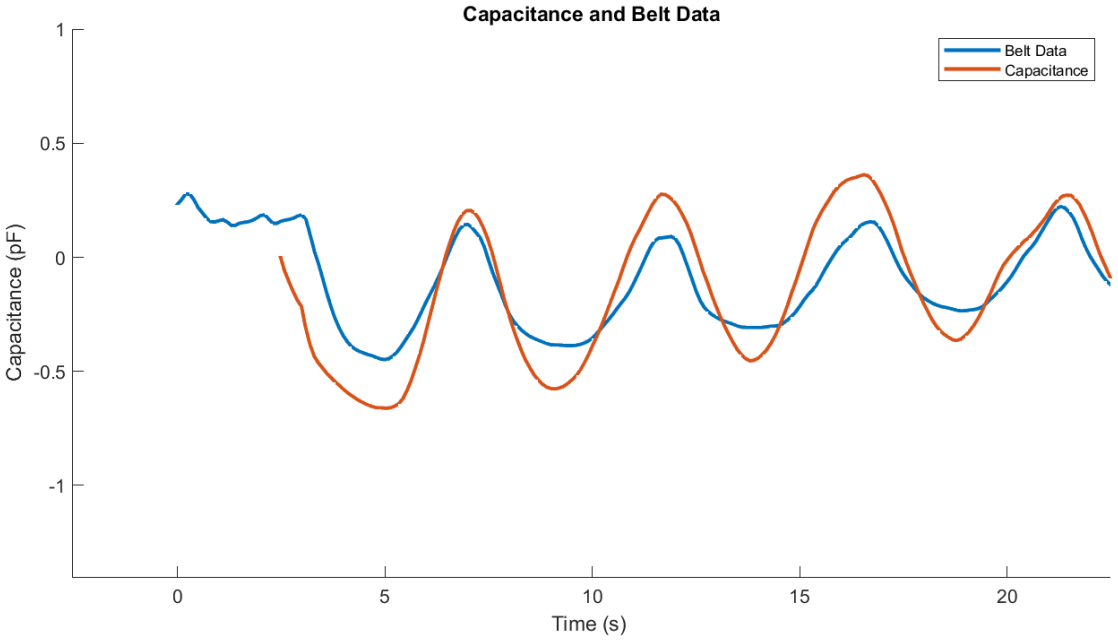

FIGURE 6.3: Capaciflector and Belt Data alignment

ones used in the tests of Chapters 4 and 5). The actual sensor plate and the gel pad's conductive material are both fully insulated to avoid any interference.

The sensor system is placed on the top left side of the chest as seen in Figure 6.4a with variability in the sensor position being either directly on the skin or the shirt, depending on the participant's preferred choice. The sensor system was placed with the button facing upward. The button alignment is done to ensure that the accelerometer would

always be in the same orientation as the current sensor system does not have a gyroscope or a compass to indicate orientation. The placement position was derived from the work done in Chapter 3, in which the capaciflector position had little to no effect on the data acquired. On the other hand the belt sensor was attached around the chest while ensuring that there is no interference between the sensor system and the belt sensor, this is show in Figure 6.4b. The data acquisition from the belt sensor is done by having an Android tablet connected to the device via Bluetooth, to continuously collect the data.

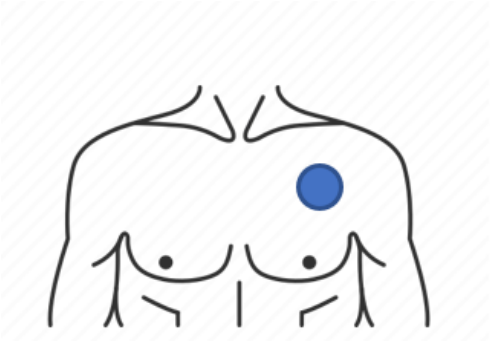

(A) Capaciflector Placement

(B) Belt Placement

FIGURE 6.4: Figures showing the placement of the sensors on the chest

6.1.2 Study 1: Metronome Tests

Study 1 is a comparative study that aims to measure the difference between the capaciflector and a reference standard belt sensor during stationary events. For this study the participants were tasked to breathe at a predefined metronome rate. The metronome values ranged from 10-19 breaths per minute. Each participant had a different rate so as to allow the system to be tested across a variety of breathing ranges. The metronome values selected were chosen to be between the average human breathing rate of 10-19 BPM (Yuan et al. (2013)). Table 6.1 shows the BPM values selected randomly for all the different tests. The values used were multiplied by two in order to allow the participant to perform a full inhale or exhale on each metronome click. This results in a continuous sinusoidal looking signal.

The tests were conducted while the participant was sitting upright on a chair, with a total duration for each test being 5 minutes long, the participant was only tasked to not speak during the test. The participants were asked to breath a full respiratory cycle on each metronome click, and are instructed to do it in a normal manner as much as possible. In cases where the participant finds breathing at the predetermined metronome rate to be difficult, this is adjusted to avoid having any inconveniences on the participant throughout the test.

TABLE 6.1: Metronome Values Selected per test

Test Number	BPM Value
1	14
2	18
3	16
4	15
5	17
6	13
7	19
8	10
9	11
10	12

6.1.3 Study 2: Walking Tests

Study 2 is also a comparative respiration rate study, but the focus is to have the participant produce movement artefacts, which can potentially interfere with the desired respiration signal. This was achieved by having the same 10 participants from study 1 walk a predefined route wearing the same sensor system and the belt sensor. The participants were asked to not talk during the test, but otherwise no further instructions were provided. The total duration for each test varied per participant from 3-5 minutes long depending on their walking speed. Two stops were introduced in the test, where the participant stops walking and were asked to take two deep breaths. These allow the signals between the belt and capaciflector system to be aligned and synchronised during the post processing stage. This test is similar to the test conducted in Chapter 5 and an example of the expected raw signal can be seen in Figure 6.5. The route for this test is done in the High-field campus of the University of Southampton.

6.1.4 Study 3: Speaking Tests

Study 3 is a comparative study that is different from study 1 and 2, the aim of this study is to explore the differences between normal breathing and breathing while speaking.

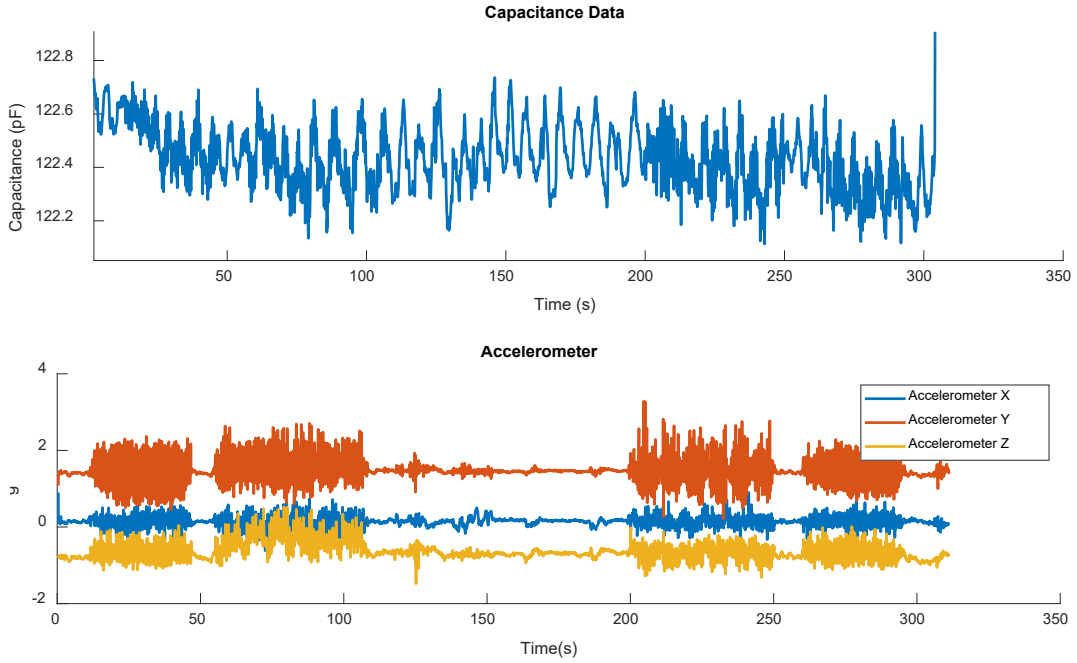

FIGURE 6.5: Example of the expected output for this part of the study.

The participant is instructed to read a paragraph of text which is the introduction section of the confirmation report (found in Appendix E), which should take approximately 5 minutes to read at a standard pace. The test is conducted with the participant seated upright on a chair with instructions to read the text out loud at a normal pace. This study will have a variable duration as each participant can read at a different pace from each other. Nonetheless, the data from all the participants should be enough to build an appropriate analysis on speaking data and enough to compare against more natural breathing data collected from the other studies.

6.1.5 Data Processing

The processing of the data was performed after the collection of the data has been completed. MATLAB (2019) was used for the data clean-up and digital filtering; an overview can be seen in Figure 6.6a. The initial step is to align the belt and capaciflector data. The offset values are the peak timestamps in which the person started the test, this is identifiable by the large breath taken before beginning the actual test. Thus, allowing a timestamp matching of both signals. The trim value is a 5 second cut off at the end of the signal, this was selected as the best value as it eliminated the sharp spike in data when the sensor was touched.

The second stage is the filtration of the data, which applies a high pass filter with a cut-off frequency of 0.02 Hz (i.e. 1.2 BPM) to the raw data and the accelerometer data,

to remove any bias in preparation for the further steps. The third step is the detection of the walking events in the signal. This is achieved by having the data segmented into time slots where the accelerometer values have a change in the mean root mean square value. This change is then identified as a movement when the mean value of the current segment is above the threshold (0.08 g) which can be seen in Figure 6.6b. This allows threshold identification of key points mainly the start and end of each sectioned event, which allows more specific filtering and data separation when generating the results. If the accelerometer is not available then this step is skipped and the entire signal is processed in the same way the stationary data is processed.

Once segmented, the signals are filtered differently for each segment. For the walking event the accelerometer noise signal is extracted and subtracted from the main signal. This is applicable because the accelerometer is directly in phase with the noise collected from the capaciflector. The data and noise is first normalised, then the noise is scaled and then subtracted from the signal. The reason behind doing the normalisation is to ensure that the scaling of the captured signal is within the same scale as the noise. Once the noise is reduced a moving average filter is applied with a window size of 10 samples is applied to suppress the higher frequencies further resulting in a clean signal with minimal loss from the movement artefacts. For the stationary event, a low-pass filter with a cut-off frequency of 1Hz is applied to the signal to remove frequencies that are higher than 1 Hz in the signal. Lastly the walking and stationary signals are combined together to form the cleaned signal, in which a power spectrogram is generated. Figure 6.6b shows the resulting stitched signal before the processing is done.

The power spectrogram used a window size of 60 seconds with an overlap of 99 percent and 0 leakage, the result is a power frequency curve over time that indicates the strongest frequencies every 0.6 seconds. The window size selected allows the full minute of the data to be analyzed including the changes that can happen over time throughout the signal. The overlap percentage used allows for a higher resolution comparison between both signals.

To extract the breathing signal, the spectrogram output is traced using MATLAB's time frequency ridge tracing function with a defined penalty of 0.05Hz which is the maximum frequency change between each window point in the spectrogram, this meant a maximum change of 3 BPM can happen in a span of 0.6 seconds. The result is a time continuous frequency signal for the strongest frequency within the set penalty. To convert the frequency data into comparable respiration data, the average of the frequency points per minute is taken to generate a result in breaths per minute.

The belt data was filtered in the same manner as the metronome data described in study 1 where a low pass-filter was used on both the stationary and walking data as the raw signal contained high frequency noise from walking. The same power spectrogram analysis is applied with the same settings to allow a direct comparison of breaths

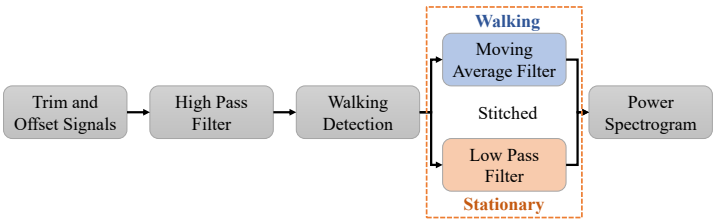

(A) Shows the method used overall to generate the respiration rate.

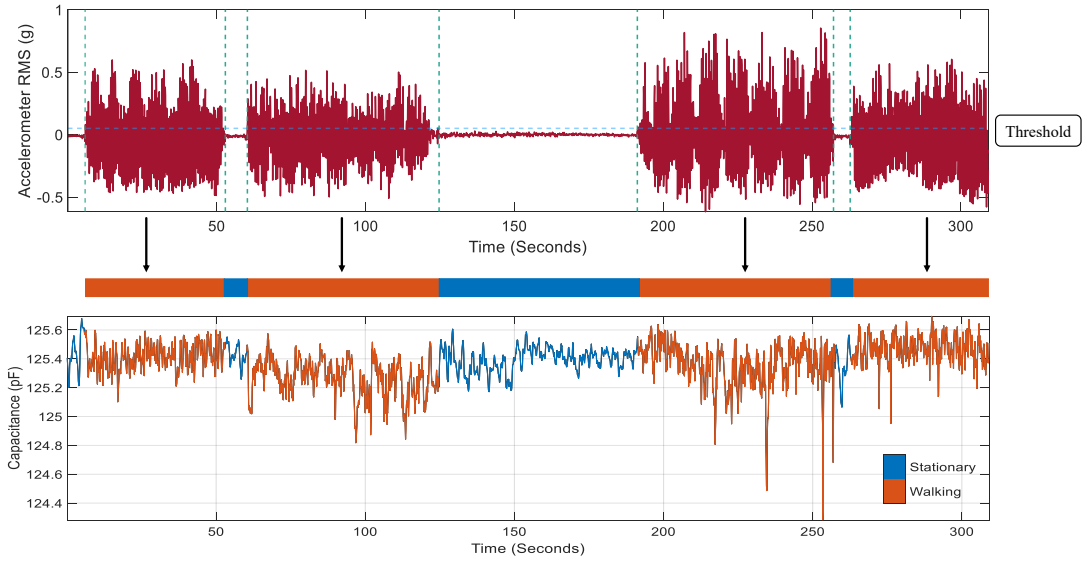

(B) Shows the detection of walking through root mean squared (RMS) threshold, and the segmented signal processing

FIGURE 6.6: Is the overview of the signal processing steps.

per minute between the belt and capaciflector sensor. A Bland-Altman plot is then generated to compare the results from the capaciflector sensor system and the belt sensor. This allows for a fairer and more visual comparison. An example Bland Altman result can be seen in Table 6.7.

6.2 Data and Results

The data will be collected and stored according to the ethics (ERGO 68839.A1). All data will be collected anonymously and cant be linked back to the subject performing the tests. The data collected from these tests were used to generate comparative Bland-Altman plots to show the system effectiveness. All studies were conducted with the

same 10 healthy participants who had a range of age between 21-52 years old, with a BMI ranging between 18.6 and 33.7.

6.2.1 Study 1: Metronome Results

For study 1, the 10 tests were used to generate a comparative Bland-Altman plot which resulted in a bias of 0.04 BPM and limits of agreement between 0.58 and -0.50 BPM (Figure 6.7). A more comparative Figure 6.7a shows the appropriate y=x line with the different metronome tests plotted along the line.

6.2.2 Study 2: Walking Results

As for Study 2 the process of comparison was split into two, due to the different method of processing, this allowed a more visual plot to be constructed by separating the results. Like study 1, all 10 participants tests were used to generate the Bland-Altman plot with a bias of -0.04 BPM and limits of agreement between 1.44 and -1.52 BPM (Figure 6.8).

And due to the method of processing, the separation of the stationary and walking data is possible, in which this can be seen in Figure 6.9. The only reason to do this is to compare the accuracy of the extraction against a known good accuracy such as the one in study 1. Where for the case of walking data there is no study at this time that compares the respiration data from walking separately. The results for the stationary separated data is much lower when compared to the walking data and it is due to the way the test was conducted in which the walking segment are more than the stationary rest segments.

6.2.3 Study 3: Speaking Results

The results from the speaking tests are 10 in total, an example of one of the results will be used for the discussion and comparison. The rest of the test results raw data can be seen in Appendix E alongside the belt equivalent.

The results from this study can be seen in one of the tests (test 8) in Figure 6.10, for which the raw data can be seen as well as the comparative plot between the belt and the collected sensor data. And by visually inspecting the data shows very good correlation between the belt and the capaciflector data.

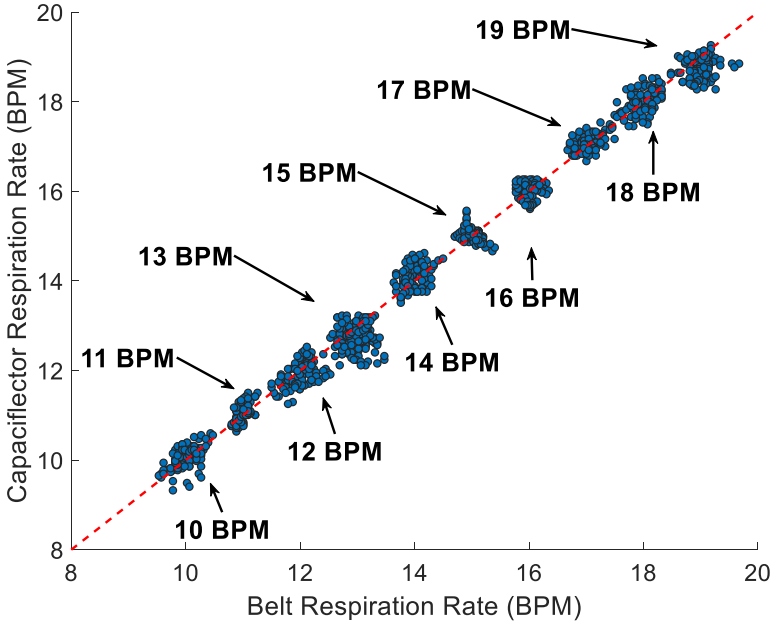

(A) Shows the linear relationship between the belt sensor and capaciflector system.

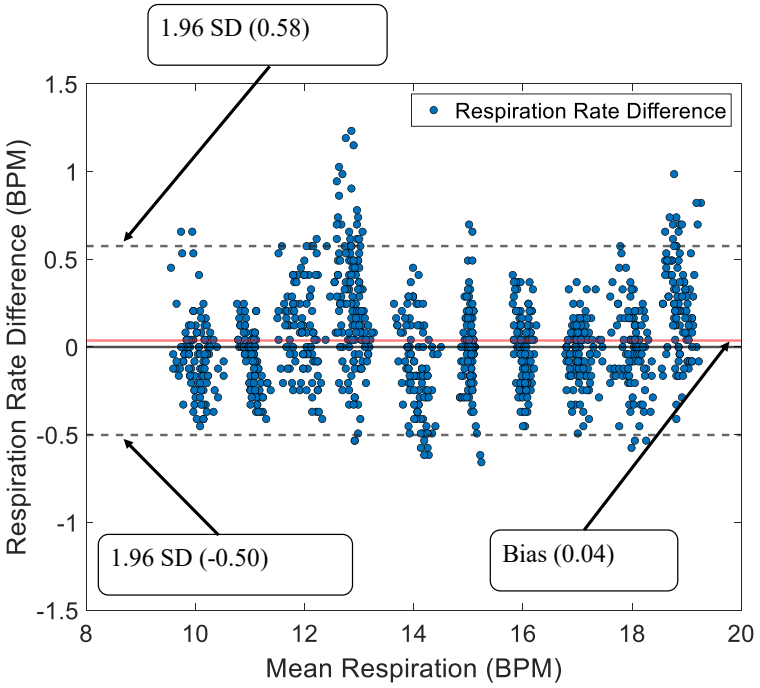

(B) Shows the Bland-Altman of the results.

FIGURE 6.7: Results from study 1 (metronome study).

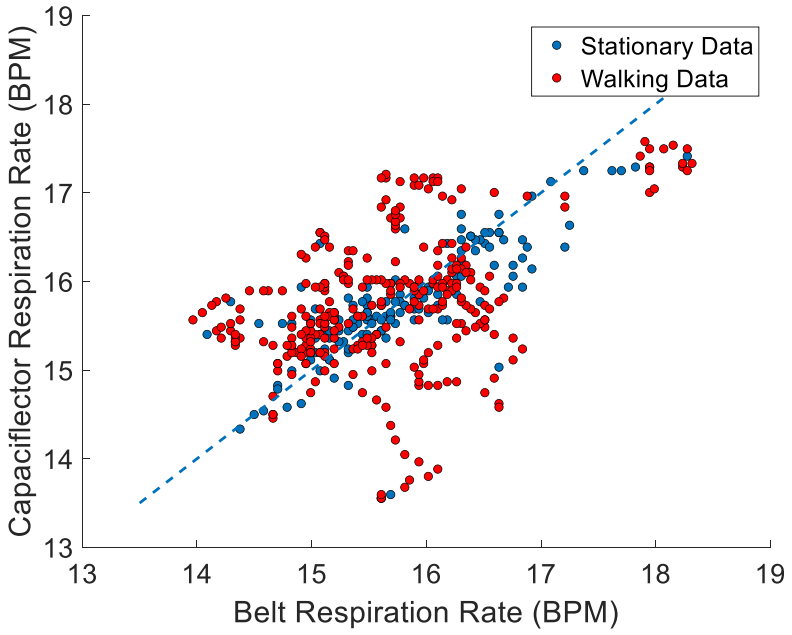

(A) Shows the linear relationship between the belt sensor and capaciflector system.

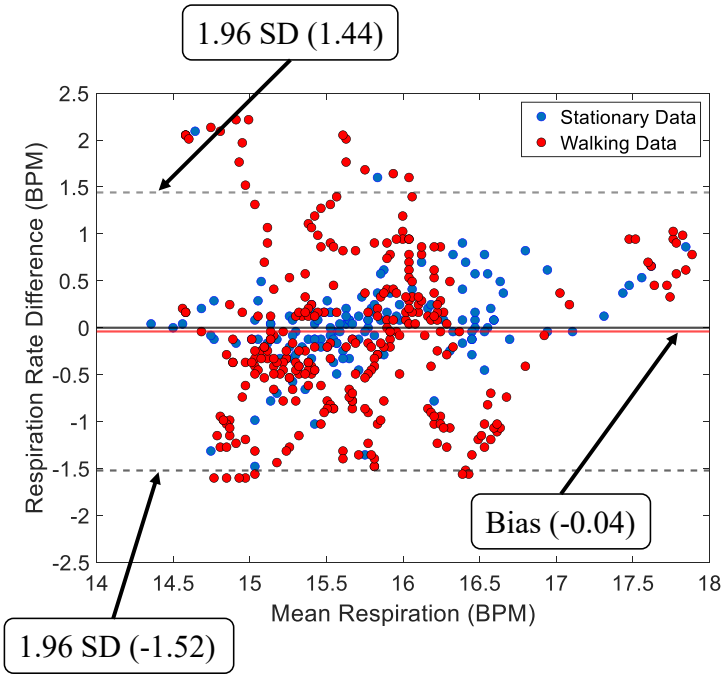

(B) Shows the Bland-Altman of the results.

FIGURE 6.8: Is the results from study 2 (walking study).

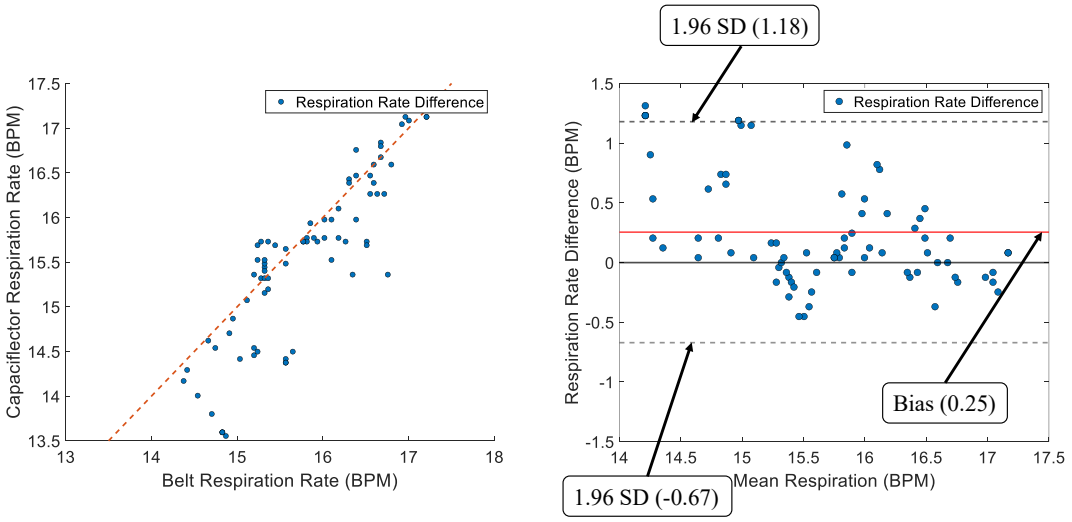

(A) Shows the separated stationary Bland Altman's.

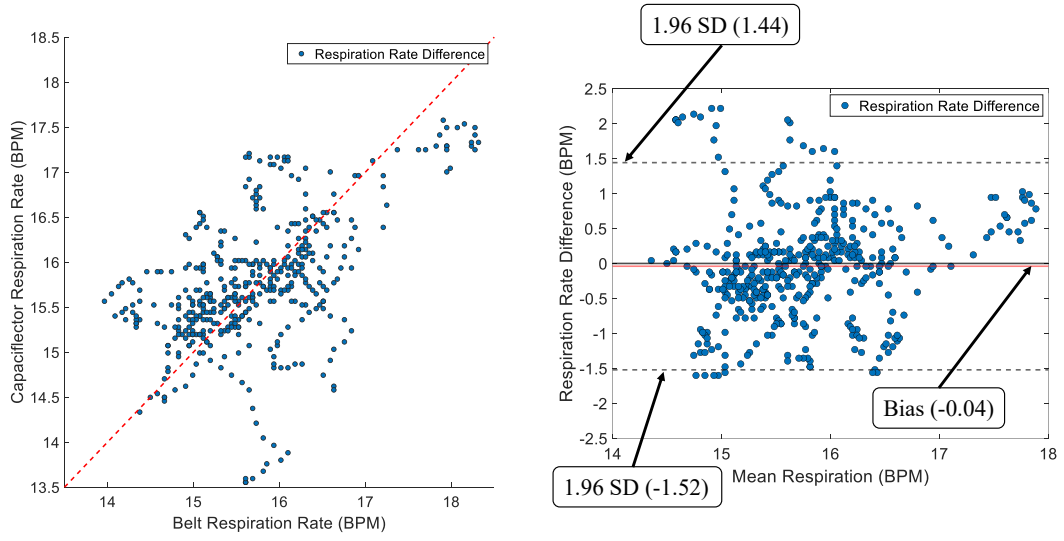

(B) Shows the separated walking Bland Altman's.

FIGURE 6.9: Results from study 2 (walking study) segmented into stationary and walking with separate Bland Atman's.

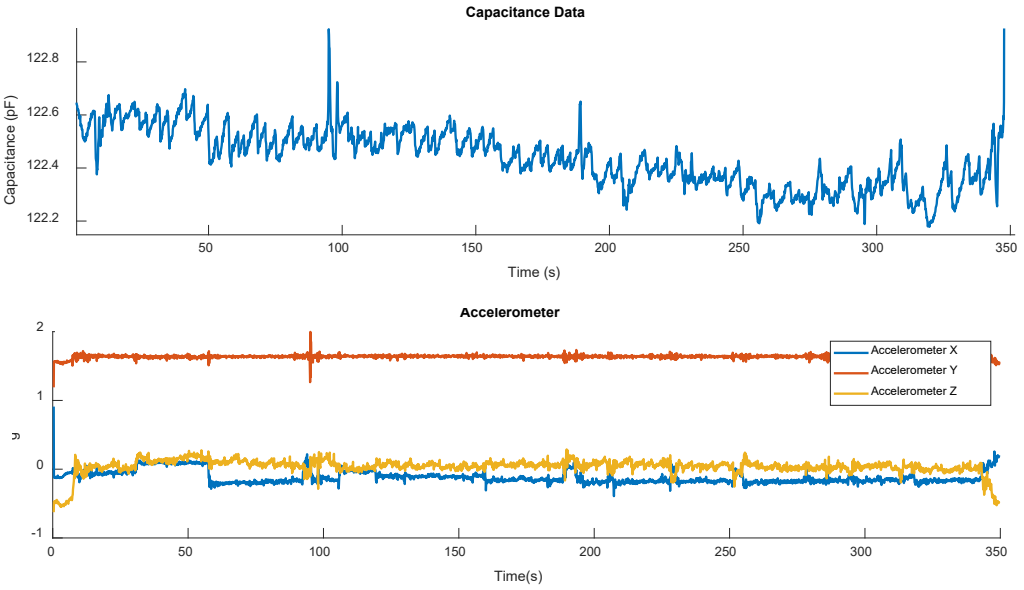

(A) Shows the raw data collected from test 8 for the speaking study.

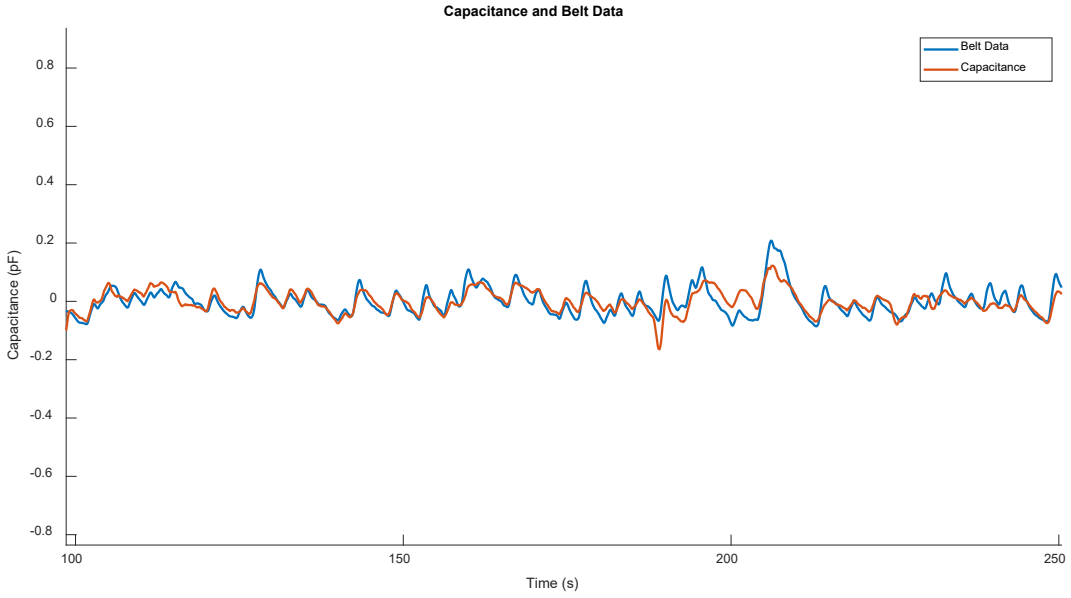

(B) Shows the comparison against the belt sensor data.

FIGURE 6.10: Results from study 3 (speaking study) for test 8, which the raw and compare figures are seen.

6.3 Discussion

Study 1 results are the results from the more controlled tests in which the sensor system is expected to perform the best in. The results in Figure 6.7 show the results to be within ± 0.54 BPM with a positive bias of 0.04 BPM. The results from study 1 are used to confirm that the system can accurately be used to measure respiration. The band of points that are together represent the different set of metronome tests that were taken. The results indicate a great upper and lower limit with a bias closer to zero, this can be compared to a study done on a commercially available sensor system by Respirasense (Subbe and Kinsella, 2018), where they achieved a bias of 0.38 BPM and limits of agreement between 1.0 and 1.8 BPM. These values are much lower (by a factor that is greater than 1 BPM) when compared to the sensor system constructed using the capaciflector. And when comparing against the previous work done in Chapter 3, the sensors did not face any deterioration due to the material used which is much more robust for these types of tests. There are however limitations to this type of test, and this mainly comes down to the periodic breathing which the metronome test artificially creates, where in a real world scenario a person's breathing will not be as continuous and will be more spontaneous and sporadic. This is also a very beneficial test towards an FFT in which the FFT benefits from a periodic signal. To improve upon this test a more relaxed breathing must be achieved, but its harder to reproduce in a more controlled test.

Study 2 results had higher limits of ± 1.48 BPM but are under the limits of what a respiratory system must achieve to be acceptable as a clinical device (±3 BPM (Chan et al., 2022)); even while measuring during motion, which introduces artefacts. The bias of the system is close to the metronome tests with a value of -0.04 BPM, which indicates that the system is repeatable between both studies, which means that its able to replicate the results within the error limits defined in Chapter2. The data from the walking study is more sporadic due to the changes in respiration in the test, this allows the system to be assessed in a more realistic scenario. This also presents a case against some of the established devices that are not capable of monitoring respiration during walking events. This mainly applies to commercial solutions such as some types of smart watches. In this sensor system, no data was left out or discarded while cleaning up the signal and during the processing stage, making it good at extracting the respiration signal from the noisy breathing data.

Study 3 results are more comparative in which an assessment against the normal breathing data collected from studies one and two show that study three exhibits a different pattern. The pattern is more of a saw tooth wave, as when the participant speaks the air is exhaled and a sharp breath intake happens once the participant is out of air. And with the sensor being able to pick up the slight changes in the breath even during speaking is promising towards developing an improved segmentation which accurately represents the respiration rate of the person. This is a key point toward systems that continuously

monitor respiration rate while the participant is doing other activities such as speaking or walking. And with most commercial solutions for measuring respiration rate this data is discarded even if there is any usable data that can correlate to the accurate respiratory rate. Thus by utilising techniques in signal processing such as comparative techniques it is possible to build a lightweight approach to detect the different wave forms. Other methods exists such as machine learning techniques which can be better in some cases. This potentially can create a more adaptive algorithm that can be used for detecting respiratory rate.

6.4 Chapter Summary

The results from both studies are good indicators towards an accurate and reliable system that can measure respiration continuously in both stationary and walking events, while also being compact in size. The system overcomes many of the missing factors in respiration sensor systems, mainly the ability to detect and retrieve respiration data from signals that have walking noise without discarding any information in the process. The technique used to remove the noise from the breathing signal is also simple enough to be implemented in the hardware itself, making the device even more standalone. And finally the third study shows a viable direction for developing the algorithm in the future. In which speaking is a uniquely identified waveform making it possible to be segmented through signal processing or through other techniques such as machine learning. This has the potential to create a more adaptive algorithm that is lightweight and easy to implement. Overall, the capaciflector based system shows promising potential for becoming reliable and low-cost sensing system for respiration monitoring in ambulatory patients.

Chapter 7

Conclusion

Different sensors are initially explored in this work, in which the capaciflector sensor was shown to be a viable sensor for use in healthcare, for both home and hospital care. The different sensor systems and sensors developed throughout this research helped build upon a more robust system that can be easily integrated and used due to its simplicity. This chapter helps summarise the outcomes and the new research developed in the field of respiration monitoring and wearables.

7.1 Chapter 3 Summary

This chapter introduced the capaciflector as a new sensor capable of measuring respiration rate, this was initially introduced in the work done by White et al. (2017), and was expanded upon in this chapter by introducing new information on the capability of using the capaciflector for respiration rate monitoring. The chapter concluded by showing that the capaciflector can be used in many different positions around the body with little restriction as long as the sensor is attached to a position which can correlate to the rib cage movement. This includes the interface medium as well, and in this case the sensor itself does not need to be directly touching the skin to work. The capaciflector sensor which was developed through screen printing for this chapter exhibited failure due to moisture, while the electronics were tethered making it hard to use for any other tests that require movement. These conclusions were used as a basis to develop the next chapters where a more robust untethered system was developed, alongside a better capaciflector sensor which was manufactured from better materials.

7.2 Chapter 4 Summary

Different capaciflector sensor designs and materials were explored in this chapter to find the optimal one for the application of respiration sensing with the capacitance to digital sensor IC. The tests were conducted through a comparative study against a belt sensor. Different configurations and modes were tested, mainly the capacitance and capaciflector mode. The outcome from this chapter showed that the capaciflector sensor had many changes in behaviour when the frequency or the configuration were changed. Thus resulting in sensor designs that were effectively assessed by finding the best response with the least amount of force. Overall the capacitance mode resulted in being as accurate as the capaciflector mode while also being easier and cheaper to manufacture and use. The only downside is that the directionality of the sensor is lost in this mode.

7.3 Chapter 5 Summary

A new sensor system is developed to allow a capaciflector to be utilised for testing. The sensor system allows the data logging of raw capacitance data from the capaciflector as well as movement data from the accelerometer. The developed hardware was put to a series of tests to ensure that the device can be used without failing, especially for continuous monitoring of respiration rate. The system was also tested for accuracy by running it through a series of short and long tests to ensure that the data captured from the sensor system is viable. The sensor system passed all the tests conducted while also being small and comfortable to wear, with the possibility of continuously monitoring for periods spanning more than 48 hours.

7.4 Chapter 6 Summary

A new algorithm was developed for the sensor system, that made use of the accelerometer data. The algorithm is tested on a small scale study of 10 participants, which showed that the algorithm works much better than the conventional processing techniques used for calculating respiration rate. The method used the accelerometer data to segment and process the different parts of the respiratory signal. The walking segments were processed in a similar way to noise cancellation in which the noise captured by the accelerometer is subtracted from the captured signal to result in a much cleaner signal. Even thought these methods exist outside the scope of respiration detection (audio noise cancelling), they are not used in the field of research for respiratory analysis. The three studies conducted also demonstrated the new sensor system with the new processing techniques, resulted in much higher accuracy's than current available

commercial systems. The sensor system serves as part of the process for building a system that can be used for respiratory monitoring continuously. And with this chapter the main aim of building a system that is able to continuously and accurately monitor respiration rate is done.

7.5 Overall Findings

The overall findings discussed in this work is the new methods and techniques that were developed and tested to get a working system that is capable of accurately and continuously collect respiratory data. The resulting algorithms developed demonstrated that the sensor system developed is as accurate as many of the gold standards used. With the benefit of being much smaller, lighter, and more comfortable to wear. This concludes the work done for this thesis in which the low cost wearable respiration sensor was the capaciflector sensor, to which a proper algorithm and hardware were developed to completion. Where Chapter 3 completed the aim of identifying whether the position of the capaciflector matters for respiration detection. While Chapter 4 identifies the best sensor to be used for respiratory detection through comparison between seven different designs. Finally Chapters 5 and 6 fulfil the main aim of developing a new respiratory sensor system that is capable of continuously monitoring respiration over long periods of time, while also being small enough to comfortably wear. The sensor system boasts an accuracy of 0.04 ± 0.54 BPM for stationary tests, and an accuracy of -0.04 ± 1.48 BPM for walking tests. This shows that even though the results are higher for the walking study they are still within the limits of accuracy ± 3 BPM that is needed to be acknowledged as a respiratory sensor for healthcare.

7.6 Future Work

For the future work much more could be done in the software side of things, mainly the interfacing of the device and the segmentation and processing algorithm. The main points to to expand upon this work are listed below:

1. The MCU software has the most potential for future work. The current post processing is done separately on a different computer, where the data must first be collected and then processed. And for the sensor system to be a more effective and self enclosed, the current post processing script must be ported from MATLAB (2019) to the micro controller. This will be a challenge in itself as most of the functions used in MATLAB (2019) will have to be used in a much more controlled manner in the MCU due to the size of the flash and RAM (Random Access Memory) of the micro controller. The key benefits to doing this is the reduction

in power consumption which in turn will create a much better overall system capable of monitoring respiration rate continuously for long periods of time.

2. The second part of the software is to improve upon the post processing methods, in which the speaking data alongside the walking data is going to be selectively filtered out. And by processing each of these segments separately the algorithm will get a much closer representation of the signal captured without any noise/ This should allow the resulting data to be much more clearer in terms of conveying the type of data resulting from the algorithm, where the good data is highlighted and the unusable data is ignored. This will create a more scale-able solution for the long term.

3. The current hardware developed has access to many features that allow the sensor system to be more versatile, mainly the BLE. And in this case part of the possibility for the future is the development of this protocol over the existing work done to allow the data to be easily accessed over Bluetooth. This means both a BLE application as well as the stack development must be done in order to effectively build the system into a cohesive unit.

4. Lastly the hardware developed has been shrunk down to a small diameter of 32 mm however with the amount of sensors used, this can be scaled further down to be closer to the original goal of being the size of a 2 pence coin. The challenge lies within developing the full system without losing out on any of the features. This should allow the senor system to become much smaller and easier to mount.

Appendix A

Schematics for Relaxation Oscillator

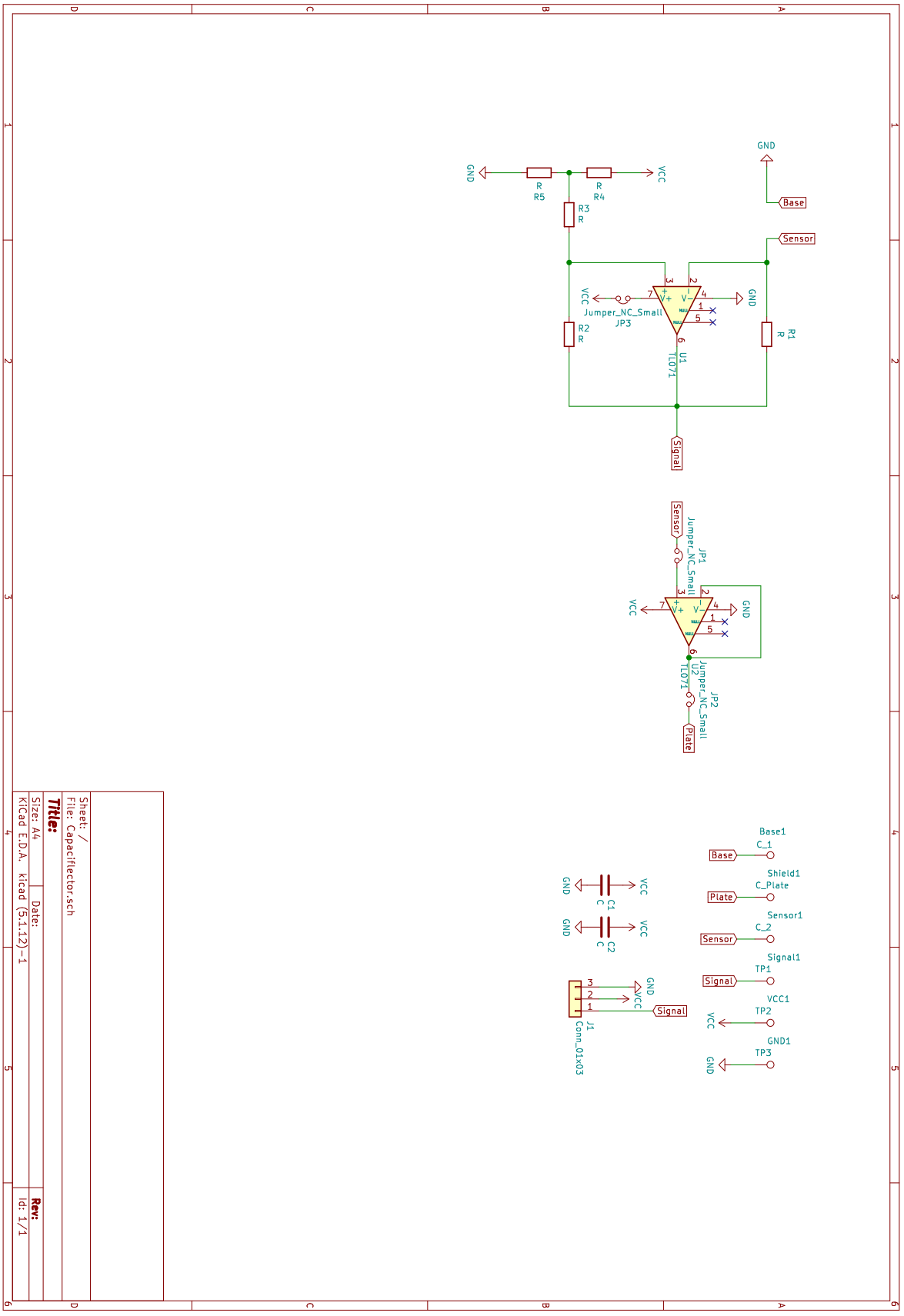

FIGURE A.1: Relaxation Oscillator schematic used for the capaciflector testing.

Appendix B

Frequency and Current table for Chapter 4

B.1 Current Reference Table

TABLE B.1: Reference table for the drive current values, sourced from the data sheet of the FDC2214 (Texas Instruments Incorporated., 2015).

Value	Current (uA)
1	18
2	21
3	25
4	28
5	33
6	38
7	44
8	52
9	60
10	69
11	81
12	93
13	108
14	126
15	146
16	169
17	196
18	228
19	264
20	307
21	356
22	413
23	479
24	555
25	644
26	747
27	867
28	1006
29	1167
30	1354
31	1571

B.2 Sensor Design and Current Drive Value

Capacitance Mode

Mode 1			Mode 1			Mode 1			Mode 2			Mode 2			Mode 2		
PAD	**CONNECTION**	**FREQ**	**PAD**	**CONNECTION**	**FREQ**	**PAD**	**CONNECTION**	**FREQ**	**PAD**	**CONNECTION**	**FREQ**	**PAD**	**CONNECTION**	**FREQ**	**PAD**	**CONNECTION**	**FREQ**
Frequency = 100kHz			**Frequency = 1MHz**			**Frequency = 10MHz**			**Frequency = 100kHz**			**Frequency = 1MHz**			**Frequency = 10MHz**		
Sensor	INA	100kHz	Sensor	INA	1MHz	Sensor	INA	10MHz	Sensor	INA	100kHz	Sensor	INA	1MHz	Sensor	INA	10MHz
Reflector	N/C	100kHz	Reflector	N/C	1MHz	Reflector	N/C	10MHz	Reflector	N/C	100kHz	Reflector	N/C	1MHz	Reflector	N/C	10MHz
Base	INB	100kHz	Base	INB	1MHz	Base	INB	10MHz	Base	GND	100kHz	Base	GND	1MHz	Base	GND	10MHz
Current	19		**Current**	6		**Current**	20		**Current**	19		**Current**	5 or 6		**Current**	21	
Sensor	INA	100kHz	Sensor	INA	1MHz	Sensor	INA	10MHz	Sensor	INA	100kHz	Sensor	INA	1MHz	Sensor	INA	10MHz
Reflector	INB	100kHz	Reflector	INB	1MHz	Reflector	INB	10MHz	Reflector	GND	100kHz	Reflector	GND	1MHz	Reflector	GND	10MHz
Base	N/C	100kHz	Base	N/C	1MHz	Base	N/C	10MHz	Base	N/C	100kHz	Base	N/C	1MHz	Base	N/C	10MHz
Current	19		**Current**	9		**Current**	22 or 23		**Current**	19		**Current**	14		**Current**	30	

Capaciflector Mode

PAD	**CONNECTION**	**FREQ**	**PAD**	**CONNECTION**	**FREQ**	**PAD**	**CONNECTION**	**FREQ**
Frequency = 100kHz			**Frequency = 1MHz**			**Frequency = 10MHz**		
Sensor	INA	100kHz	Sensor	INA	1MHz	Sensor	INA	10MHz
Reflector	N/C	100kHz	Reflector	N/C	1MHz	Reflector	N/C	10MHz
Base	INB	100kHz	Base	INB	1MHz	Base	INB	10MHz
Current	21		**Current**	8		**Current**	24	
Sensor	INA	100kHz	Sensor	INA	1MHz	Sensor	INA	10MHz
Reflector	INB	100kHz	Reflector	INB	1MHz	Reflector	INB	10MHz
Base	N/C	100kHz	Base	N/C	1MHz	Base	N/C	10MHz
Current			**Current**			**Current**		

FIGURE B.1: Current Settings for Rigid Design 1 for both the capaciflector and capacitance mode

Capacitance Mode

Mode 1			Mode 1			Mode 1			Mode 2			Mode 2			Mode 2		
PAD	**CONNECTION**	**FREQ**	**PAD**	**CONNECTION**	**FREQ**	**PAD**	**CONNECTION**	**FREQ**	**PAD**	**CONNECTION**	**FREQ**	**PAD**	**CONNECTION**	**FREQ**	**PAD**	**CONNECTION**	**FREQ**
Frequency = 100kHz			**Frequency = 1MHz**			**Frequency = 10MHz**			**Frequency = 100kHz**			**Frequency = 1MHz**			**Frequency = 10MHz**		
Sensor	INA	100kHz	Sensor	INA	1MHz	Sensor	INA	10MHz	Sensor	INA	100kHz	Sensor	INA	1MHz	Sensor	INA	10MHz
Reflector	N/C	100kHz	Reflector	N/C	1MHz	Reflector	N/C	10MHz	Reflector	N/C	100kHz	Reflector	N/C	1MHz	Reflector	N/C	10MHz
Base	INB	100kHz	Base	INB	1MHz	Base	INB	10MHz	Base	GND	100kHz	Base	GND	1MHz	Base	GND	10MHz
Current	19		**Current**	6 or 7		**Current**	19 or 20		**Current**	19		**Current**	6		**Current**	21 or 22	
Sensor	INA	100kHz	Sensor	INA	1MHz	Sensor	INA	10MHz	Sensor	INA	100kHz	Sensor	INA	1MHz	Sensor	INA	10MHz
Reflector	INB	100kHz	Reflector	INB	1MHz	Reflector	INB	10MHz	Reflector	GND	100kHz	Reflector	GND	1MHz	Reflector	GND	10MHz
Base	N/C	100kHz	Base	N/C	1MHz	Base	N/C	10MHz	Base	N/C	100kHz	Base	N/C	1MHz	Base	N/C	10MHz
Current	19		**Current**	8 or 9		**Current**	20 or 21		**Current**	19		**Current**	11		**Current**	26 to 30	

Capaciflector Mode

PAD	**CONNECTION**	**FREQ**	**PAD**	**CONNECTION**	**FREQ**	**PAD**	**CONNECTION**	**FREQ**
Frequency = 100kHz			**Frequency = 1MHz**			**Frequency = 10MHz**		
Sensor	INA	100kHz	Sensor	INA	1MHz	Sensor	INA	10MHz
Reflector	N/C	100kHz	Reflector	N/C	1MHz	Reflector	N/C	10MHz
Base	INB	100kHz	Base	INB	1MHz	Base	INB	10MHz
Current	20		**Current**	8		**Current**	22	
Sensor	INA	100kHz	Sensor	INA	1MHz	Sensor	INA	10MHz
Reflector	INB	100kHz	Reflector	INB	1MHz	Reflector	INB	10MHz
Base	N/C	100kHz	Base	N/C	1MHz	Base	N/C	10MHz
Current			**Current**			**Current**		

FIGURE B.2: Current Settings for Rigid Design 2 for both the capaciflector and capacitance mode

Capacitance Mode

Mode 1			Mode 1			Mode 1			Mode 2			Mode 2			Mode 2		
PAD	**CONNECTION**	**FREQ**	**PAD**	**CONNECTION**	**FREQ**	**PAD**	**CONNECTION**	**FREQ**	**PAD**	**CONNECTION**	**FREQ**	**PAD**	**CONNECTION**	**FREQ**	**PAD**	**CONNECTION**	**FREQ**
Frequency = 100kHz			**Frequency = 1MHz**			**Frequency = 10MHz**			**Frequency = 100kHz**			**Frequency = 1MHz**			**Frequency = 10MHz**		
Sensor	INA	100kHz	Sensor	INA	1MHz	Sensor	INA	10MHz	Sensor	INA	100kHz	Sensor	INA	1MHz	Sensor	INA	10MHz
Reflector	N/C	100kHz	Reflector	N/C	1MHz	Reflector	N/C	10MHz	Reflector	N/C	100kHz	Reflector	N/C	1MHz	Reflector	N/C	10MHz
Base	INB	100kHz	Base	INB	1MHz	Base	INB	10MHz	Base	GND	100kHz	Base	GND	1MHz	Base	GND	10MHz
Current	18 or 19		**Current**	5 or 6		**Current**	19		**Current**	19		**Current**	5 or 6		**Current**	19	
Sensor	INA	100kHz	Sensor	INA	1MHz	Sensor	INA	10MHz	Sensor	INA	100kHz	Sensor	INA	1MHz	Sensor	INA	10MHz
Reflector	INB	100kHz	Reflector	INB	1MHz	Reflector	INB	10MHz	Reflector	GND	100kHz	Reflector	GND	1MHz	Reflector	GND	10MHz
Base	N/C	100kHz	Base	N/C	1MHz	Base	N/C	10MHz	Base	N/C	100kHz	Base	N/C	1MHz	Base	N/C	10MHz
Current	18 or 19		**Current**	6 or 7		**Current**	21		**Current**	19		**Current**	5 or 6		**Current**	21	

Capaciflector Mode

PAD	**CONNECTION**	**FREQ**	**PAD**	**CONNECTION**	**FREQ**	**PAD**	**CONNECTION**	**FREQ**
Frequency = 100kHz			**Frequency = 1MHz**			**Frequency = 10MHz**		
Sensor	INA	100kHz	Sensor	INA	1MHz	Sensor	INA	10MHz
Reflector	N/C	100kHz	Reflector	N/C	1MHz	Reflector	N/C	10MHz
Base	INB	100kHz	Base	INB	1MHz	Base	INB	10MHz
Current	21		**Current**	8		**Current**	26	
Sensor	INA	100kHz	Sensor	INA	1MHz	Sensor	INA	10MHz
Reflector	INB	100kHz	Reflector	INB	1MHz	Reflector	INB	10MHz
Base	N/C	100kHz	Base	N/C	1MHz	Base	N/C	10MHz
Current			**Current**			**Current**		

FIGURE B.3: Current Settings for Rigid Design 3 for both the capaciflector and capacitance mode

Appendix C

Schematics for Developed Sensor System

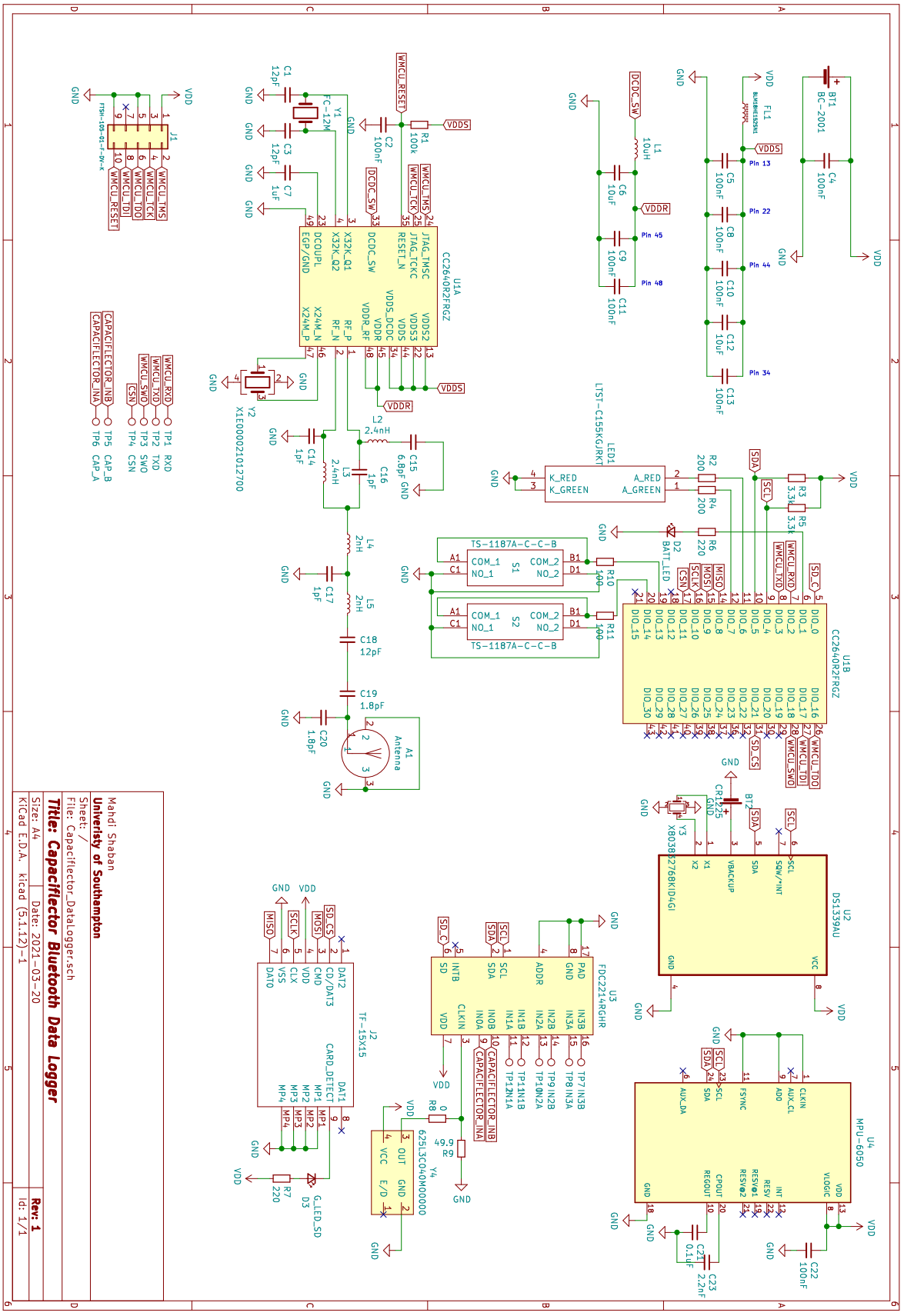

FIGURE C.1: Schematic for the first version of the sensor system.

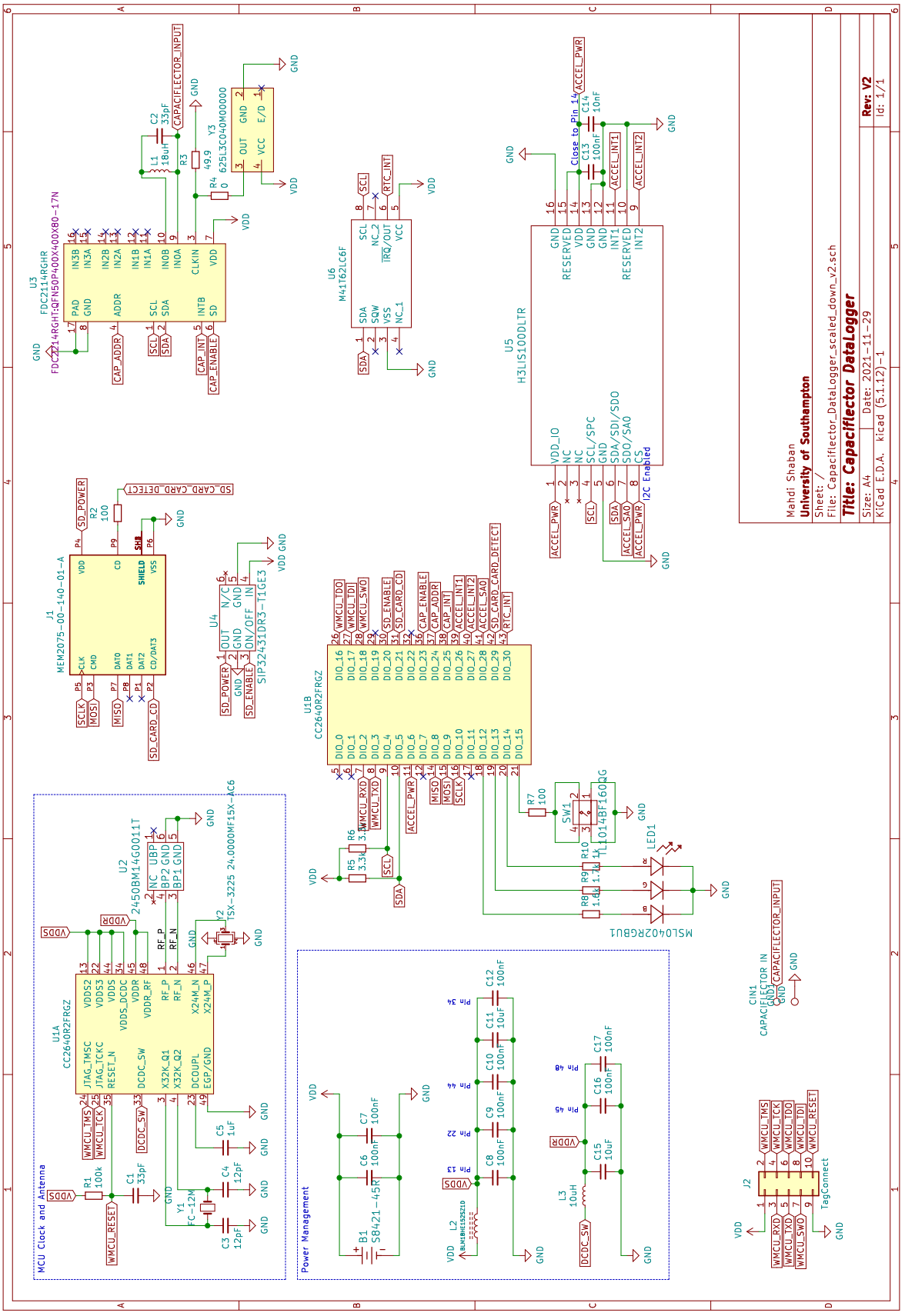

FIGURE C.2: Schematic for the second version of the sensor system.

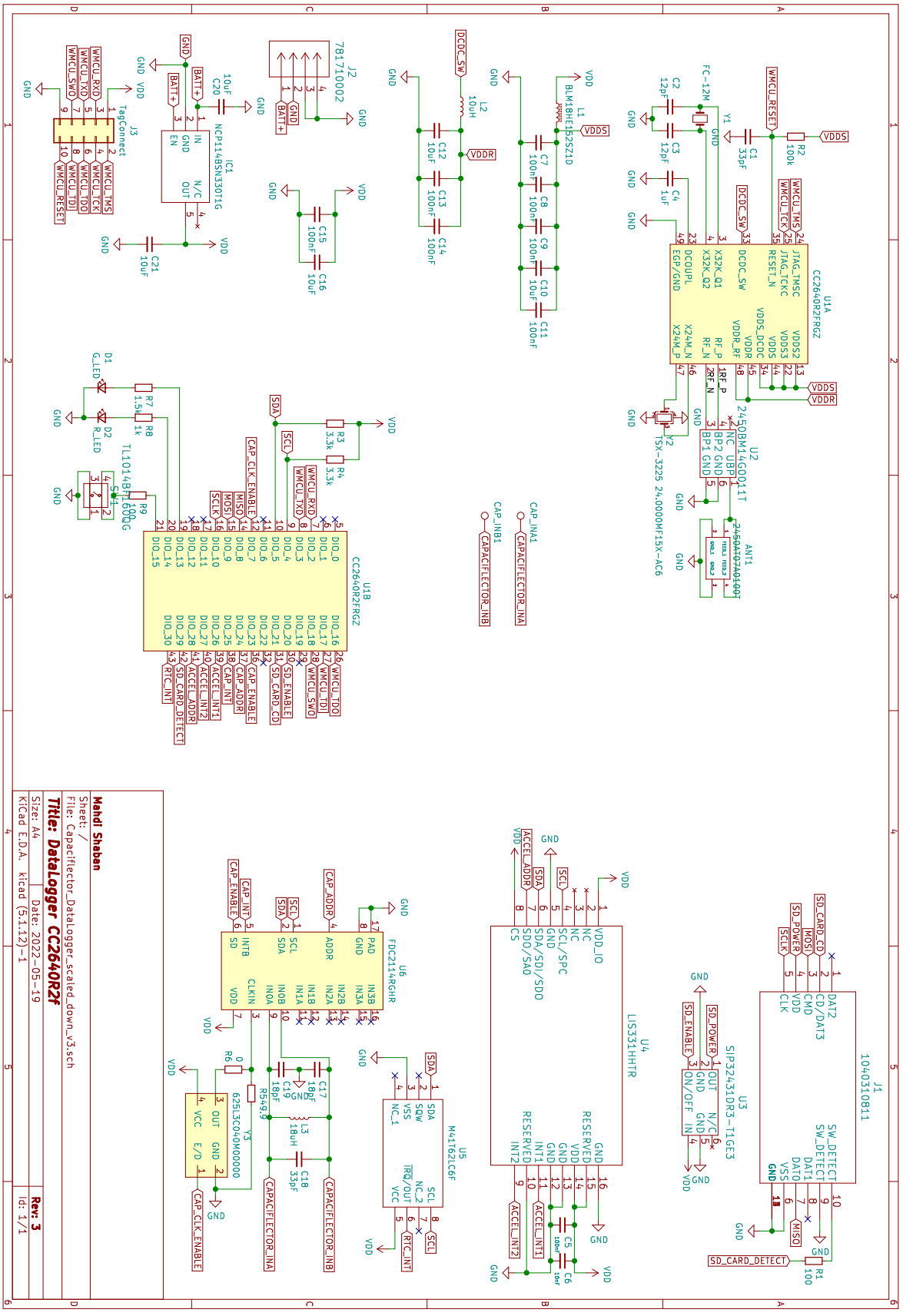

FIGURE C.3: Schematic for the final version of the sensor system, this version was modified to accept the inputs from two different sources (CR2032 and Li-Po Battery).

Appendix D

MCU Firmware and MATLAB Processing Code

This appendix shows the code used for the post processing algorithm as well as the micro controller firmware.

D.1 MATLAB Code

```
close all;

DataFormat = readtable('DataLocation.xlsx','PreserveVariableNames',true);
DataName = readtable('DataFormat.xlsx','PreserveVariableNames',true);

Excluded = DataName{:,6};

TestLocation = DataFormat{:,1};
TestLocation = string(TestLocation);

TestString = DataName{:,1};
TestString = string(TestString);

channelTested = 3;

ChannelInfo = DataName{:,2+channelTested};

ridgeWidth = 0.005;
timeRatio = 60;
freqLimits = [0.1 0.8];
overlapPercent = 90;
leakage = 0;

filterHP = designfilt('highpassiir','FilterOrder',2, ...
         'PassbandFrequency',0.02, ...
```

```
        'SampleRate',10);

% Check if output directory exists
if ~exist(strjoin(["Channel", channelTested],''), 'dir')
    mkdir(strjoin(["Channel", channelTested],''));
end

if ~exist(strjoin(["Channel", channelTested,'/Output'],''), 'dir')
    mkdir(strjoin(["Channel", channelTested,'/Output'],''));
end

if ~exist(strjoin(["Channel", channelTested, '/Output/Spectogram'],''), '
    dir')
        mkdir(strjoin(["Channel", channelTested,'/Output/Spectogram'],'')
    );
end

if ~exist(strjoin(["Channel", channelTested,'/Output/Compare'],''), 'dir'
    )
        mkdir(strjoin(["Channel", channelTested,'/Output/Compare'],''));
end

C_BA = [];
B_BA = [];

for testNum = 5:length(TestLocation)
    close all;

    if not(Excluded(testNum))
        continue;
    end

    if ChannelInfo(testNum) == 0
        continue;
    end

    disp(['Testing: ' TestString(testNum)]);

    fileName = fullfile(pwd,string('Data/' + TestLocation(testNum) + '.
    lvm'));
    opts = delimitedTextImportOptions("NumVariables", 6);
    opts.DataLines = [23, Inf];
    opts.Delimiter = "\t";
    opts.VariableNames = ["LabVIEWMeasurement", "VarName2", "VarName3", "
    VarName4", "VarName5", "Var6"];
    opts.SelectedVariableNames = ["LabVIEWMeasurement", "VarName2", "
    VarName3", "VarName4", "VarName5"];
    opts.VariableTypes = ["double", "double", "double", "double", "double
    ", "string"];
    opts.ExtraColumnsRule = "ignore";
    opts.EmptyLineRule = "read";
```

```
70      opts = setvaropts(opts, "Var6", "WhitespaceRule", "preserve");
71      opts = setvaropts(opts, "Var6", "EmptyFieldRule", "auto");
72      Data_C = readtable(fileName, opts);
73      clear opts;
74
75      % Load Pnemograph
76      fileToLoad2=strrep(fileName,'C.lvm','P_BPM.xlsx');%Pnemo_data
77      opts = spreadsheetImportOptions("NumVariables", 1);
78      opts.Sheet = "BPM";
79      opts.DataRange = "F2:F14";
80      opts.VariableNames = "BPM";
81      opts.VariableTypes = "double";
82      PBPMS1 = readtable(fileToLoad2, opts, "UseExcel", false);
83      PnemoData=table2array(PBPMS1);
84      PnemoData(PnemoData==0)=NaN;
85      PnemoData = rmmissing(PnemoData);
86      clear opts;
87
88      % Extract Channel data
89      data_C = flipud(table2array(Data_C(2:end,1:5)));
90      C_data=data_C(:,channelTested+2);
91      t_C=flipud(data_C(:,1));
92
93      % Apply High pass filter and remove offset
94      C_data = filtfilt(filterHP,C_data);
95
96      % Run Spectogram
97  %     [p_c,f_c,t_c]=pspectrum(C_data,seconds(t_C),'spectrogram',...
98  %         'TimeResolution',timeRatio,...
99  %         'Reassign',false,...
100 %         'FrequencyLimits',freqLimits,...
101 %         'OverlapPercent',overlapPercent,...
102 %         'Leakage',leakage);
103
104     [p_c,f_c,t_c]=pspectrum(C_data,10.4,'spectrogram',...
105         'TimeResolution',timeRatio,...
106         'Reassign',false,...
107         'FrequencyLimits',freqLimits,...
108         'OverlapPercent',overlapPercent,...
109         'Leakage',leakage);
110
111     % Ridge Detection
112     %[fridge_c,~,lr_c] = tfridge(p_c,f_c,ridgeWidth);
113     [fridge_c,~,lr_c] = tfridge(p_c,f_c,ridgeWidth);
114
115     % Average Data
116     tt_secs_c = array2timetable(fridge_c.*60,'RowTimes',seconds(t_c));
117     tt_mins_c=retime(tt_secs_c,'minutely','mean');
118     time_av_c = seconds(tt_mins_c.Time);
119
120     % Plot and Save Spectogram and ridge output
```

```
121     Spectogram = figure();
122     title("Spectogram Output");
123     imagesc(t_c,f_c,log(p_c));
124     set(gca, 'YDir', 'normal');
125     colorbar();
126     xlabel('Time (Samples)');
127     ylabel('Frequency (mHz)');
128 
129     hold on;
130     plot(t_c,fridge_c,'r','LineWidth',2);
131     hold off;
132 
133     savefile = strjoin(["Channel", channelTested,'/Output/Spectogram/',
        TestString(testNum), '_Spectogram.png'],'');
134     saveas(Spectogram,savefile)
135 
136     % Calculate and Plot BPM comparasion
137     B_BPM = PnemoData(1:end-1);
138     C_BPM = tt_mins_c.Var1(1:length(B_BPM));
139 
140     Compare = figure();
141 
142     C_BA = [C_BA; C_BPM];
143     B_BA = [B_BA; B_BPM];
144 
145 %
146 %     if length(PnemoData)<length(C_BPM)
147 %         C_BA = [C_BA; C_BPM(1:length(PnemoData))];
148 %         B_BA = [B_BA; B_BPM];
149 %     else
150 %         C_BA = [C_BA; C_BPM];
151 %         B_BA = [B_BA; PnemoData(1:length(C_BPM))];
152 %     end
153 
154     plot(time_av_c(1:length(C_BPM))./60,C_BPM,'linewidth',2);
155     hold on;
156     t_Pnemo = 0:1:length(B_BPM)-1;
157     plot(t_Pnemo,B_BPM,'linewidth',2);
158 
159     legend('Capaciflector','CPET');
160     title('CPET BPM vs Capaciflector BPM');
161     xlabel('Time (Minutes)');
162     ylabel('Breaths Per Minute (BPM)');
163 
164     savefile = strjoin(["Channel", channelTested,'/Output/Compare/',
        TestString(testNum), '_Compare.png'],'');
165     saveas(Compare,savefile)
166 
167 end
168 
```

```
save(strjoin(["Channel", channelTested,'/Output/Capaciflector.mat'],''),'B_BA');
save(strjoin(["Channel", channelTested,'/Output/Belt.mat'],''),'C_BA');

% Calculate Bland Altman Plot Values
d_dif = B_BA-C_BA;
d_mean = [B_BA,C_BA];
d_mean = nanmean(d_mean,2);
d_bias = nanmean(d_dif);
d_std = nanstd(d_dif);

d_LLOA = d_bias - (1.96*d_std);
d_ULOA = d_bias + (1.96*d_std);


% Plot Bland Altman Plot
BlandAltman = figure();

plot(d_mean, d_dif,'*r','MarkerFaceColor','k','MarkerSize',6);

title('Bland Altman Plot');
xlabel('Mean Respiration (BPM)');
ylabel('RR Difference (BPM)');

%Drawing the center line
yline(0,'k','LineWidth',2);

%Drawing the Bias
yline(d_bias,'b','Bias ('+string(d_bias)+')','FontSize', 18,'LineWidth',2);

%Drawing Upper and lower Limits
yline(d_LLOA,'--o','-1.96 SD ('+string(d_LLOA)+')','FontSize', 18,'LineWidth',2);
yline(d_ULOA,'--o','+1.96 SD ('+string(d_ULOA)+')','FontSize', 18,'LineWidth',2);

% Save Bland Altman Plot
savefile = strjoin(["Channel", channelTested, '_BlandAltman.png'],'');
saveas(BlandAltman,savefile)
```

LISTING D.1: Matlab Code used to process the data in Chapter 3

```
close all;


[file,path] = uigetfile('*.txt');
if isequal(file,0)
   %disp('User selected Cancel');
else
   %disp(['User selected ', fullfile(path,file)]);
```

```
    fileLoc = fullfile(path,file);
end

%% Filter Settings
filterHP = designfilt('highpassiir','FilterOrder',2, ...
         'PassbandFrequency',0.02, ...
         'SampleRate',10);

%% Settings

% Spectogram Settings
ridgeWidth = 0.005;
timeRatio = 60;
freqLimits = [0.1 0.8];
overlapPercent = 90;
leakage = 0;

divider = 1;
twoPow28 = 2^28;
fref = 43400000/divider;
C = 33;
L = 18;

belt = 0;

%% Import Data
Data = readData(fileLoc);
Data = table2array(Data);

if(belt)
    Data_B = readData(fileLoc, true);
end


t_raw = str2double(Data(3:end,1));
capRaw = str2double(Data(3:end,4));
accelX = str2double(Data(3:end,5));
accelY = str2double(Data(3:end,6));
accelZ = str2double(Data(3:end,7));
bat = str2double(Data(3:end,8));

% t = t(1:2600);
% capRaw = capRaw(1:2600);
% accelX = accelX(1:2600);
% accelY = accelY(1:2600);
% accelZ = accelZ(1:2600);

sampleRate =  str2double(regexprep(Data(1:1),{'\D*([\d\.]+\d)[^\d]*', '
    [^\d\.]*'},{'$1 ', ' '}));

t = (t_raw.*(sampleRate/1000));
```

```
capHz = fref.* (capRaw./twoPow28);
cap = 10E12 * (1./(L*10E-6 .* power(capHz .* 2 .* pi,2)));
cap = cap - C;
%cap = capRaw;
accelX = accelX./8192;
accelY = accelY./8192;
accelZ = accelZ./8192;
bat = bat./1000;

% dur = t;
d_t = t_raw.*sampleRate;
dur = duration(0,0,0,d_t,'Format','hh:mm:ss.SSSS');

figure();
subplot(2,1,1);
plot(dur,cap,'LineWidth',2);
title("Capacitance Data");
xlabel("Time (hh:mm:ss)");
ylabel("Capacitance (pF)");

subplot(2,1,2);
plot(dur,accelX,'LineWidth',2);
hold on;
plot(dur,accelY,'LineWidth',2);
plot(dur,accelZ,'LineWidth',2);
title("Accelerometer Data");
xlabel("Time (hh:mm:ss)");
ylabel("Accelerometer (g)");
legend("Accel X", "Accel Y", "Accel Z");
hold off;

%% Testing
C_BPM = [];
B_BPM = [];

C_data = filtfilt(filterHP,cap);
%C_data = cap;
figure();
plot(C_data,'LineWidth',2);

%C_data = lowpass(C_data, 60, 20);
C_data = movmean(C_data,10);

figure();
plot(C_data,'LineWidth',2)

if(belt)
    [p_b,f_b,t_b]=pspectrum(Data_B(:,2),10,'spectrogram','TimeResolution'
    ,timeRatio,'Reassign',false,'FrequencyLimits',freqLimits,'
    OverlapPercent',overlapPercent,'Leakage',leakage);
    [fridge_b,~,lr_b] = tfridge(p_b,f_b,ridgeWidth);
```

```
108
109     figure();
110     % Capaciflector
111     imagesc(t_b,f_b,log(p_b));
112     set(gca, 'YDir', 'normal');
113     colorbar();
114     xlabel('Time (Seconds)');
115     ylabel('Frequency (Hz)');
116
117     hold on;
118     plot(t_b,fridge_b,'r','LineWidth',2);
119     hold off;
120
121     title("Belt");
122
123     tt_secs_b = array2timetable(fridge_b.*60,'RowTimes',seconds(t_b));
124     tt_mins_b=retime(tt_secs_b,'minutely','mean');
125     time_av_b = seconds(tt_mins_b.Time);
126
127     B_BPM(:,1) = time_av_b./60;
128     B_BPM(:,2) = tt_mins_b.Var1;
129
130      % Plot Data Ouput
131     figure();
132     plot(B_BPM(:,1),B_BPM(:,2),'linewidth',2);
133     xlabel('Time (Minutes)');
134     ylabel('Respiration Rate  (Breaths Per Minute)');
135     title('Belt Respiration Rate vs Time');
136 end
137
138 [p_c,f_c,t_c]=pspectrum(C_data,1000/sampleRate,'spectrogram','
        TimeResolution',timeRatio,'Reassign',false,'FrequencyLimits',
        freqLimits,'OverlapPercent',overlapPercent,'Leakage',leakage);
139
140 % Ridge Detection
141 [fridge_c,~,lr_c] = tfridge(p_c,f_c,ridgeWidth);
142
143 % Test = figure();
144 % % t_m = seconds(t);
145 % % t_m = t_m.Format('mm');
146 % plot(t_m,bat,'linewidth',2);
147 % title('Battery Voltage vs Time');
148 % xlabel('Time (Seconds)');
149 % ylabel('Battery (V)');
150
151 % Plot and Save Spectogram and ridge output
152 Spectogram = figure();
153 % Capaciflector
154 imagesc(t_c,f_c,log(p_c));
155 set(gca, 'YDir', 'normal');
156 colorbar();
```

```
157 xlabel('Time (Seconds)');
158 ylabel('Frequency (Hz)');
159
160 hold on;
161 plot(t_c,fridge_c,'r','LineWidth',2);
162 hold off;
163
164 title("Capaciflector");
165
166 tt_secs_c = array2timetable(fridge_c.*60,'RowTimes',seconds(t_c));
167 tt_mins_c=retime(tt_secs_c,'minutely','mean');
168 time_av_c = seconds(tt_mins_c.Time);
169
170 C_BPM(:,1) = time_av_c./60;
171 C_BPM(:,2) = tt_mins_c.Var1;
172
173  % Plot Data Ouput
174 Compare = figure();
175 plot(C_BPM(:,1),C_BPM(:,2),'linewidth',2);
176 xlabel('Time (Minutes)');
177 ylabel('Respiration Rate  (Breaths Per Minute)');
178 title('Capaciflector Respiration Rate vs Time');
179
180 %%
181 if(belt)
182 % Calculate Bland Altman Plot Values
183     d_dif = B_BPM(:,2)-C_BPM(:,2);
184     d_mean = [B_BPM(:,2),C_BPM(:,2)];
185     d_mean = nanmean(d_mean,2);
186     d_bias = nanmean(d_dif);
187     d_std = nanstd(d_dif);
188
189     d_LLOA = d_bias - (1.96*d_std);
190     d_ULOA = d_bias + (1.96*d_std);
191
192
193     % Plot Bland Altman Plot
194     BlandAltman = figure();
195
196     plot(d_mean, d_dif,'*r','MarkerFaceColor','k','MarkerSize',6);
197
198     %ylim([-1 2]);
199
200     title('Bland Altman Plot');
201     xlabel('Mean Respiration (BPM)');
202     ylabel('RR Difference (BPM)');
203
204     %Drawing the center line
205     yline(0,'k','LineWidth',2);
206
207     %Drawing the Bias
```

```
208     yline(d_bias,'b','Bias ('+string(d_bias)+')','FontSize', 18,'
    LineWidth',2, 'LabelVerticalAlignment', 'middle');
209
210     %Drawing Upper and lower Limits
211     yline(d_LLOA,'--o','-1.96 SD ('+string(d_LLOA)+')','FontSize', 18,'
    LineWidth',2, 'LabelVerticalAlignment', 'bottom');
212     yline(d_ULOA,'--o','+1.96 SD ('+string(d_ULOA)+')','FontSize', 18,'
    LineWidth',2, 'LabelVerticalAlignment', 'top');
213 end
```

LISTING D.2: Matlab Code used to process the data in Chapter 5

D.2 Micro controller Firmware Code

```
1  // Enable Capacitance Chip
2  gpioClearOutput(AUXIO_0_CONTROL_FDC2214);
3
4  // CAPACITANCE SENSOR Config
5
6  // Init Channel 0
7  i2cDeviceWriteReg16MsbFirst(FDC2214_I2C_ADDR,FDC2214_SETTLECOUNT_CH0,0
       x0400);
8
9  //rcount maximized for low power operation
10 i2cDeviceWriteReg16MsbFirst(FDC2214_I2C_ADDR,FDC2214_RCOUNT_CH0,0xFFFF);
11
12 i2cDeviceWriteReg16MsbFirst(FDC2214_I2C_ADDR,FDC2214_ERROR,0x0001);
13
14 //no offset
15 i2cDeviceWriteReg16MsbFirst(FDC2214_I2C_ADDR,FDC2214_OFFSET_CH0,0x0000);
16
17 //Set clock dividers
18 i2cDeviceWriteReg16MsbFirst(FDC2214_I2C_ADDR,FDC2214_CLOCK_DIVIDERS_CH0,
       0x1001);
19
20 //set drive register
21 i2cDeviceWriteReg16MsbFirst(FDC2214_I2C_ADDR,FDC2214_DRIVE_CH1, 0x8C40);
22
23 //Set MUX
24 i2cDeviceWriteReg16MsbFirst(FDC2214_I2C_ADDR,FDC2214_MUX_CONFIG, 0x020D);
25
26 // Config with Sleep Still enabled
27 i2cDeviceWriteReg16MsbFirst(FDC2214_I2C_ADDR,FDC2214_CONFIG,0x1441);
28
29 U16 devId = 0;
30 state.capReady = 0;
31
32 i2cDeviceReadReg16MsbFirst(FDC2214_I2C_ADDR,FDC2214_DEVICE_ID;devId);
33
```

```
if (devId == 0x3055){
    state.capReady = 1;
}

i2cDeviceWriteReg8(MPU_ADDR,MPU_GYRO_CONFIG,0x00);
i2cDeviceWriteReg8(MPU_ADDR,MPU_ACCEL_CONFIG,0x08);

if(cfg.gyroEnable == 1){
    i2cDeviceWriteReg8(MPU_ADDR,MPU_PWR_MGMT_2,0x00);
}else{
    i2cDeviceWriteReg8(MPU_ADDR,MPU_PWR_MGMT_2,0x07);
}

i2cDeviceWriteReg8(MPU_ADDR,MPU_PWR_MGMT_1,0x08);

i2cDeviceReadReg8(MPU_ADDR,MPU_DEV_ID;devId);

if(devId == 104){
    state.mpuReady = 1;
}
```

LISTING D.3: Initialisation Code for the Sensor Controller Studio Tasks

```
U16 msb = 0;
U16 lsb = 0;
U16 n = 0;
U16 readyBit = 0;

for(U16 n = 0; n < BUFF_MIN; n++){
    // RTC READ
    i2cDeviceReadReg8(RTC_ADDR,RTC_SEC;output.rtcSec[n]);
    i2cDeviceReadReg8(RTC_ADDR,RTC_MIN;output.rtcMin[n]);
    i2cDeviceReadReg8(RTC_ADDR,RTC_HRS;output.rtcHrs[n]);

    // CAPACITANCE READ
    i2cDeviceReadReg16MsbFirst(FDC2214_I2C_ADDR,FDC2214_DATA_CH0_MSB;
    output.capMsb[n]);
    i2cDeviceReadReg16MsbFirst(FDC2214_I2C_ADDR,FDC2214_DATA_CH0_LSB;
    output.capLsb[n]);

    // MPU READ
    i2cDeviceReadReg8(MPU_ADDR,MPU_ACCEL_X_H;msb);
    i2cDeviceReadReg8(MPU_ADDR,MPU_ACCEL_X_L;lsb);

    output.accelX[n] = lsb | (msb << 8);

    i2cDeviceReadReg8(MPU_ADDR,MPU_ACCEL_Y_H;msb);
    i2cDeviceReadReg8(MPU_ADDR,MPU_ACCEL_Y_L;lsb);

    output.accelY[n] = lsb | (msb << 8);

```

```
    i2cDeviceReadReg8(MPU_ADDR,MPU_ACCEL_Z_H;msb);
    i2cDeviceReadReg8(MPU_ADDR,MPU_ACCEL_Z_L;lsb);

    output.accelZ[n] = lsb | (msb << 8);

    if(cfg.gyroEnable == 1){
        i2cDeviceReadReg8(MPU_ADDR,MPU_GYRO_X_H;msb);
        i2cDeviceReadReg8(MPU_ADDR,MPU_GYRO_X_L;lsb);

        output.gyroX[n] = lsb | (msb << 8);

        i2cDeviceReadReg8(MPU_ADDR,MPU_GYRO_Y_H;msb);
        i2cDeviceReadReg8(MPU_ADDR,MPU_GYRO_Y_L;lsb);

        output.gyroY[n] = lsb | (msb << 8);

        i2cDeviceReadReg8(MPU_ADDR,MPU_GYRO_Z_H;msb);
        i2cDeviceReadReg8(MPU_ADDR,MPU_GYRO_Z_L;lsb);

        output.gyroZ[n] = lsb | (msb << 8);
    }

    // Delay Sample Rate
    fwDelayUs(50000, FW_DELAY_RANGE_100_MS);
}

i2cDeviceReadReg8(RTC_ADDR,RTC_DAY;output.rtcDay);
i2cDeviceReadReg8(RTC_ADDR,RTC_DATE;output.rtcDate);
i2cDeviceReadReg8(RTC_ADDR,RTC_MONTH;msb);
i2cDeviceReadReg8(RTC_ADDR,RTC_YEAR;output.rtcYear);

output.rtcMonth = msb & 0x7F;

fwGenAlertInterrupt();
```

LISTING D.4: Execution Code for the Sensor Controller Studio Tasks

```
/*
 *  ======== Main function ========
 */
void SD_DataLogger_taskFxn(UArg a0, UArg a1)
{
    SD_DataLogger_init();

    if (isWakingFromShutdown) {
        uint32_t sleepUs = 300000;
        GPIO_write(Board_GPIO_RED_LED, 1);
        Task_sleep(sleepUs / Clock_tickPeriod);
        GPIO_write(Board_GPIO_RED_LED, 0);
        Task_sleep(sleepUs / Clock_tickPeriod);
    }
```

```
15
16      for(;;){
17          uint32_t events;
18
19          // Waits for an event to be posted associated with the calling
    thread.
20          // Note that an event associated with a thread is posted when a
21          // message is queued to the message receive queue of the thread
22          events = Event_pend(syncEvent, Event_Id_NONE, SD_ALL_EVT,
23                              BIOS_WAIT_FOREVER);
24
25          // Process Events
26          if(events){
27
28              // Long Button Press Event
29              if(events & SD_PWR_BTN_LONG_EVT){
30                  if(!isSampling){
31                      // Do Nothing
32                      //stopSampling();
33                      powerOff();
34                  }else{
35                      isSampling = false;
36
37                      // Close File After Sampling is done and go to sleep
38                      stopSampling();
39                  }
40              }
41
42              // Short Button Press Event
43              if(events & SD_PWR_BTN_SHORT_EVT){
44
45                  // Check if Sampling Stopped or Started
46                  if(isSampling){
47                      //Currently Sampling DO NOTHING
48                      //isSampling = false;
49                      //stopSampling();
50                  }else{
51                      isSampling = true;
52
53                      // Mount and register the SD Card
54                      sdfatfsHandle = SDFatFS_open(Board_SD0, DRIVE_NUM);
55                      if (sdfatfsHandle == NULL) {
56                          Display_printf(display, 0, 0, "Error starting the
     SD card\n");
57                          //HAL_SYSTEM_RESTART();
58                      }
59                      else {
60                          Display_printf(display, 0, 0, "Drive %u is
    mounted\n", DRIVE_NUM);
61                      }
62
```

```
63                      // SCS Start Task and enter sleep mode
64                      //scifStartTasksNbl(1 << SCIF_SENSORS_TASK_ID);
65                      //DELAY_MS(100);
66                      if (scifWaitOnNbl(1000000) != SCIF_SUCCESS) {
67                          Display_printf(display, 0, 0, "Error");
68                      } else if (scifStartTasksNbl(1 <<
    SCIF_SENSORS_TASK_ID) != SCIF_SUCCESS) {
69                          Display_printf(display, 0, 0, "Started Task");
70                      }
71
72                      // Open a new file for Sampling
73                      fileOpen = openFile(&dataFile);
74
75                      if(fileOpen){
76                          // Start Sampling Timer
77                          //Util_startClock(&periodicClock);
78
79                          // Run the "Sensors" Execution Code
80                          if (scifWaitOnNbl(1000000) != SCIF_SUCCESS) {
81                              Display_printf(display, 0, 0, "Error");
82                              isSampling = false;
83                              if (scifWaitOnNbl(1000000) != SCIF_SUCCESS) {
84                                  Display_printf(display, 0, 0, "Error");
85                              } else if (scifStopTasksNbl(1 <<
    SCIF_SENSORS_TASK_ID) != SCIF_SUCCESS) {
86                                  Display_printf(display, 0, 0, "Error
    Stoping Task");
87                              }
88                              SDFatFS_close(sdfatfsHandle);
89                              blinkLed(Board_GPIO_RED_LED,1);
90                          } else if (scifSwTriggerExecutionCodeNbl(1 <<
    SCIF_SENSORS_TASK_ID) != SCIF_SUCCESS) {
91                              Display_printf(display, 0, 0, "Error Starting
     Task");
92                              isSampling = false;
93                              if (scifWaitOnNbl(1000000) != SCIF_SUCCESS) {
94                                  Display_printf(display, 0, 0, "Error");
95                              } else if (scifStopTasksNbl(1 <<
    SCIF_SENSORS_TASK_ID) != SCIF_SUCCESS) {
96                                  Display_printf(display, 0, 0, "Error
    Stopping Task");
97                              }
98                              SDFatFS_close(sdfatfsHandle);
99                              blinkLed(Board_GPIO_RED_LED,1);
100                         }else{
101                             blinkLed(Board_GPIO_GREEN_LED,1);
102                             //Util_stopClock(&ledClock);
103                             Display_printf(display, 0, 0, "Started
    Sampling");
104                         }
105                     }else{
```

```
106                         isSampling = false;
107                         if (scifWaitOnNbl(1000000) != SCIF_SUCCESS) {
108                             Display_printf(display, 0, 0, "Error");
109                         } else if (scifStopTasksNbl(1 <<
    SCIF_SENSORS_TASK_ID) != SCIF_SUCCESS) {
110                             Display_printf(display, 0, 0, "Error Stoping
    Task");
111                         }
112                         SDFatFS_close(sdfatfsHandle);
113                         blinkLed(Board_GPIO_RED_LED,1);
114                     }
115                 }
116             }
117
118             // Sampling Event
119             if((events & SD_PERIODIC_EVT) && isSampling){
120
121                 // Run the "Sensors" Execution Code
122                 if (scifWaitOnNbl(20000) != SCIF_SUCCESS) {
123                     Display_printf(display, 0, 0, "Error Timeout Fail");
124                     isSampling = false;
125                     if (scifWaitOnNbl(20000) != SCIF_SUCCESS) {
126                         Display_printf(display, 0, 0, "Error \n");
127                     }else if (scifStopTasksNbl((1 << SCIF_SENSORS_TASK_ID
    )) != SCIF_SUCCESS) {
128                         Display_printf(display, 0, 0, "Error Stopping
    Task \n");
129                     }
130                     SDFatFS_close(sdfatfsHandle);
131                     Util_stopClock(&periodicClock);
132                     blinkLed(Board_GPIO_RED_LED,1);
133                 } else if (scifSwTriggerExecutionCodeNbl(1 <<
    SCIF_SENSORS_TASK_ID) != SCIF_SUCCESS) {
134                     Display_printf(display, 0, 0, "Error Starting Task");
135                     isSampling = false;
136                     if (scifWaitOnNbl(20000) != SCIF_SUCCESS) {
137                         Display_printf(display, 0, 0, "Error \n");
138                     }else if (scifStopTasksNbl((1 << SCIF_SENSORS_TASK_ID
    )) != SCIF_SUCCESS) {
139                         Display_printf(display, 0, 0, "Error Stopping
    Task \n");
140                     }
141                     SDFatFS_close(sdfatfsHandle);
142                     Util_stopClock(&periodicClock);
143                     blinkLed(Board_GPIO_RED_LED,1);
144                 }
145
146                 // Start Periodic Clock
147                 //Util_startClock(&periodicClock);
148             }
149
```

```
150             // SCS Event
151             if((events & SD_SCS_SAMPLE_EVT) && isSampling){
152                 // Acknowledge Incoming Data
153                 processData();
154 
155                 Event_post(syncEvent, SD_PERIODIC_EVT);
156 
157                 // Post Event to write to SD card
158                 Event_post(syncEvent,SD_WRITE_EVT);
159 
160 
161             }
162 
163             if((events & SD_WRITE_EVT) && isSampling){
164                 // Write Event
165                 result = writeData(&dataFile,dataSample);
166 
167                 if(result){
168                     // Do Nothing
169 
170                 }else{
171                     // Stop Sampling and go to Standby Mode
172                     isSampling = false;
173                     if (scifWaitOnNbl(20000) != SCIF_SUCCESS) {
174                         Display_printf(display, 0, 0, "Error \n");
175                     }else if (scifStopTasksNbl((1 << SCIF_SENSORS_TASK_ID
    )) != SCIF_SUCCESS) {
176                         Display_printf(display, 0, 0, "Error Stopping
    Task \n");
177                     }
178                     SDFatFS_close(sdfatfsHandle);
179                     Util_stopClock(&periodicClock);
180                     blinkLed(Board_GPIO_RLED, 1);
181                 }
182 
183                 Display_printf(display, 0, 0, "Cap: %d, Accel: %d", cap
    [0],accelX[0]);
184             }
185 
186             // Event for LED Blinking
187             if(events & SD_LED_EVT){
188                 Util_startClock(&ledClock);
189                 if(!isSampling){
190                     blinkLed(Board_GPIO_RED_LED,1);
191                 }else{
192                     //blinkLed(Board_GPIO_GREEN_LED,1);
193                 }
194             }
195 
196         }
197     }
```

```
198 }
```

LISTING D.5: Data Logger Main Code (Simplified View)

Appendix E

Speaking Tests And Supplementary Materials

This appendix has the raw test results for all the speaking tests. As well as the document read for the work done in Chapter 6. The text is the previous introduction which was written for the confirmation reveiw.

E.1 Text Read

Breathing is a vital part of every human's body and is a set of sophisticated processes that help regulate and clean the incoming gases that we breathe. Breathing has many forms and rhythmic movement that links it to other organs movement such as the heart and lungs.

While breathing occurs on a physical level of the human body, respiration occurs at the cellular level; due to the key functionalities of both, they become part of the full breathing cycle in a human body (Negro et al., 2018). The speed of this cycle changes from age to age as a healthy person normally breathes at a standard rate of 12-20 breaths per minute while an infant can breath 25-40 breaths per minute (Yuan et al., 2013). Having slight changes in respiration rate can also be an early indicator of deteriorating health, where respiration rates of $\geq$ 27 BPM can predict cardiac arrest from up to 72 hours (Kelly, 2018).

In hospitals there are multiple methods for detecting respiration, some of the methods are in the form of machines such as a pneumotachometer or by manually counting the number of times the chest rises over a set period of time. This is typically done in 1 minute intervals at set intervals. This become a long and tedious tasks for nurses that are in charge of this process (Wheatley, 2018). The pneumotachometer is an accurate machine which can continuously monitor the respiration of a patient, this is considered

a gold standard machine in respiration detection, due to the accuracy and reliability, as it measures the amount of airflow and pressure coming from the body (Donnelly et al., 2013). The only downside is that this method takes time and requires a machine that is not portable or comfortable to wear.

This shows the need for a respiration monitoring system that is able to continuously monitor the changes in breathing over long periods of time, while also being easy to wear and portable. This type of system should allow the detection of many different types of disorders and conditions that are directly related to respiration, such as obstructive sleep apnoea/hypopnoea (OSAHS), central sleep apnoea (CSA), and hypoventilation syndromes which are all different forms of sleeping disorders (Riha, 2015). While conditions like sepsis, pneumonia, and cardiac arrest can all be identified early by looking at a continuous respiration signal (Ginsburg et al., 2018).

In an analysis done by Lynn and Curry (2011) on unexpected hospital deaths, shows that the early detection of respiration rate changes in disease like sepsis could potentially be avoided if the proper monitoring and alarm systems are set up to identify the changes. Where one of the main factors that change in a predictable manner is the respiratory rate. Figure 1.1 shows an example of an unexpected hospital death signals, where the respiration rate can be seen to have a steady increase over time in an event such as sepsis.

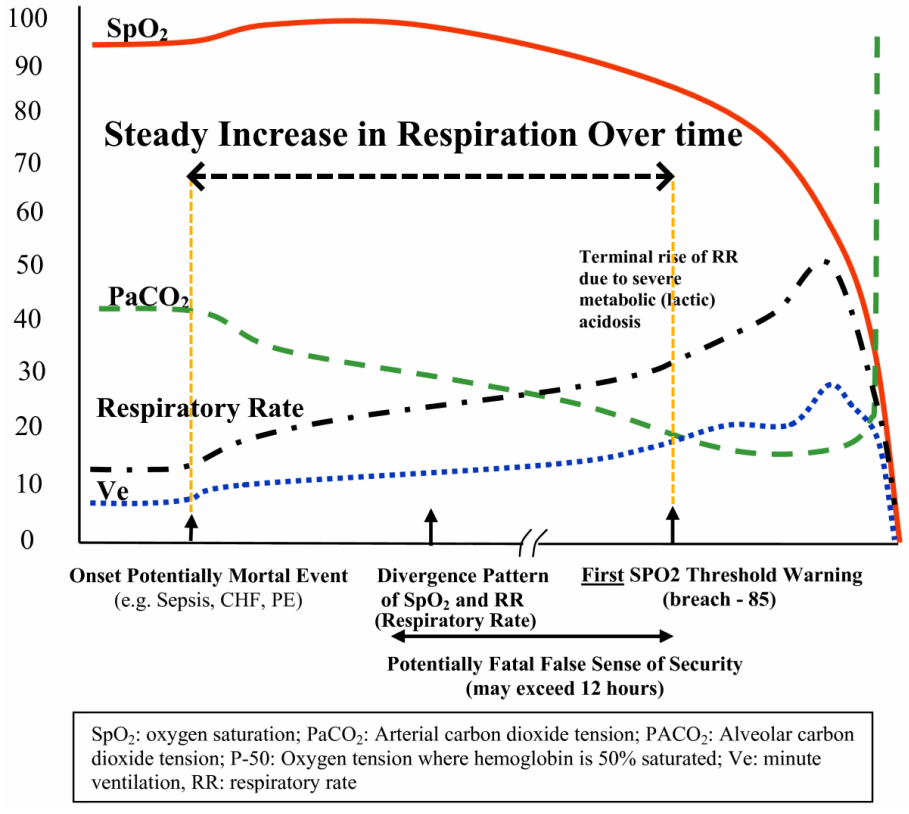

FIGURE E.1: Pattern in unexpected deaths, where respiration can be linked to possible early detection (Sourced and edited from (Lynn and Curry, 2011))

This need for respiration data is reflected by the many different types of scoring systems that are developed to prevent many of these unexpected deaths. The widely used one in the United Kingdom National Health Service (NHS) is the National Early Warning Score (NEWS) developed the Royal College of Physicians, which was updated recently in 2017 to NEWS2. The main aim of this system is to create a standardised system for assessing illness (RCP, 2020). The scoring system uses six physiological parameters that produces a score representing the risk of the patient (RCP, 2020). The NEWS2 score emphasises the need of respiration as a primary parameter, that is important in determining the severity of the patient. And recently there is work done on a new risk score for assessing corona virus patients, which adopts respiration as a primary parameter due to the effects the virus has on the lungs (Knight et al., 2020).

Similarly, the Quick SOFA score that is used for scoring sepsis patients uses respiration as one of the primary parameters for assessing a patients health and their appropriate mortality risk value.

This brings the topic of building such systems that can detect many of these changes in respiration by continuously monitoring the patient and potentially avoiding these deaths. An example is towards Figure E.1 where potentially a continuous monitoring of the respiration could have given an early warning, while potentially preventing the unexpected death. However, for the system to be effectively used in many environments such as the home and hospital, as well as potentially be used in low-resource environments, the system must have a low manufacturing cost while not affecting the accuracy of the sensor/system. In this paper a low-cost sensor system is attributed to be in the range of £100 - £500, which was chosen by the exploration of the average market prices of respiration sensors.

Currently there are sensors that exist in the market to fill the gaps of continuous respiration monitoring while also being relatively cheap (between £500 - £1000), however many of these technologies are not well suited to be easily wearable and portable or more importantly continuous in monitoring over long periods of time. Hence this research aims to produce a better sensor system that can fill in the gap in which many sensor technologies could not, while also having the goal of being low cost, continuous and accurate to be deployed in both home and hospital environments.

The sensor technology that has been decided upon to be used to fill this gap is the capaciflector. The sensor is a essentially a distance sensor that measures respiration by correlating the distance between the chest and the sensor to be attributed as breathing data. This capaciflector is evaluated by testing it in a clinical environment with a total of 70 participants. Two studies were undertaken to assess the effectiveness under stationary conditions, while the other study is to assess the effectiveness and accuracy under the movement of the body by the use of a bicycle.

The results from the studies were used to develop a different form of system that can utilise the capaciflector sensor effectively.

E.2 Raw Test Results

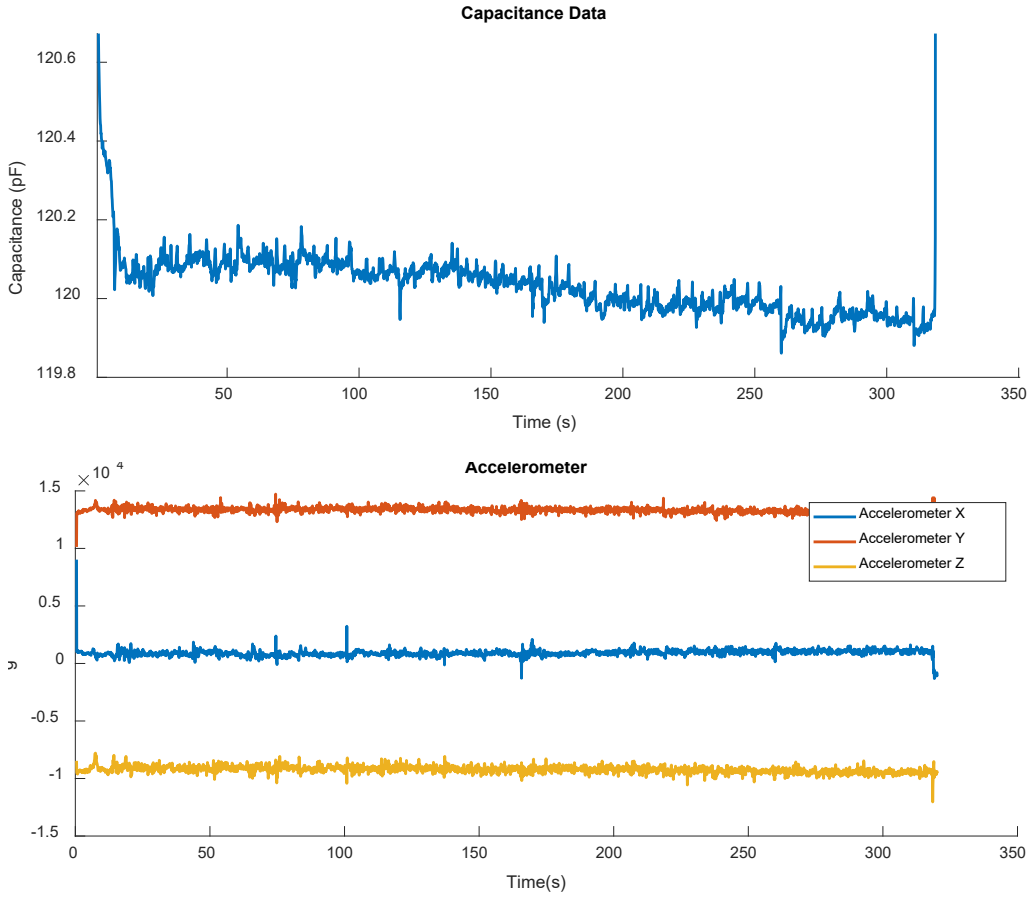

FIGURE E.2: Raw results for test 1 in the speaking study.

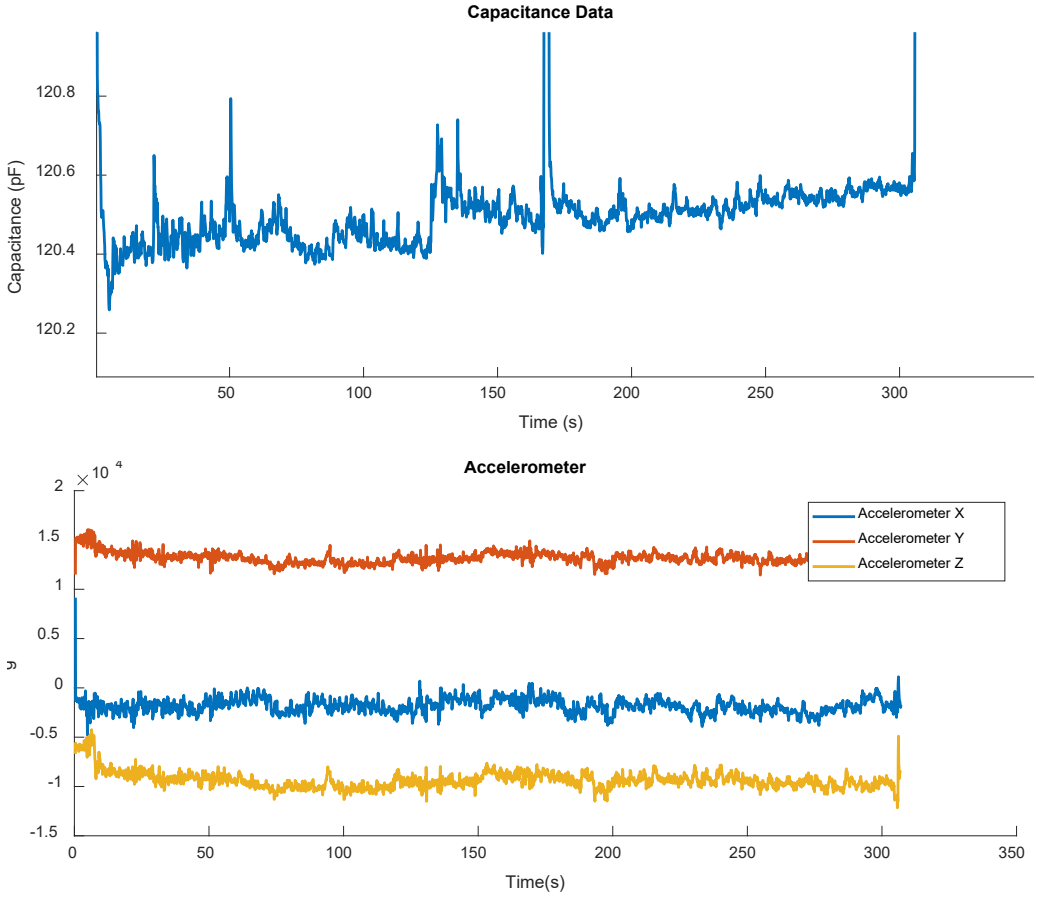

FIGURE E.3: Raw results for test 2 in the speaking study.

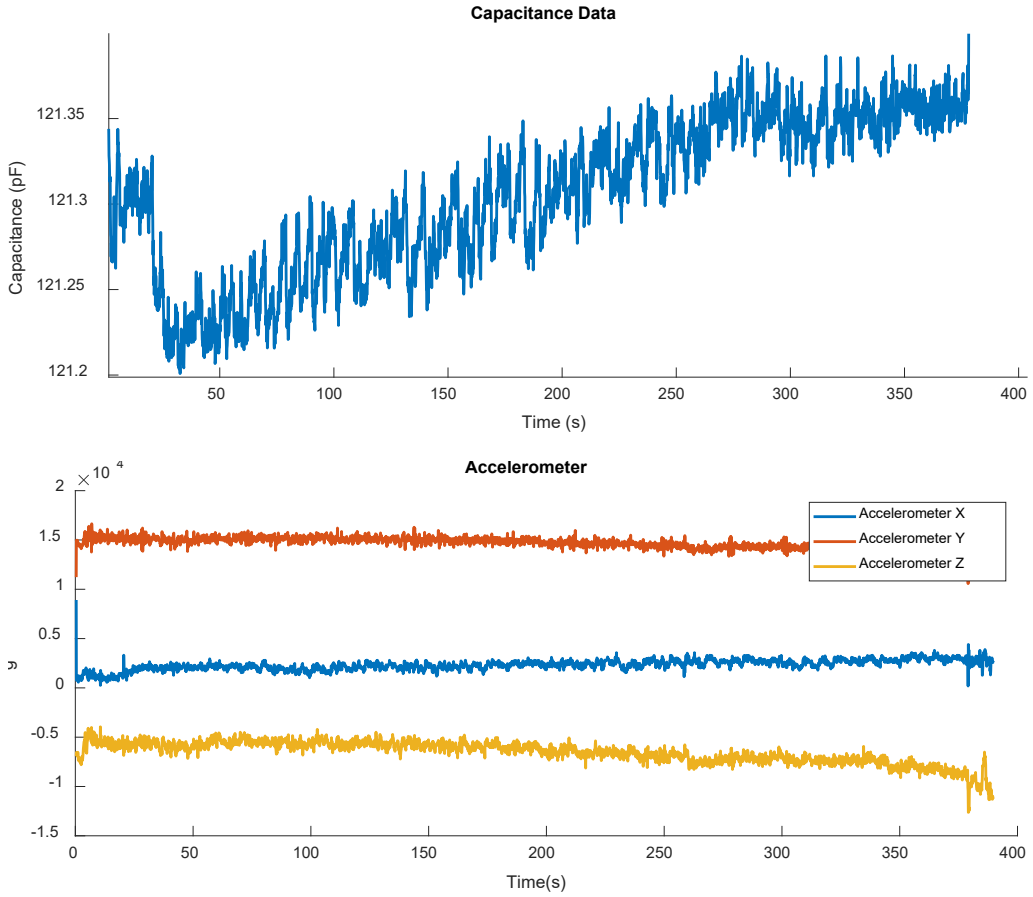

FIGURE E.4: Raw results for test 3 in the speaking study.

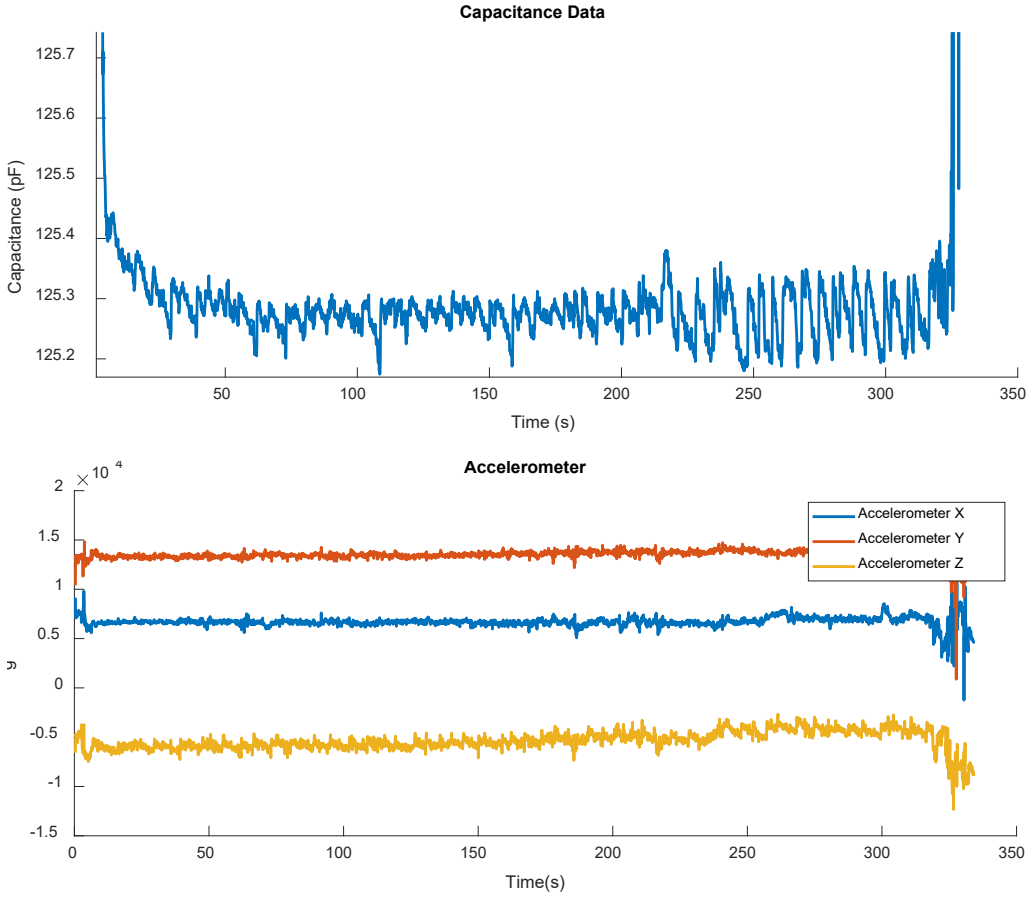

FIGURE E.5: Raw results for test 4 in the speaking study.

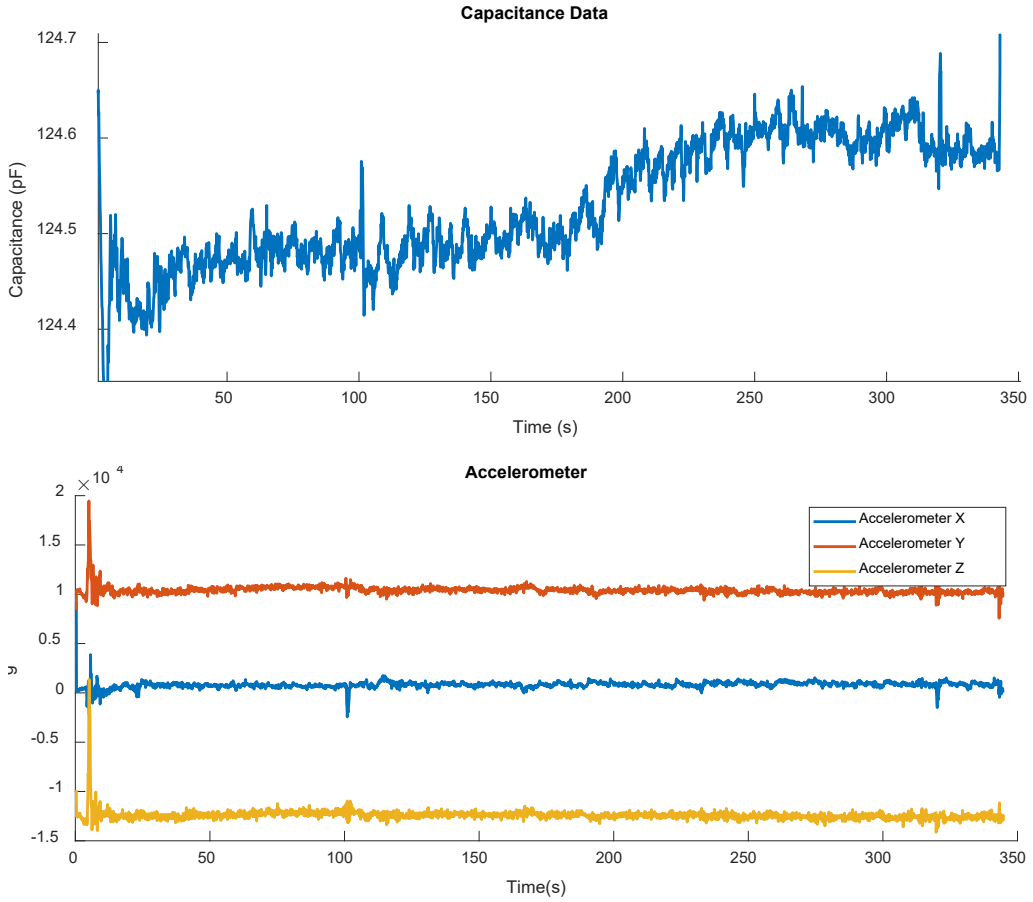

FIGURE E.6: Raw results for test 5 in the speaking study.

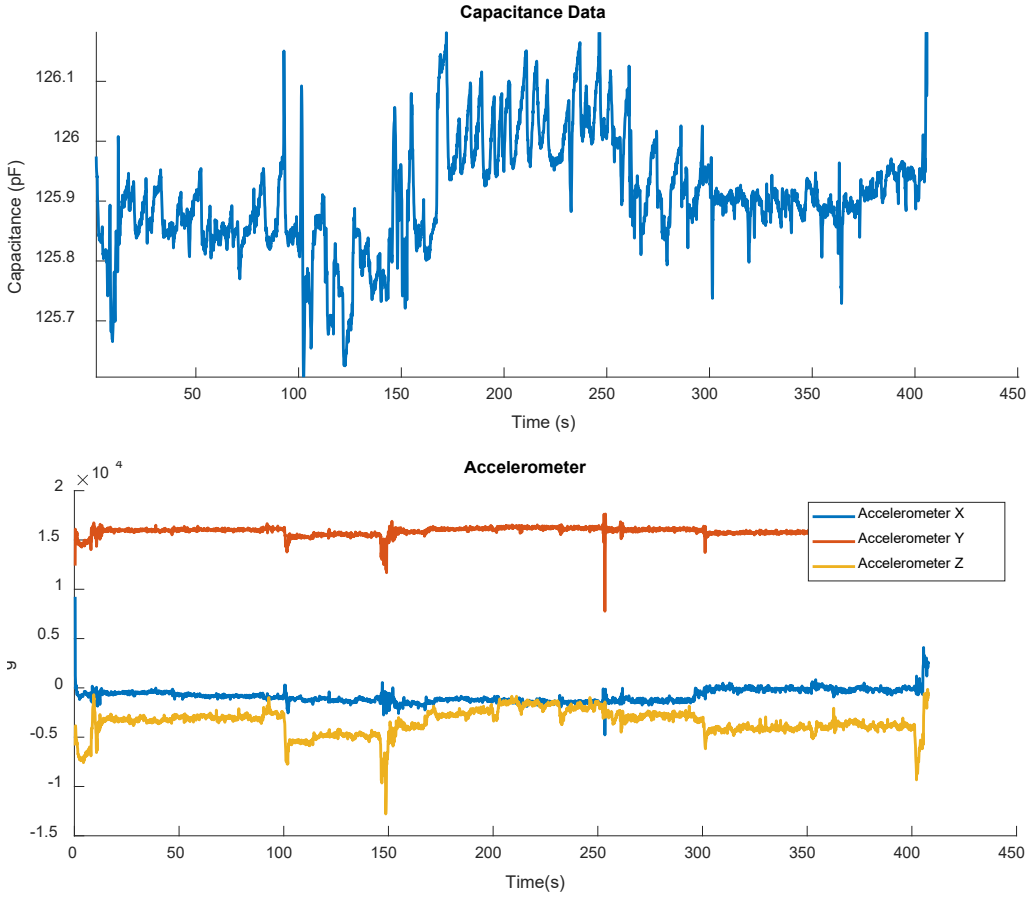

FIGURE E.7: Raw results for test 6 in the speaking study.

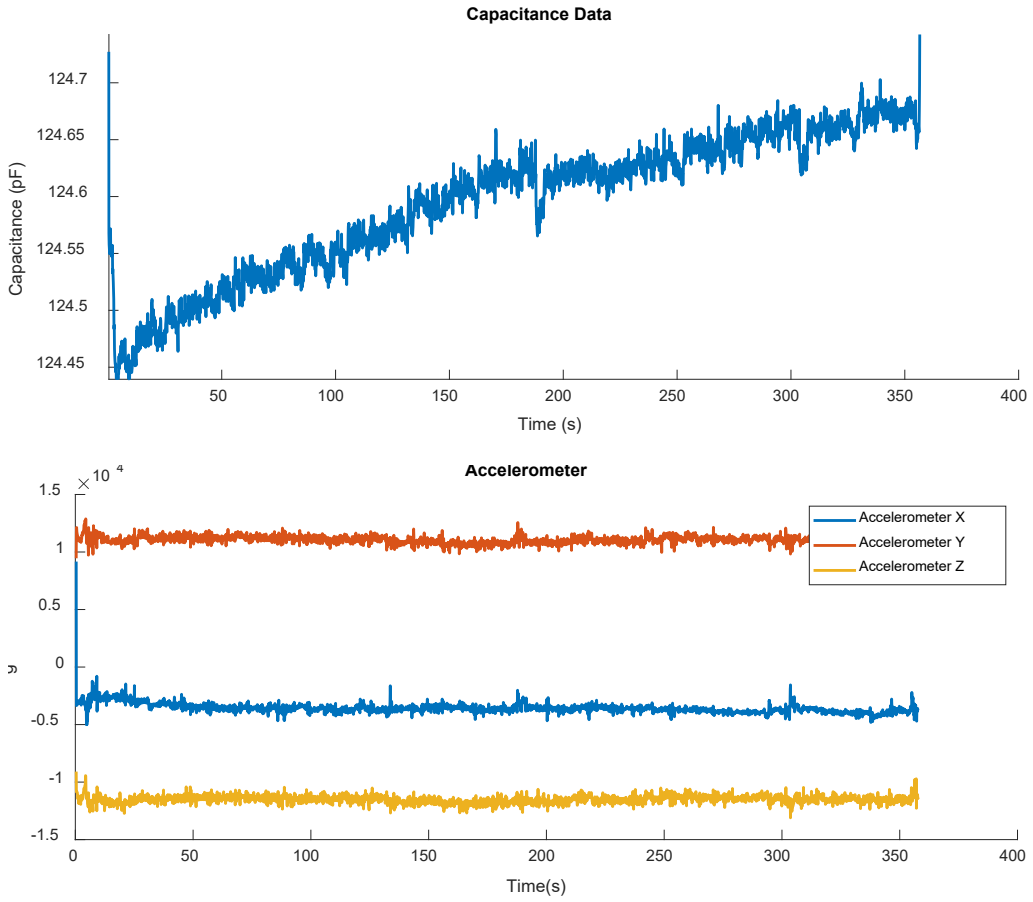

FIGURE E.8: Raw results for test 7 in the speaking study.

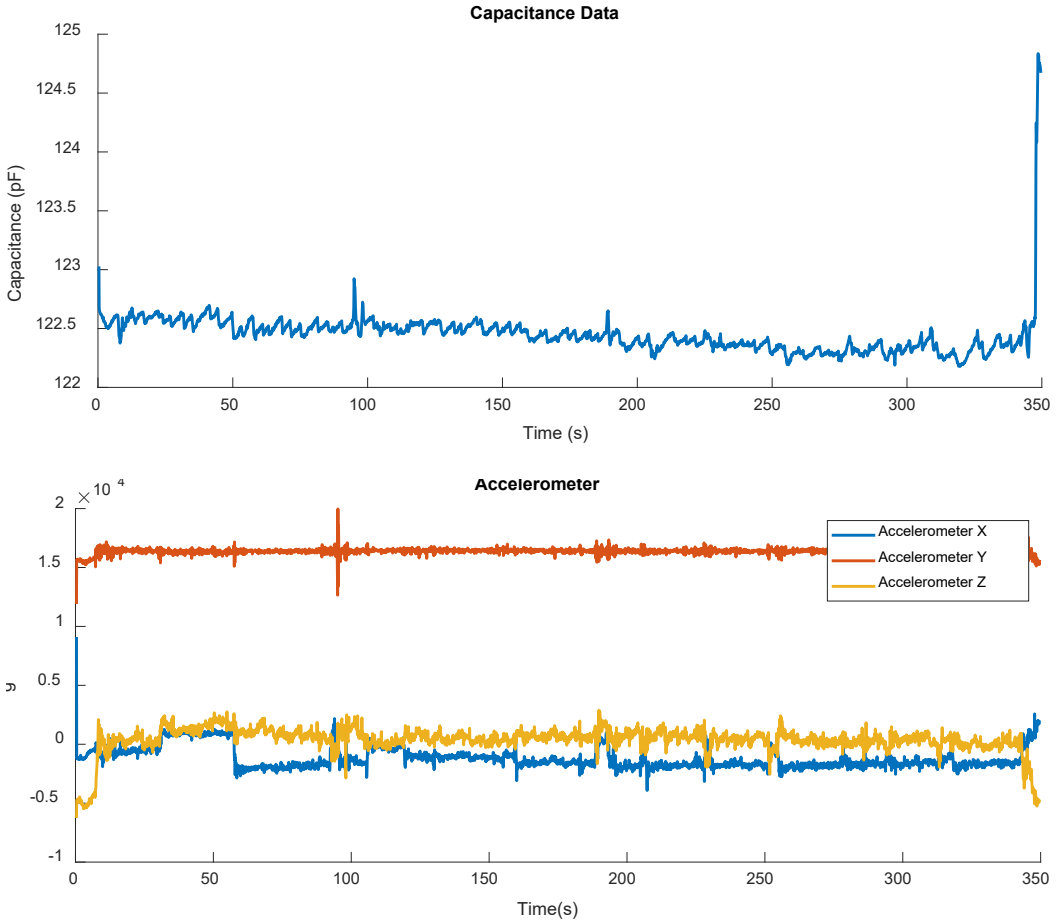

FIGURE E.9: Raw results for test 8 in the speaking study.

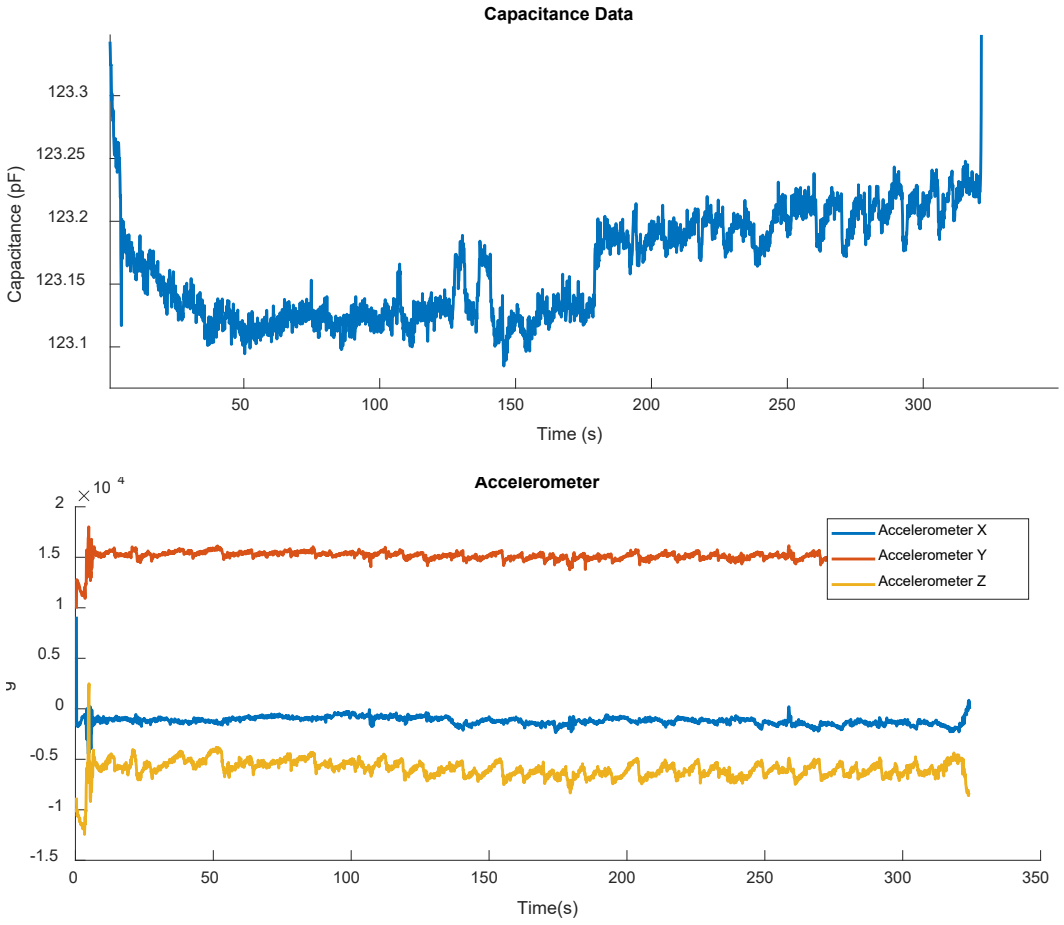

FIGURE E.10: Raw results for test 9 in the speaking study.

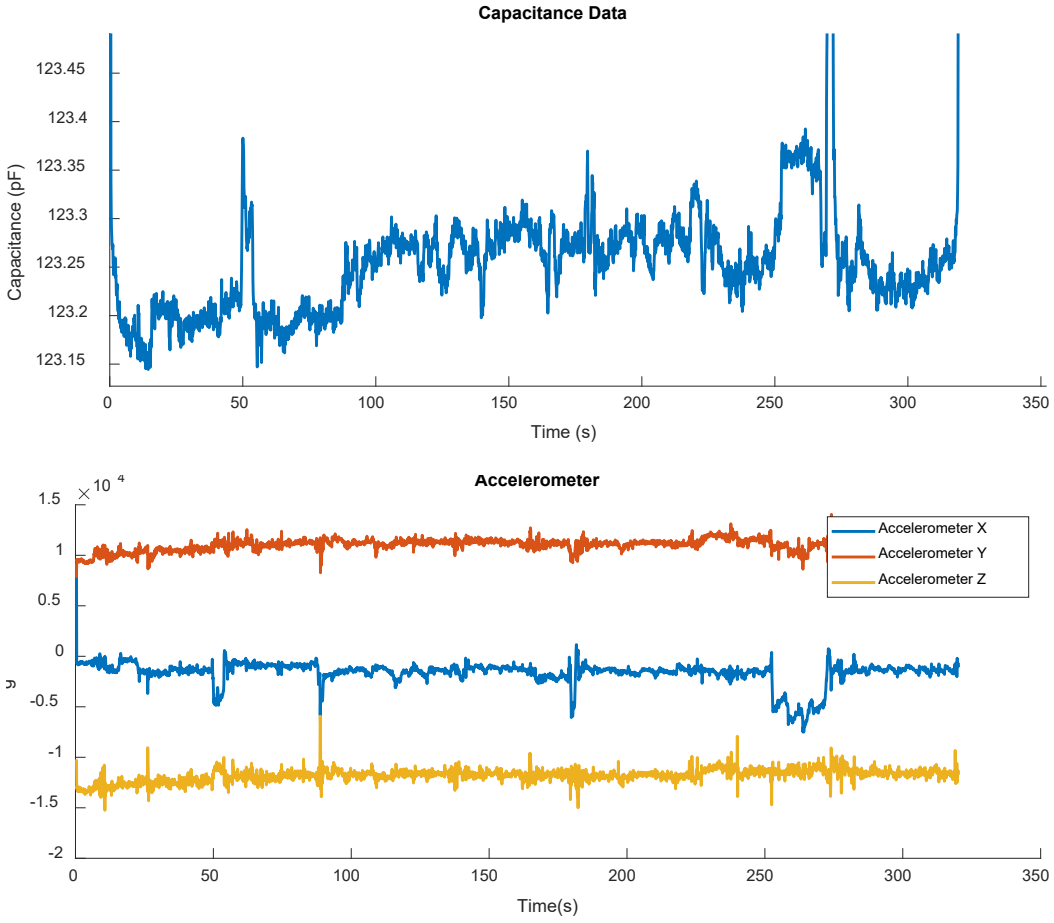

FIGURE E.11: Raw results for test 10 in the speaking study.

Appendix F

Gantt Chart

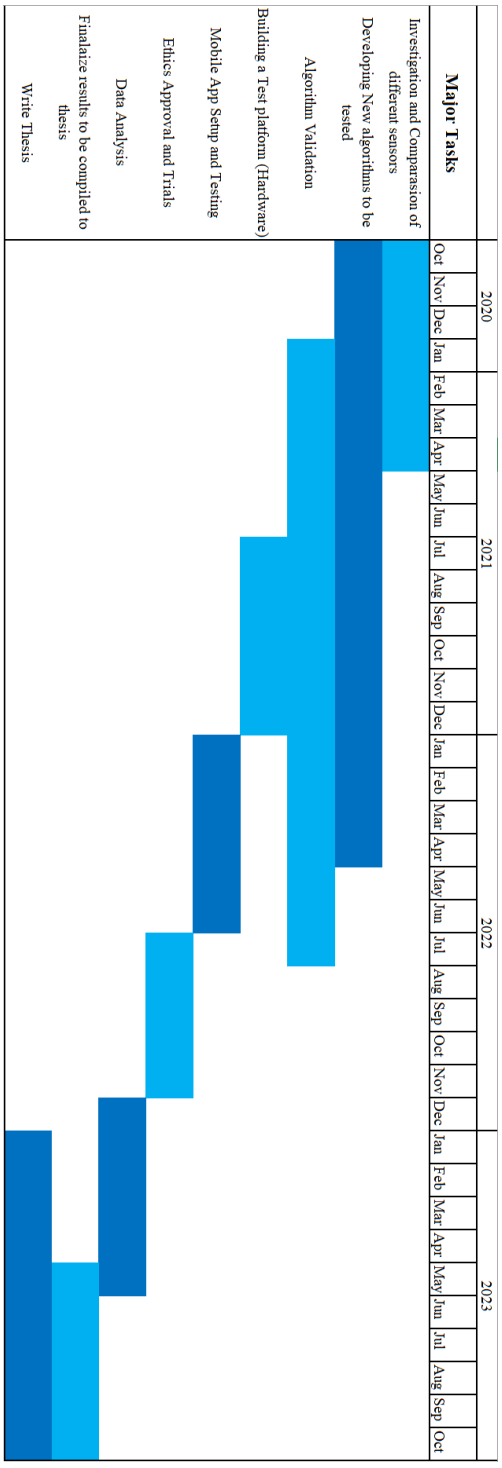

FIGURE F.1: Original Gantt Chart laying out the most major tasks in the PhD

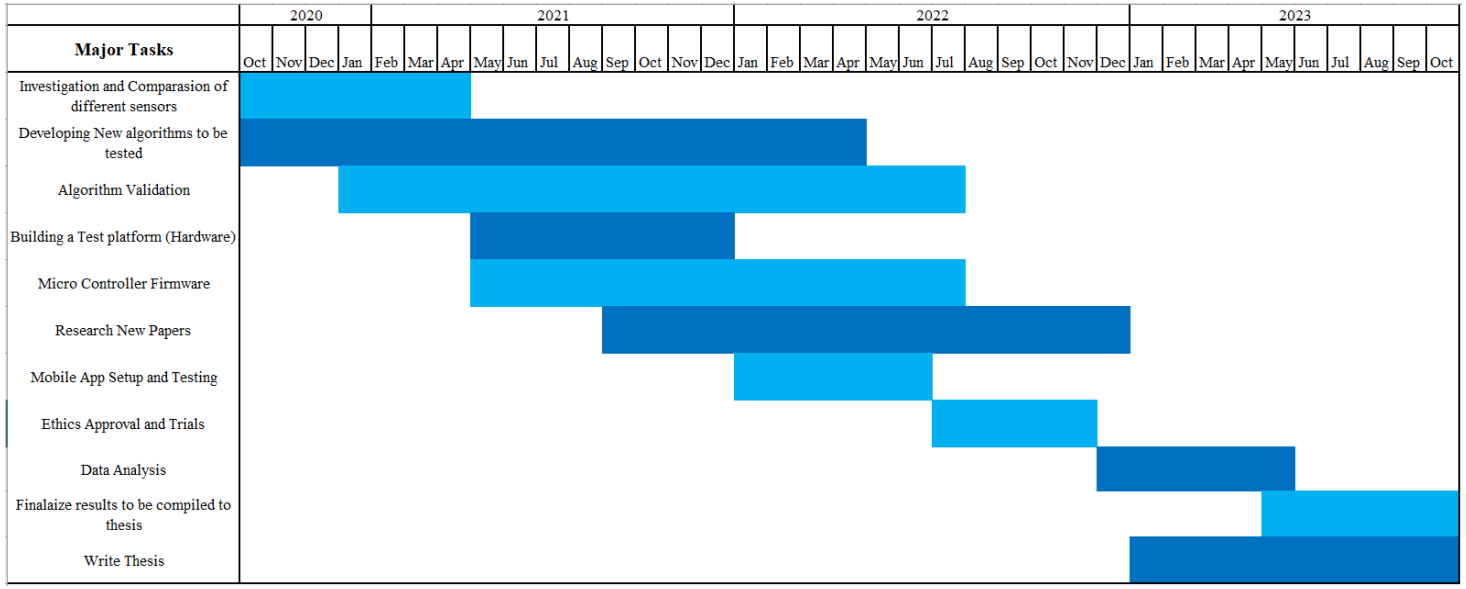

FIGURE F.2: Updated Gantt Chart laying out the most major tasks in the PhD

Appendix G

IEEE Sensors Conference Paper

A New Type of Respiration Sensing System for Continuous Monitoring

Mahdi Shaban[a] Daniel Spencer[a] Neil White[a]

[a] School of Electronics and Computer Science, University of Southampton, Southampton, United Kingdom

ms17g16@soton.ac.uk

0000-0002-7219-3708

***Abstract*—Respiration rate is the number of breaths per minute and is a vital signal that is used readily in the medical field. The gold standard that is currently used is the manual breath count, while there are other methods, these are not suitable for continuous wearable monitoring. Where the need for sensors that can continuously measure respiration rate is important in the detection of respiratory diseases. We have developed a new sensor system capable of measuring respiration continuously for a duration spanning more than 24 hours on a single CR2032 coin cell battery. The system utilities a capaciflector sensor which is a 3-electrode proximity-based capacitance sensor, that works by measuring the capacitance between the sensor electrode and ground. The sensor measures the breathing signal as the modulated change of the skin thickness as the chest expands due to a respiration cycle. The use of a capacitance sensor allowed the device to be more compactly designed and suitable for long term measurements, as well as being capable of capturing respiration data while walking. Two studies were done to measure the accuracy of the system. The first study was taken under a predefined metronome tone between 10 and 19 breaths per minute, where the participants were stationary throughout the test. The second study is a walking test in which the participants walk a predefined route to introduce motion to the respiration data. The tests were compared against a belt sensor by Vernier (Go Direct Respiration Belt) and were analyzed by generating a Bland Altman of the results. The results from the direct comparison of the respiration rate between the two systems in the metronome study resulted in an excellent result of ± 0.68 Breaths Per Minute (BPM) for the variance, with a bias of 0.06 BPM. The second study resulted in ± 1.32 BPM for the variance, and a bias of 0.01 BPM. Concluding the system would be viable for long term monitoring.**

Keywords—Respiration, Breathing, Capaciflector, Sensor, Wearable Sensor, Capacitance, Continuous Monitoring

I. INTRODUCTION

Respiration is a vital parameter in healthcare monitoring, in which it is useful in identifying and preventing illnesses such as sleep apnea and sepsis [1]. It has been shown that respiration is an early indicator of sepsis, where failing to detect changes in respiratory rate can often result in poorer outcomes for the patient, and in serious cases mortality [2]. In some cases where respiratory rates are ≥ 27 Breaths Per Minute (BPM), this can be an early indicator of cardiac arrest [3]. In a recent study about COVID effects on respiration, the respiration rate during COVID correlates with higher mortality risk [4]. The current gold standard for measuring respiration rate is the manual count, which is not a viable option for continuous long-term monitoring, and there are no systems suitable for long term monitoring. This brings up the importance of continuous respiration monitoring, where potentially monitoring the changes in respiration rate can help in identifying illness, thus having the ability to monitor respiration continuously is very beneficial. Many sensors that exist such as force, piezoelectric, ECG, and PPG already are capable of continuous respiration monitoring with some limitations, however many of these sensors fail to satisfy other factors such as comfortability, size, and cost, as well as detection of movement events, which is an important factor for a more robust monitoring system [5]-[8]. The movement events have been a challenge for many sensors as they introduce a uniform noise in the signal. The capaciflector has been shown to detect and measure respiration rate in previous work [9], and for the performance of the sensor under exercise conditions it was presented in previous work done [10], however, both the system that were tested were not wearable and required a tethered connection. We have developed a compact sensor system that uses the capaciflector and is capable of continuously and accurately measuring respiration over long periods of time, while also being capable of discerning between walking events and stationary breathing events.

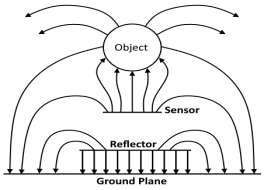

Fig. 1. Capaciflector Sensor Cross Section View.

II. RESPIRATION SENSING SYSTEM

We have developed a new sensor system which can accurately capture respiration rate using a 3-electrode capacitance-based sensor called a capaciflector. The sensor is

a proximity-based sensor that works by measuring the capacitance between the sense-electrode and ground-electrode, which is modulated during breathing (Fig. 1). The third electrode (reflector) is driven to the same potential as the sensor and is used to direct the field into the body [11]. This allows the sensor to be manufactured out of basic components that are commonly found. The size and shape of the three electrodes have a direct impact on the performance of the sensor, in which the change of capacitance is based off the change in distance between the chest and the sensor plate.

Using a capacitance-based sensor allows the sensor to be compactly designed and suitable for long-term measurements unlike many other approaches and in this case an FR-4 PCB based version is manufactured on a 4-layer board. Our miniature system (see Fig. 4) also contains an IMU (Inertial Measurement Unit) for collecting accelerometer data and can continuously measure for periods spanning more than 24 hours using a single CR2032 coin cell battery. The device constructed has an overall diameter of 32 mm with a thickness of 7mm, this can be seen next to a British 2 pence coin for scale in Fig. 4. The sensor can be used wirelessly without attaching it to any external components, allowing the system to be used untethered. The system works by sampling

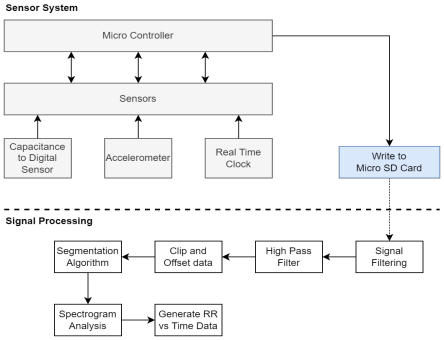

Fig. 3. System Block diagram for the sensor running in datalogger mode and the signal processing.

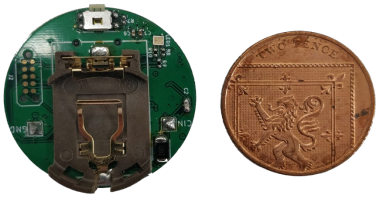

Fig. 4. The developed sensor system next to a 2 Pence British Coin.

the sensors at a defined sample rate of 10 Hz this data is then written to the micro-SD card at a much slower rate (every 20 samples).

III. Methodology

To test the device accuracy, two studies were done to assess the sensor under stationary controlled conditions and while walking. The tests were done under the ERGO ethics in the University of Southampton (ERGO 68839.A1). The first study has ten 5-minute-long tests with a controlled metronome tone, that was done with the capaciflector based system against a gold standard belt sensor by Vernier (Go Direct Respiration Belt). The tests contained metronome values from 10 to 19 BPM. The sensor system was mounted in the top right side of the chest, while the belt sensor was strapped across the chest. The second study has ten 5-minute-tests with the same mounting methods as the first study, where the task is to walk across a predefined route which contains walking up and down a staircase. The aim of the second study is to compare the system performance against movement artifacts.

The processing of the data was done through an algorithm that uses spectrogram processing in order to process the data into frequency against time data. The data is then averaged for that minute to get the minutely breathing data. For study 2, the data was segmented with the use of the IMU data. This was done to apply pre-processing to the walking signals where the noise from the capacitance data is canceled with the data collected from the IMU. This segmentation allows the detected motion events to be processed differently from the stationary events. A block diagram of the overview of the signal processing can be seen in Fig. 3. The same data extracted from the belt is also processed using the same algorithm and parameters for a fair comparison.

The data from the algorithm is analyzed using the Bland Altman statistical method which is a faster way to visually compare between large data sets. This allows direct point to point comparison of both the gold standard and the capaciflector based system.

The system was also power tested by getting the average current consumed during operation, which correlated to 3.3mAH, and on a CR2032 cell which has 200mAH this results in around 60 Hours of theoretical run time. The system was further tested with a new coin cell to cross check the maximum run time of the sensor system. The system ran a total of 45 hours on a fresh battery; the difference is due to the capacity of the battery decreasing due to the large current consumption from the micro-SD card which shortens the lifespan in the process.

IV. Results and Discussion

The results from the tests were processed into respiration values which were then compiled into a Bland Altman Plot to show the accuracy of the developed system from the gold standard belt sensor. An example of the resulting data from system and the belt sensor can be seen in Fig. 5, where breathing peaks are correlated exactly with the belt data.

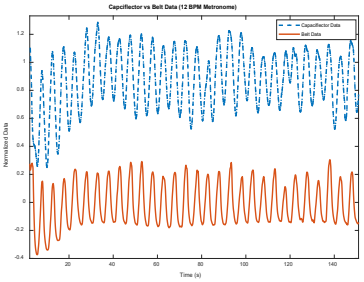

Fig. 5. A test signal from one of the metronome tests (12 Breaths Per Minute), showing the capaciflector data collected by the sensor system against the belt data.

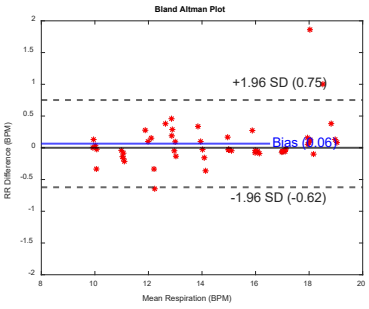

Fig. 6. Bland Altman for the ten metronome tests, comparing the belt data with the new sensor system. Each vertical band represents the different metronome value tested.

A. Study 1 (Metronome Results)

Study 1 results are the results from the more controlled tests in which the sensor system is expected to perform the best in. The results in Fig. 6 show the results to be within ± 0.68 BPM with a negative bias of 0.06 BPM. The results from study 1 are used to confirm that the system can accurately be used to measure respiration. The band of points that are together represent the different set of metronome tests that were taken. The results indicate a great upper and lower limit with a bias closer to zero, this can be compared to a study done on a sensor system by Respirasense, where they achieved a bias of 0.38 BPM and limits of agreement between 1.0 and 1.8 BPM. These values are much lower (by a factor that is greater than 1 BPM) when compared to the sensor system constructed using the capaciflector [6].

B. Study 2 (Walking Results)

Study 2 results had much higher variances of ± 1.32 BPM but are within the limits of an accurate system that utilizes the movement data to extract the breathing data. The bias of the

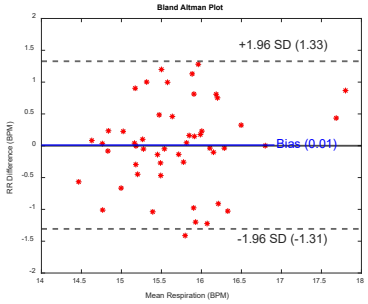

Fig. 7. Bland Altman for the ten walking tests, comparing the belt data with the new sensor system.

system is similar to the metronome tests with a value of 0.01 BPM, which indicates that the system is repeatable. This can be seen in Fig. 7. The data from the walking study is more sporadic due to the changes in respiration in the test, this allows the system to be assessed in a more realistic scenario. This also presents a case against some of the established devices that are not capable of monitoring respiration during walking events. This mainly applies to more commercial ready solutions such as Apple Watches. And in this sensor system no data was left out or discarded while cleaning up the signal and during the processing stage, making it better at extracting the respiration signal from the noisy breathing data.

V. Conclusion

The results from both studies are good indicators towards an accurate system that can measure respiration continuously in both stationary and walking events, while also being compact in size. The system utilizes many of the missing factors in respiration sensor systems, mainly the ability to detect and retrieve respiration data from signals that have walking noise without discarding any information in the process. The technique used to remove the noise from the breathing signal is also simple enough to be implemented in the hardware itself, making the device even more compact. And with the sensor itself being simple to manufacture the cost of the device becomes much lower.

Overall, the capaciflector based system shows big potential in becoming one of the gold standards of respiration monitoring due to the simplicity of the sensor as well as the ease of use in both home and hospital environments.

REFERENCES

[1] R. L. Riha. Diagnostic approaches to respiratory sleep disorders. J Thorac Dis, 7(8): 1373–1384, Aug 2015.

[2] Amy Sarah Ginsburg, Jennifer L. Lenahan, Rasa Izadnegahdar, and J. Mark Ansermino. A systematic review of tools to measure respiratory rate in order to identify childhood pneumonia. American Journal of Respiratory and Critical Care Medicine, 197(9): 1116–1127, May 2018.

[3] Carol Kelly. Respiratory rate 1: why measurement and recording are crucial. Nursing Times [online], 114(4):23–24, April 2018.

[4] Booth A, Reed AB, Ponzo S, Yassaee A, Aral M, et al. (2021) Population risk factors for severe disease and mortality in COVID-19: A global systematic review and meta-analysis. PLOS ONE 16(3): e0247461.

[5] Chu, M., Nguyen, T., Pandey, V. et al. Respiration rate and volume measurements using wearable strain sensors. npj Digital Med 2, 8 (2019).

[6] Subbe CP, Kinsella S. Continuous Monitoring of Respiratory Rate in Emergency Admissions: Evaluation of the RespiraSense™ Sensor in Acute Care Compared to the Industry Standard and Gold Standard. Sensors (Basel). 2018;18(8):2700. Published 2018 Aug 17.

[7] P. H. Charlton, T. Bonnici, L. Tarassenko, D. A. Clifton, R. Beale, and P. J. Watkinson, "An assessment of algorithms to estimate respiratory rate from the electrocardiogram and photoplethysmogram," Physiological Measurement, vol. 37, no. 4. IOP Publishing, pp. 610–626, Mar. 30, 2016.

[8] V. Mouradian, A. Poghosyan, and L. Hovhannisyan, "Continuous wearable health monitoring using novel PPG optical sensor and device," 2014 IEEE 10th International Conference on Wireless and Mobile Computing, Networking and Communications (WiMob). IEEE, Oct. 2014.

[9] Neil M. White, Jordan Ash, Yang Wei, and Harry Akerman. A planar respiration sensor based on a capaciflector structure. IEEE Sensors Letters, 1(4):1–4, August 2017.

[10] Hayward, N., Shaban, M., Badger, J. et al. A capaciflector provides continuous and accurate respiratory rate monitoring for patients at rest and during exercise. Journal of Clinical Monitoring and Computing (2022).

[11] J. Vranish. Commercial "capaciflector." Computers \& Electrical Engineering, 1991.

Appendix H

Ethics Supplementary Materials and Consent Forms

H.1 Consent Forms

UNIVERSITY OF Southampton

CONSENT FORM

Study title: Investigation of Respiration Signals

Researcher names: Mahdi Mohamed Saleh Abdulla Ahmed Shaban
Harry Ackerman
Isobel Jones
ERGO number: ERGO/FEPS/68839

Please initial the box(es) if you agree with the statement(s):

I have read and understood the information sheet ([28/04/2022] / Version 1.2) and have had the opportunity to ask questions about the study.	
I agree to take part in this research project and agree for my data to be used for the purpose of this study.	
I understand my participation is voluntary and I may withdraw for any reason without my participation rights being affected.	
I understand that should I withdraw from the study then the information collected about me up to this point may still be used for the purposes of achieving the objectives of the study only.	
I understand that I will not be directly identified in any reports of the research.	
I understand that I am not wearing a pacemaker, and if I do, I am to notify the researcher.	
I understand that I am happy to be contacted for the 4th Study on a separate date.	
I understand that I have the choice on the way I can be contacted for the 4th Study.	

Name of participant (print name).....

Signature of participant.....

Date.....

Name of researcher (print name).....

Signature of researcher .....

Date.....

H.2 Participant Information Sheet

UNIVERSITY OF Southampton

Participant Information Sheet

Study Title: Investigation of Respiration Signals

Researchers: Mahdi Mohamed Saleh Abdulla Ahmed Shaban
Harry Ackerman
Isobel Jones
ERGO number: ERGO/FEPS/68839

You are being invited to take part in the above research study. To help you decide whether you would like to take part or not, it is important that you understand why the research is being done and what it will involve. Please read the information below carefully and ask questions if anything is not clear or you would like more information before you decide to take part in this research. You may like to discuss it with others, but it is up to you to decide whether to take part in the project. If you are happy to participate you will be asked to sign a consent form.

What is the research about?
I'm a PhD Student in Electrical and Electronics Engineering doing a study on a low-cost sensor hardware, this study will be part of my work towards completing my thesis. The study is conducted to collect enough data to allow the hardware and the software to be optimised and calibrated. The objective for this study is to assess the effectiveness and accuracy of the device throughout daily activities. The expected outcome of this study is to have the data be used to effectively develop newer methods of detection towards the research.

Why have I been asked to participate?
You have been asked to do this study as you fit the requirement of being healthy and can wear the sensor for a full 24-hour period.

What will happen to me if I take part?
The participation should take a maximum of two days to fully complete with the first day doing three short tests, which should last a maximum duration of an hour. And at the end of those tests a device will be placed to be used throughout the next day (if possible). No changes in your daily activities will change, and all normal activities should be performed as usual except for anything involving water, in which the device may be removed for the period. There will be no audio or video recording in this study, and everything will be anonymous. The research data collected will be done quantitatively.

Are there any benefits in my taking part?
Taking part in this study will help this research to further understand respiration signals and the proper detection methods that can be used to effectively gather respiration data. This study will have no reimbursements for participation.

Are there any risks involved?
No risk is involved in this study as the device is not invasive and only contact the skin indirectly. The device may cause discomfort for some people (while wearing it over long periods of time). If in any case the device does cause discomfort, the device can be removed easily.

What data will be collected?
The data collected will be from a sensor that reads respiration data in the form of capacitance, while the belt sensor will measure the force on the chest. Weight, height, and age data will be collected with no personal information, or any information that links you to the data will be collected. The consent data will be stored securely in a locked drawer. The main data from the tests will be stored in a password locked USB device. As for during the study where the sensor will be collected after the last test; the contact information (email) will be kept in the same USB device in the form of an Excel file which will be deleted as soon as the tests are over. The emails are only collected to keep in contact until the participant fully completes or withdraws from the study.

Will my participation be confidential?
Your participation and the information we collect about you during the research will be kept strictly confidential.

Only members of the research team and responsible members of the University of Southampton may be given access to data about you for monitoring purposes and/or to carry out an audit of the study to ensure that the research is complying with applicable regulations. Individuals from regulatory authorities (people who check that we are carrying out the study correctly) may require access to your data. All these people have a duty to keep your information, as a research participant, strictly confidential.

Do I have to take part?
No, it is entirely up to you to decide whether to take part or not. If you decide you want to take part, you will need to sign a consent form to show you have agreed to take part. The way to contact Mahdi Shaban for this study is by using email (**ms17g16@soton.ac.uk**) in which a consent form will be provided to be signed.

What happens if I change my mind?
You have the right to change your mind and withdraw at any time without giving a reason and without your participant rights being affected. If you do withdraw from the study, we will keep the information about you that we have already obtained for the purposes of achieving the objectives of the study only. In the case of withdrawal, the same contact email for Mahdi Shaban (**ms17g16@soton.ac.uk**) must be used to inform of any changes.

What will happen to the results of the research?
Your personal details will remain strictly confidential. Research findings made available in any reports or publications will not include information that can directly identify you. The results will be used to write a publication on the sensor hardware and the algorithms. Where the information from this study will help it but will not include any information that links or identifies you.

Where can I get more information?
Please contact Mahdi Shaban by email for any more information
Mahdi Shaban **(ms17g16@soton.ac.uk)**

What happens if there is a problem?
If you have a concern about any aspect of this study, you should speak to Mahdi Shaban (ms17g16@soton.ac.uk) who will do their best to answer your questions.
If you remain unhappy or have a complaint about any aspect of this study, please contact the University of Southampton Research Integrity and Governance Manager (023 8059 5058, rgoinfo@soton.ac.uk).

Thank you for your time.

References

K. Albouaini, M. Egred, A. Alahmar, and D. J. Wright. Cardiopulmonary exercise testing and its application. *Postgraduate Medical Journal*, 83(985):675–682, November 2007. doi: 10.1136/hrt.2007.121558. URL https://doi.org/10.1136/hrt.2007.121558.

Sami El Arja, Titus Jayarathna, Felipe Ulloa, Gaetano Gargiulo, and Paul Breen. Characterization of coated piezo-resistive fabric for respiration sensing. In *2019 International Conference on Electrical Engineering Research & Practice (ICEERP)*. IEEE, November 2019. doi: 10.1109/iceerp49088.2019.8956989. URL https://doi.org/10.1109/iceerp49088.2019.8956989.

E. Oran Brigham. *FFT TRANSFORM APPLICATIONS*, page 167–199. Prentice-Hall, 1988.

P. Y. Chan, N. P. Ryan, D. Chen, J. McNeil, and I. Hopper. Novel wearable and contactless heart rate, respiratory rate, and oxygen saturation monitoring devices: a systematic review and meta-analysis. *Anaesthesia*, 77(11):1268–1280, August 2022. doi: 10.1111/anae.15834. URL https://doi.org/10.1111/anae.15834.

Hsiao-Huang Chang, Chuan-Chih Hsu, Chia-Yuen Chen, Wai-Keung Lee, Hao-Teng Hsu, Kuo-Kai Shyu, Jia-Rong Yeh, Pin-Jun Lin, and Po-Lei Lee. A method for respiration rate detection in wrist PPG signal using holo-hilbert spectrum. *IEEE Sensors Journal*, 18(18):7560–7569, September 2018. doi: 10.1109/jsen.2018.2855974. URL https://doi.org/10.1109/jsen.2018.2855974.

Peter H Charlton, Timothy Bonnici, Lionel Tarassenko, David A Clifton, Richard Beale, and Peter J Watkinson. An assessment of algorithms to estimate respiratory rate from the electrocardiogram and photoplethysmogram. *Physiological Measurement*, 37 (4):610–626, March 2016. doi: 10.1088/0967-3334/37/4/610. URL https://doi.org/10.1088/0967-3334/37/4/610.

Michael Chu, Thao Nguyen, Vaibhav Pandey, Yongxiao Zhou, Hoang N. Pham, Ronen Bar-Yoseph, Shlomit Radom-Aizik, Ramesh Jain, Dan M. Cooper, and Michelle Khine. Respiration rate and volume measurements using wearable strain sensors.

npj Digital Medicine, 2(1), February 2019. doi: 10.1038/s41746-019-0083-3. URL https://doi.org/10.1038/s41746-019-0083-3.

Ku Young Chung, Bong-Ki Lee, Kwangsub Song, Kangsoo Shin, Seok Hyun Cho, and Joon-Hyuk Chang. An experimental study: The sufficient respiration rate detection technique via continuous wave doppler radar. In *2016 IEEE International Conference on Network Infrastructure and Digital Content (IC-NIDC)*. IEEE, September 2016. doi: 10.1109/icnidc.2016.7974619. URL https://doi.org/10.1109/icnidc.2016.7974619.

James W. Cooley, Peter A. W. Lewis, and Peter D. Welch. The fast fourier transform and its applications. *IEEE Transactions on Education*, 12(1):27–34, 1969. doi: 10.1109/te.1969.4320436. URL https://doi.org/10.1109/te.1969.4320436.

Toan Dinh, Thanh Nguyen, Van Thanh Dau, Foisal Abu Riduan, Canh-Dung Tran, Hoang-Phuong Phan, Tuan-Khoa Nguyen, Pablo Guzman, Nam-Trung Nguyen, and Dzung Viet Dao. Flexible and wearable flow sensor using spinnable carbon nanotube nanofilm for respiration monitoring. In *2020 IEEE 33rd International Conference on Micro Electro Mechanical Systems (MEMS)*. IEEE, January 2020. doi: 10.1109/mems46641.2020.9056423. URL https://doi.org/10.1109/mems46641.2020.9056423.

N. Donnelly, T. Hunniford, R. Harper, A. Flynn, A. Kennedy, D. Branagh, and J. McLaughlin. Demonstrating the accuracy of an in-hospital ambulatory patient monitoring solution in measuring respiratory rate. In *2013 35th Annual International Conference of the IEEE Engineering in Medicine and Biology Society (EMBC)*. IEEE, July 2013. doi: 10.1109/embc.2013.6611096. URL https://doi.org/10.1109/embc.2013.6611096.

Validyne Engineering. Basics of pneumotach flow measurement, Apr 2018. URL https://www.validyne.com/blog/basics-pneumotach-flow-measurement.

Atena Roshan Fekr, Katarzyna Radecka, and Zeljko Zilic. Tidal volume variability and respiration rate estimation using a wearable accelerometer sensor. *Proceedings of the 4th International Conference on Wireless Mobile Communication and Healthcare - "Transforming healthcare through innovations in mobile and wireless technologies"*, 2014. doi: 10.4108/icst.mobihealth.2014.257528.

A.C. Fischer-Cripps. Digital signal processing. In *Newnes Interfacing Companion*, pages 269–283. Elsevier, 2002. doi: 10.1016/b978-075065720-4/50121-2. URL https://doi.org/10.1016/b978-075065720-4/50121-2.

Davide Giavarina. Understanding bland altman analysis. *Biochemia Medica*, 25(2):141–151, 2015. doi: 10.11613/bm.2015.015. URL https://doi.org/10.11613/bm.2015.015.

Amy Sarah Ginsburg, Jennifer L. Lenahan, Rasa Izadnegahdar, and J. Mark Ansermino. A systematic review of tools to measure respiratory rate in order to identify childhood pneumonia. *American Journal of Respiratory and Critical Care Medicine*, 197(9): 1116–1127, May 2018. doi: 10.1164/rccm.201711-2233ci. URL https://doi.org/10.1164/rccm.201711-2233ci.

Google. Track your respiratory rate, 2021. URL https://support.google.com/fit/answer/10478084?hl=en-GB.

Nick Hayward, Mahdi Shaban, James Badger, Isobel Jones, Yang Wei, Daniel Spencer, Stefania Isichei, Martin Knight, James Otto, Gurinder Rayat, Denny Levett, Michael Grocott, Harry Akerman, and Neil White. A capaciflector provides continuous and accurate respiratory rate monitoring for patients at rest and during exercise. *Journal of Clinical Monitoring and Computing*, January 2022. doi: 10.1007/s10877-021-00798-7. URL https://doi.org/10.1007/s10877-021-00798-7.

Zhengling He, Xianxiang Chen, Zhen Fang, Tingyu Sheng, and Shanhong Xia. Fusion estimation of respiration rate from ECG and PPG signal based on android platform and wearable watch. In *2nd IET International Conference on Biomedical Image and Signal Processing (ICBISP 2017)*. Institution of Engineering and Technology, 2017. doi: 10.1049/cp.2017.0096. URL https://doi.org/10.1049/cp.2017.0096.

Tao Jiang, Junwen Zhong, Jiaming Liang, Yichuan Wu, Zehui Li, Xiaohao Wang, Liwei Lin, and Xiang Qian. Wearable airflow sensor for nasal symmetric evaluation and respiration monitoring. In *2019 IEEE SENSORS*. IEEE, October 2019. doi: 10.1109/sensors43011.2019.8956504. URL https://doi.org/10.1109/sensors43011.2019.8956504.

JLCPCB. Pcb capabilities, 2021. URL https://jlcpcb.com/capabilities/Capabilities.

Carol Kelly. Respiratory rate 1: why measurement and recording are crucial. *Nursing Times [online]*, 114(4):23–24, April 2018. URL https://www.nursingtimes.net/clinical-archive/respiratory-clinical-archive/respiratory-rate-1-why-measurement-and-recording-are-crucial-26-03-2018/.

Ian Kerslake and Fiona Kelly. Uses of capnography in the critical care unit. *BJA Education*, 17(5):178–183, May 2017. doi: 10.1093/bjaed/mkw062. URL https://doi.org/10.1093/bjaed/mkw062.

KiCad Development Team. Kicad eda, 2021. URL https://www.kicad.org/about/kicad/. v5.1.7.

Jong Deok Kim, Won Hyuk Lee, Yonggu Lee, Hyun Ju Lee, Teahyen Cha, Seung Hyun Kim, Ki-Min Song, Young-Hyo Lim, Seok Hyun Cho, Sung Ho Cho, and Hyun-Kyung Park. Non-contact respiration monitoring using impulse radio ultrawide-band radar in neonates. *Royal Society Open Science*, 6(6), June 2019. doi: 10.1098/rsos.190149. URL https://doi.org/10.1098/rsos.190149.

Stephen R Knight, Antonia Ho, Riinu Pius, Iain Buchan, Gail Carson, Thomas M Drake, Jake Dunning, Cameron J Fairfield, Carrol Gamble, Christopher A Green, Rishi Gupta, Sophie Halpin, Hayley E Hardwick, Karl A Holden, Peter W Horby, Clare Jackson, Kenneth A Mclean, Laura Merson, Jonathan S Nguyen-Van-Tam, Lisa Norman, Mahdad Noursadeghi, Piero L Olliaro, Mark G Pritchard, Clark D Russell, Catherine A Shaw, Aziz Sheikh, Tom Solomon, Cathie Sudlow, Olivia V Swann, Lance CW Turtle, Peter JM Openshaw, J Kenneth Baillie, Malcolm G Semple, Annemarie B Docherty, and Ewen M Harrison. Risk stratification of patients admitted to hospital with covid-19 using the ISARIC WHO clinical characterisation protocol: development and validation of the 4c mortality score. *BMJ*, page m3339, September 2020. doi: 10.1136/bmj.m3339. URL https://doi.org/10.1136/bmj.m3339.

LabVIEW. Labview 2018, 2018. URL https://www.ni.com/en-gb/shop/labview.html.

Lawrence A Lynn and J Paul Curry. Patterns of unexpected in-hospital deaths: a root cause analysis. *Patient Safety in Surgery*, 5(1):3, 2011. doi: 10.1186/1754-9493-5-3. URL https://doi.org/10.1186/1754-9493-5-3.

Carlo Massaroni, Daniel Simões Lopes, Daniela Lo Presti, Emiliano Schena, and Sergio Silvestri. Contactless monitoring of breathing patterns and respiratory rate at the pit of the neck: A single camera approach. *Journal of Sensors*, 2018:1–13, September 2018. doi: 10.1155/2018/4567213. URL https://doi.org/10.1155/2018/4567213.

MATLAB. Matlab r2019b, 2019. URL https://www.mathworks.com/products/matlab.html.

Vahram Mouradian, Armen Poghosyan, and Levon Hovhannisyan. Continuous wearable health monitoring using novel PPG optical sensor and device. In *2014 IEEE 10th International Conference on Wireless and Mobile Computing, Networking and Communications (WiMob)*. IEEE, October 2014. doi: 10.1109/wimob.2014.6962159. URL https://doi.org/10.1109/wimob.2014.6962159.

National Instruments. Usb-6003, 2020. URL https://www.ni.com/en-gb/support/model.usb-6003.html.

Christopher A. Del Negro, Gregory D. Funk, and Jack L. Feldman. Breathing matters. *Nature Reviews Neuroscience*, 19(6):351–367, May 2018. doi: 10.1038/s41583-018-0003-6. URL https://doi.org/10.1038/s41583-018-0003-6.

Novelda. Slmx4 - uwb radar module, 2021. URL https://sensorlogic.store/products/slmx4-uwb-radar-module?pr_prod_strat=copurchase&pr_rec_pid=6636734742683&pr_ref_pid=4438933700667&pr_seq=uniform.

Robert Oshana. Overview of digital signal processing algorithms. In *DSP Software Development Techniques for Embedded and Real-Time Systems*, pages 59–121. Elsevier, 2006. doi: 10.1016/b978-075067759-2/50006-5. URL https://doi.org/10.1016/b978-075067759-2/50006-5.

Panasonic. Manganese dioxide lithium coin batteries: Individual specifications : Cr2032, August 2005.

PCBWay. Stack-up for fpc, 2022. URL https://www.pcbway.com/pcb_prototype/Stack_up_for_FPC.html.

Pmd-solutions. Sensor technology — pmd solutions, 2020. URL http://www.pmd-solutions.com/sensortechnology/.

M. Pohanka. Overview of Piezoelectric Biosensors, Immunosensors and DNA Sensors and Their Applications. *Materials (Basel)*, 11(3), Mar 2018.

Aleksandra Rashkovska, Matjaž Depolli, Ivan Tomašić, Viktor Avbelj, and Roman Trobec. Medical-grade ECG sensor for long-term monitoring. *Sensors*, 20(6):1695, March 2020. doi: 10.3390/s20061695. URL https://doi.org/10.3390/s20061695.

Vignesh Ravichandran, Balamurali Murugesan, Vaishali Balakarthikeyan, Keerthi Ram, S.P. Preejith, Jayaraj Joseph, and Mohanasankar Sivaprakasam. RespNet: A deep learning model for extraction of respiration from photoplethysmogram. In *2019 41st Annual International Conference of the IEEE Engineering in Medicine and Biology Society (EMBC)*. IEEE, July 2019. doi: 10.1109/embc.2019.8856301. URL https://doi.org/10.1109/embc.2019.8856301.

RCP. National early warning score (news) 2, Jul 2020. URL https://www.rcplondon.ac.uk/projects/outputs/national-early-warning-score-news-2.

R. L. Riha. Diagnostic approaches to respiratory sleep disorders. *J Thorac Dis*, 7(8): 1373–1384, Aug 2015.

SanDisk Corporation. Sandisk datasheet industrial microsd card, December 2015. Rev 1.0.

Nandakumar Selvaraj and Ravi Narasimhan. Detection of sleep apnea on a per-second basis using respiratory signals. In *2013 35th Annual International Conference of the IEEE Engineering in Medicine and Biology Society (EMBC)*. IEEE, July 2013. doi: 10.1109/embc.2013.6609953. URL https://doi.org/10.1109/embc.2013.6609953.

Sensirion. Flow sensor solutions in modern medical ventilators, 2021. URL https://www.sensirion.com/en/about-us/newsroom/sensirion-specialist-articles/flow-sensor-solutions-in-modern-medical-ventilators/.

Mahdi M S A A Shaban, Daniel C Spencer, and Neil M. White. A new type of respiration sensing system for continuous monitoring. *IEEE Sensors Conference*, 2022.

Mahdi M S A A Shaban, Daniel C Spencer, Harry Akerman, Isobel Jones, and Neil M. White. A new type of respiration sensing system for continuous monitoring. *IEEE Sensors Journal*, 2023.

Christian Subbe and Sean Kinsella. Continuous monitoring of respiratory rate in emergency admissions: Evaluation of the RespiraSense™ sensor in acute care compared to the industry standard and gold standard. *MDPI Sensors*, 18(8), August 2018. doi: 10.3390/s18082700. URL https://doi.org/10.3390/s18082700.

Texas Instruments Incorporated. *4-Ch, 28-bit, capacitance to digital converter*. Texas Instruments Incorporated., 2015. URL https://www.ti.com/lit/gpn/fdc2214. Rev. A.

Texas Instruments Incorporated. Code composer studio integrated development environment (ide), 2020. URL https://www.ti.com/tool/CCSTUDIO. v10.2.0.

Texas Instruments Incorporated. *FAQ FDC2214*. Texas Instruments Incorporated., 2021. URL https://e2e.ti.com.

Vernier. Go direct respiration belt, 2020. URL https://www.vernier.com/product/go-direct-respiration-belt/.

J. Vranish. Commercial "capaciflector." computers & electrical engineering, 1991. URL https://ntrs.nasa.gov/archive/nasa/casi.ntrs.nasa.gov/19920013480.pdf.

Iain Wheatley. Respiratory rate 3: how to take an accurate measurement. *Nursing Times [online]*, 114(7):21–22, July 2018. URL https://www.nursingtimes.net/clinical-archive/respiratory-clinical-archive/respiratory-rate-3-how-to-take-an-accurate-measurement-25-06-2018/.

Neil M. White, Jordan Ash, Yang Wei, and Harry Akerman. A planar respiration sensor based on a capaciflector structure. *IEEE Sensors Letters*, 1(4):1–4, August 2017. doi: 10.1109/lsens.2017.2722481. URL https://doi.org/10.1109/lsens.2017.2722481.

Xim. Lifelight, 2020. URL https://lifelight.ai/.

Chenxi Yang, Brendan Bruce, Xiaofan Liu, Behnood Gholami, and Negar Tavassolian. A hybrid radar-camera respiratory monitoring system based on an impulse-radio ultrawideband radar. In *2020 42nd Annual International Conference of the IEEE Engineering in Medicine & Biology Society (EMBC)*. IEEE, July 2020. doi: 10.1109/embc44109.2020.9175267. URL https://doi.org/10.1109/embc44109.2020.9175267.

George Yuan, Nicole A. Drost, and R. Andrew McIvor. Clinical review - respiratory rate and breathing pattern. *McMaster University Medical Journal (MUMJ)*, 10(1), 2013. URL https://mdprogram.mcmaster.ca/docs/default-source/MUMJ-Library/v10_23.pdf?sfvrsn=0.